



# Distribution Models for Vulnerable Marine Ecosystem Indicator Taxa in the Cobb-Eickelberg Seamount Chain

Christopher N. Rooper<sup>1</sup>, Pamela Goddard<sup>2</sup>, Christina Conrath<sup>3</sup>,  
Lauri Sadorus<sup>2</sup>, Kim Rand<sup>2</sup>, Vanessa Lowe<sup>2</sup>

05 December 2024

## Contents

<b>1</b>	<b>Introduction</b>	<b>3</b>
<b>2</b>	<b>Vulnerable Marine Indicator Taxa Group: <i>Gorgonians</i></b>	<b>4</b>
2.1	Study resolution . . . . .	4
2.2	Dependent data . . . . .	6
2.3	Independent data . . . . .	7
2.4	Modelling approach . . . . .	8
2.5	Model uncertainty . . . . .	10
2.6	Model validation . . . . .	11
2.7	Model outputs . . . . .	12
2.8	Conclusions . . . . .	13
<b>3</b>	<b>Vulnerable Marine Indicator Taxa Group: <i>Antipatharians</i></b>	<b>25</b>
3.1	Study resolution . . . . .	25
3.2	Dependent data . . . . .	25
3.3	Independent data . . . . .	27
3.4	Modelling approach . . . . .	28
3.5	Model uncertainty . . . . .	30
3.6	Model validation . . . . .	31
3.7	Model outputs . . . . .	32
3.8	Conclusions . . . . .	33
<b>4</b>	<b>Vulnerable Marine Indicator Taxa Group: <i>ScleractinianReefs</i></b>	<b>45</b>
4.1	Study resolution . . . . .	45
4.2	Dependent data . . . . .	45
4.3	Independent data . . . . .	47
4.4	Modelling approach . . . . .	48
4.5	Model uncertainty . . . . .	50
4.6	Model validation . . . . .	51
4.7	Model outputs . . . . .	52
4.8	Conclusions . . . . .	53
<b>5</b>	<b>Vulnerable Marine Indicator Taxa Group: <i>Hexactinellids</i></b>	<b>65</b>
5.1	Study resolution . . . . .	65
5.2	Dependent data . . . . .	65
5.3	Independent data . . . . .	67
5.4	Modelling approach . . . . .	68
5.5	Model uncertainty . . . . .	70

5.6	Model validation . . . . .	71
5.7	Model outputs . . . . .	72
5.8	Conclusions . . . . .	73
<b>6</b>	<b>Vulnerable Marine Indicator Taxa Group: <i>Demosponges</i></b>	<b>85</b>
6.1	Study resolution . . . . .	85
6.2	Dependent data . . . . .	85
6.3	Independent data . . . . .	87
6.4	Modelling approach . . . . .	88
6.5	Model uncertainty . . . . .	90
6.6	Model validation . . . . .	91
6.7	Model outputs . . . . .	92
6.8	Conclusions . . . . .	93
<b>7</b>	<b>Vulnerable Marine Indicator Taxa Group: <i>Pennatulaceans</i></b>	<b>105</b>
7.1	Study resolution . . . . .	105
7.2	Dependent data . . . . .	105
7.3	Independent data . . . . .	107
7.4	Modelling approach . . . . .	108
7.5	Model uncertainty . . . . .	110
7.6	Model validation . . . . .	111
7.7	Model outputs . . . . .	112
7.8	Conclusions . . . . .	113
<b>8</b>	<b>Vulnerable Marine Indicator Taxa Group: <i>Hydrocorals</i></b>	<b>125</b>
8.1	Study resolution . . . . .	125
8.2	Dependent data . . . . .	125
8.3	Independent data . . . . .	127
8.4	Modelling approach . . . . .	128
8.5	Model uncertainty . . . . .	130
8.6	Model validation . . . . .	131
8.7	Model outputs . . . . .	132
8.8	Conclusions . . . . .	133
<b>9</b>	<b>Summary</b>	<b>145</b>
<b>10</b>	<b>References</b>	<b>145</b>

# 1 Introduction

The objective of these analyses were to develop species distribution models for VME indicator taxa in the Cobb-Eickelberg seamount chain (Figure 1). These models were developed using survey data collected in 2022 and tested against survey data collected in 2024. The species distributions will be used to assess risk of VME impacts by fishing and other human activities on these seamounts.

Historically (1970's – 1990's) many of the seamounts in this chain were fished by both domestic (Canadian and USA) and foreign (Russia, Korea and Japan) fishing fleets. Currently, there is limited fishing at the seamounts in international waters. The only fishing currently occurring is by the Canadian Sablefish longline trap fleet. The intersection between deep-sea coral and sponge distribution and fisheries is an ongoing concern of the North Pacific Fisheries Commission, the Regional Fisheries Management Organization for international waters of the North Pacific Ocean ([www.npfc.int](http://www.npfc.int)). The NPFC manages fisheries and vulnerable marine ecosystems (VME's) to monitor potential significant and adverse impacts on deep sea corals and sponges. Thus, there is interest in these offshore seamount chains, both in terms of their biological characteristics and for management issues related to international fisheries.

The data used in this modeling effort were collected during two surveys in 2022 and 2024. The main tool used in this work was the underwater stereo camera system developed during the Alaska Coral and Sponge Initiative in 2012-2015. The stereo-camera survey followed a standard protocol outlined in Rooper et al. (2016), with a target of 15 minutes of on-bottom time for each transect. Images were processed to determine substrate type, density and size of structure forming invertebrates and density and size of fish species using *Sebastes* software (Williams et al. 2015). The visual survey was designed in a robust statistically sound method so that inferences about the deep-sea coral and sponge communities on seamounts can be made. The survey used a stratified-random sampling design using depth strata on 5 seamounts (Figure 1). Five depth strata (0-200 m, 200 – 400 m, 400 – 600 m, 600 – 800 m and 800 -1100).

In total 77 transects were occupied in 2022 (Figure 2). These transects were used to generate models of species distribution for seven taxonomic groups of VME indicators (Gorgonians, Antipatharians, Reef-building Scleractinians, Demosponge, Hexactinellid sponge, Pennatulaceans, and Hydrocorals). The models were tested against the presence and absence data from 58 transects that were occupied in 2024 (Figure 2).

In the following sections each taxonomic group is presented. The template for each of the model presentations is modified from the ICES PHM advice template (ICES 2020).

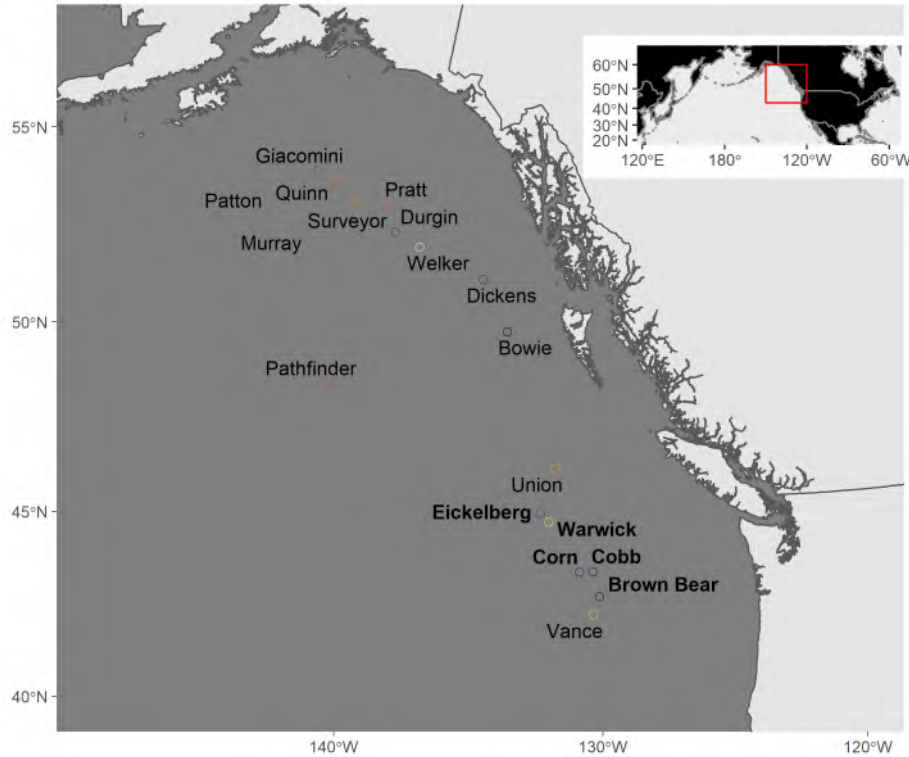


Figure 1: Map of eastern North Pacific Ocean seamounts showing the five seamount complexes where the Canadian Sablefish fishery operates and where VME indicator taxa distribution was modeled for this study in bold text (Eickelberg, Warwick, Corn, Cobb and Brown Bear).

## 2 Vulnerable Marine Indicator Taxa Group: *Gorgonians*

### 2.1 Study resolution

#### 2.1.1 Location of the study area (or management region)

This modelling was carried out for five seamounts in the Northeastern Pacific Ocean where fisheries are managed by the North Pacific Fisheries Commission. The five seamounts are shown in Figure 1 and are part of the Cobb-Eickelberg seamount chain.

**2.1.1.1 Spatial extent of the modelled area** The specific seamounts modeled were five North Pacific Seamounts (Cobb, Brown Bear, Eickelberg, Warwick and Corn). Modeling was conducted from depths of 0 - 1250 m. Data was collected from 0 to ~850 m.

**2.1.1.2 Spatial resolution of the model and independent variables** The spatial resolution of the modeling was 100 m by 100 m grid cells. The all data was projected into an Albers equal area projection (proj4 description = “+proj=aea +lat\_0=45 +lon\_0=-126 +lat\_1=50 +lat\_2=58.5 +x\_0=1000000 +y\_0=0 +ellps=GRS80 +towgs84=0,0,0,0,0,0 +units=m +no\_defs”).

**2.1.1.3 Spatial precision (of observations and independent variables)** The spatial precision of the observations was taken from the gps mounted on the research vessel. Based on tracking information, the camera system was towed slightly behind the vessel (~200 m typically), but along the same path as the vessel. The anticipated precision of the variation of the camera path was expected to be less than 20 m across the trackline.

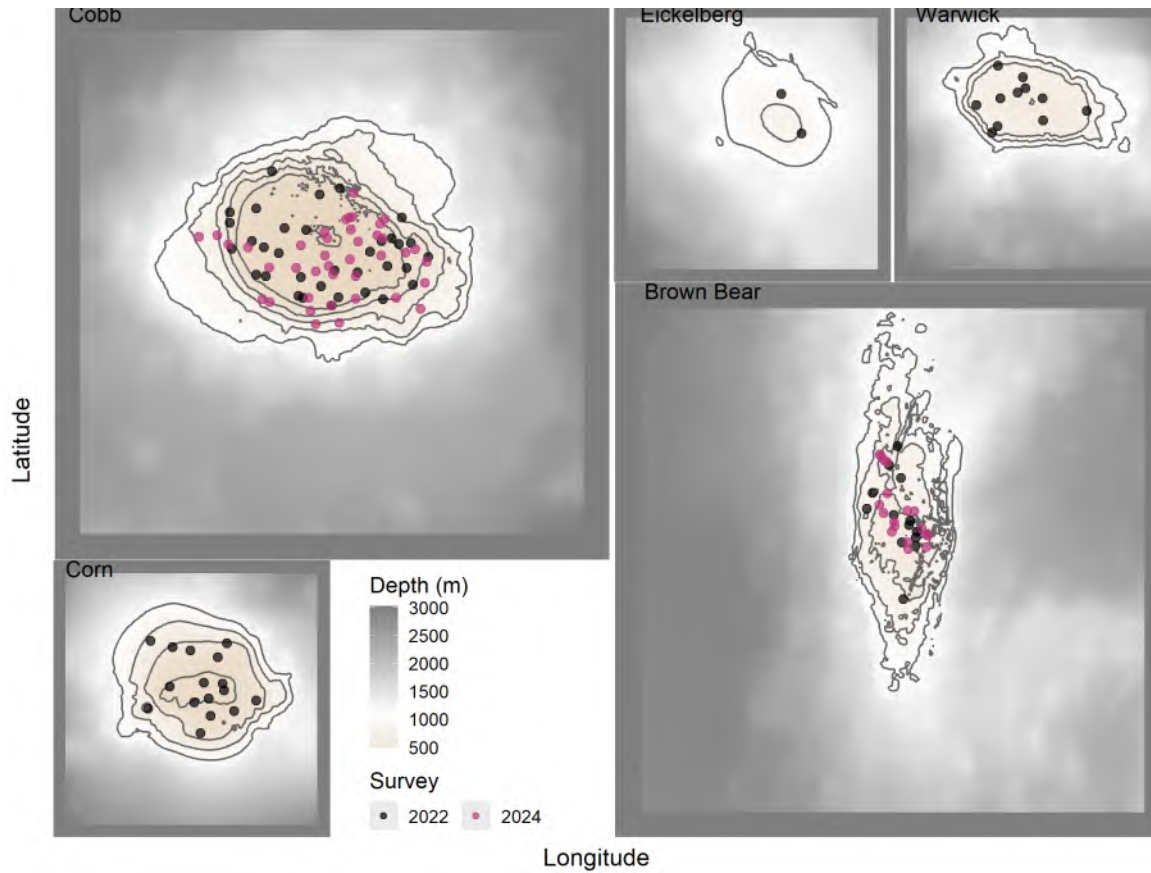


Figure 2: Map of survey transect locations in 2022 and 2024 at eastern North Pacific Ocean seamounts where the Canadian Sablefish fishery operates (Eickelberg, Warwick, Corn, Cobb and Brown Bear).

**2.1.1.4 Depth resolution/range/extent (of the observations and independent variables)** The depth range of the observations of *Gorgonians* (from the depth sensor mounted on the camera) was from 61 to 808 m (mean = 442 m, SE = 206.28). The depth range of the modeled area was from 34 (the summit depth of Cobb Seamount) to 1250 m.

## 2.1.2 Temporal extent of the data

**2.1.2.1 Dates of data extent** The dates observations used in model development were collected were September 6, 2022 to September 20, 2022. The dates for observations used for model testing were from September 3, 2024 to September 11, 2024.

**2.1.2.2 Precision of date/time** The precision of the date and the time of the data was assumed to be the closest second.

**2.1.2.3 Data/time resolution** The resolution of the date and time was fraction of a second.

**2.1.2.4 Impacts over time to consider in the data set (e.g. historical fishing effort)** Fishing occurred over the entire time frame from which these data points were collected. Fishing also has occurred historically since the 1970's. We did not attempt to account for historical fishing effort over this time. There may have been climate impacts occurring over the time frame of the data observations as well, however, these were not accounted for in the analyses.

## 2.2 Dependent data

The dependent data are shown in Figure 3.

Table 1. Number of records for each taxonomic grouping in the order *Gorgonians* from the survey database.

	Species or Taxa group	Count
15	Swiftia	342
5	Keratoisididae	303
9	Paragorgiidae	209
14	Primnoidae	140
11	Plexauridae	105
10	Parastenella	102
2	Gorgonacea	38
3	Isidella	24
7	Paragorgia	11
4	Isidella tentaculum	9
1	Acanthogorgiidae	1
6	Keratoisis	1
8	Paragorgia stephencairnsi	1
12	Plumarella superba	1
13	Primnoa pacifica	1

### 2.2.1 Data type (presence, absence, abundance)

The data used for modeling *Gorgonians* distribution were observed presences ( $n = 68$ ) and absences ( $n = 9$ ) that occurred at the five seamounts.

### 2.2.2 Data source (e.g. type of survey(s) combined)

The data were entirely from random stratified surveys of the Cobb-Eickelberg seamount chain conducted in 2022.

### 2.2.3 Measure of sampling effort

Sampling effort was estimated by the distance the camera traveled along each transect multiplied by the field of view observed along the transect (Rooper et al. 2016). This provided an area observed for each transect which was used as the effort measure. Area observed ranged from 254 to 2469 with a median area observed of 1197.

### 2.2.4 Detectability

Detectability of the width of the viewing area of the camera along the transect (area observed) was assumed to be 100% for VME indicator taxa. However, there were likely some individuals that were too small to be detected.

### 2.2.5 Taxonomic level

The taxonomic level modeled here was the taxonomic group *Gorgonians* (see Table 1 for individual families included in this grouping and refer to CMM for NPFC definitions).

### 2.2.6 Functional attributes (its ecology)

*Gorgonians* are a diverse, long-lived and fragile species. They occur in deep-water and are habitat forming structures important to many fishes, invertebrates other taxonomic groups.

### **2.2.7 Taxonomic confidence of species/assemblages**

The taxonomic confidence of the assemblage was assumed to be good. Experts experienced in identification of corals and sponges from visual imagery in the North Pacific Ocean did all the identification and image analyses.

### **2.2.8 Rationale for taxonomic/assemblage level modeled**

*Gorgonians* as defined here are a group that shares common habitat requirements and depth distribution. They are closely related and the order is globally distributed at deep depths. This Order has been previously modelled using Maximum entropy methods on a global extent and regional extent (Yesson et al., 2017, Chu et al. 2018, Doherty et al. 2019).

### **2.2.9 Source of absence data**

Absences were observations of no individuals at transects. In total there were 944 absences in the dataset.

### **2.2.10 Other potential errors or biases in the data**

There are some potential sources of error in the data, including errors in positioning of the records, errors in species identification (including both false positives and false negatives).

### **2.2.11 Data filtering steps**

No data filtering was conducted.

### **2.2.12 Taxonomic aggregation steps**

The records for the Order *Gorgonians* were aggregated by transect into presence or absence observations.

### **2.2.13 Method for combining dependent data sources (if done outside the modelling)**

No other dependent data sources were used in this modelling.

## **2.3 Independent data**

### **2.3.1 Independent data (environmental variables used)**

Five independent variables were used in building a model of *Gorgonians* distribution; bathymetry, topographic position index, seafloor slope, Oxygen concentration and northness (Figure 4).

### **2.3.2 Independent data source (source of raw or derived data)**

The bathymetry used here was downloaded from the NOAA website (<https://www.ncei.noaa.gov/maps/bathymetry/>). It consists of gridded bathymetry from a multibeam sources on a 3 arc-second grid for the region of interest. The details of the data sources can be found on the NOAA website. There were some gaps in the NOAA bathymetry layers. These were filled using single beam echosounder data collected during the 2022 and 2024 cruises and GEBCO bathymetry ([www.gebco.net/data\\_and\\_products/gridded\\_bathymetry\\_data](http://www.gebco.net/data_and_products/gridded_bathymetry_data)). The single beam echosounder data and GEBCO bathymetry was sampled into the missing grids in the NOAA bathymetry, with preference to the single beam echosounder data.

From the bathymetry two derived variables (slope and topographic position index) were calculated using the raster package (Hijmans 2019). Slope was calculated from the nearest 8 neighbors and TPI was calculated with a focal distance of ~300 m.

Northness was calculated as the cosine of the aspect (direction relative to 0 degrees that the slope was facing) for each grid cell based on bathymetry.

Oxygen data were based on the World Ocean Atlas data (2018 update). These data were clipped to the area of interest and resampled into the bathymetry grid using bilinear interpolation. The five explanatory variables are shown in Figure 4.

### 2.3.3 Native spatial and temporal resolution of the independent data

The native spatial resolution of the NOAA bathymetry was 3 arc-second grid. The native spatial resolution for the Oxygen data was 0.5 degrees longitude and latitude. It should be noted that the Oxygen data sources are conglomerations of data collected over varying spatial and temporal scales (e.g. the temporal scale is since ~1900's in the case of some measurements). For complete documentation of the spatial and temporal scale of the raw data the NODC respective website should be consulted ([www.gebco.net/data\\_and\\_products/gridded\\_bathymetry\\_data](http://www.gebco.net/data_and_products/gridded_bathymetry_data) and <https://www.nodc.noaa.gov/OC5/woa18/>).

All independent data layers were trimmed to include only observations and explanatory variables from this region and to depths of 1250 m.

### 2.3.4 Data processing and scaling (method for downscaling or aggregation)

Both the bathymetry (for gap filling) and oxygen layers were downscaled to a 100 m by 100 m grid in order to match the scale of the bathymetry. This downscaling was completed using bilinear interpolation.

**2.3.4.1 Goodness of fit for downscaled aggregated data** The downscaled data at the dependent data sites for both Oxygen and bathymetry represented the lower resolution very well ( $r > 0.9$ ).

**2.3.4.2 Measurement errors and bias** Measurement errors in the data or bias in the data were not accounted for beyond the processing conducted on the raw measurements by GEBCO or NODC.

### 2.3.5 Derivation methods and calculations for derived variables

From the bathymetry three derived variables (aspect, slope and topographic position index) were calculated using the raster package (Hijmans 2019). These variables were calculated on bathymetry aggregated (see below) to a 100 m by 100 m grid. The aspect variable was then converted to northness using a cosine function.

### 2.3.6 Rationale for inclusion of independent variables clearly stated and ecologically relevant

These five variables (depth, slope, topographic position index, northness and oxygen) have been found in previous studies to influence the distribution of *Gorgonians* (Huff et al., 2013, Yesson et al., 2017, Etnoyer et al., 2018).

## 2.4 Modelling approach

In this study generalized additive models (GAM) were developed to predict species distribution (Wood 2006).

### 2.4.1 Model steps

**2.4.1.1 Code for model provided** The code and data used for this model are not currently publicly available, but can be available on request from Chris Rooper ([chris.rooper@dfo-mpo.gc.ca](mailto:chris.rooper@dfo-mpo.gc.ca)).

**2.4.1.2 Packages used are referenced** The packages used to develop this model are referenced in the above .Rmd file. The key packages used were “sf”, “rnatuarearth”, “ggplot2”, “rgdal”, “rgeos”, “gstat”, “raster”, “mgcv” and are all available for download from CRAN. The R version used here was R version 3.6.0 (2019-04-26) – “Planting of a Tree” (R Core Development Team 2019).

**2.4.1.3 Data is made available as supplementary material** The independent variables are available from Chris Rooper ([chris.rooper@dfo-mpo.gc.ca](mailto:chris.rooper@dfo-mpo.gc.ca)).

## 2.4.2 Biases (spatial, temporal and other) acknowledged and described

There were no inherent biases in the modeling method (although there may be biases in the dependent and independent data described above).

## 2.4.3 Methods and approaches to collinearity in independent variables

**2.4.3.1 Collinearity in independent variables** The five explanatory variables were examined for collinearity using a pearson correlations (Figure 5). Variance inflation factors (Zuur et al. 2002) were also examined. In both cases the values were low, suggesting that the variables were fairly independent of each other.

Table 2. Variance inflation factors for independent variables using in modeling.

Variable	VIF
Depth	3.592
Slope	1.231
TPI	1.091
Oxygen	3.372
Northness	1.065

**2.4.3.2 Criteria for variable/dimension reduction provided** None of the variance inflation factors exceeded 5, indicating that dimension reduction was not warranted.

## 2.4.4 Choice of modelling method is explained and justified

The modelling method chosen was a generalized additive model (GAM). This model was primarily chosen for its simplicity of assumptions (stated below), its usefulness in fitting binomial (presence-absence) data, and the many previous applications of this method to predicting species distributions.

**2.4.4.1 Modelling assumptions are clearly stated** The basic GAM assumptions are; 1) Independence among data points, 2) The distribution of the residuals is binomially distributed, 3) homogenous variance across the fitted values, and 4) a non-linear relationship between response and predictor.

**2.4.4.2 Potential violations of model assumptions are explored** Diagnostic plots of Pearson residuals are shown in Figure 6. The residuals did not indicate any serious violations of GAM assumptions.

## 2.4.5 Model application

To build the model of *Gorgonians* a generalized additive model was constructed that contained five explanatory variables (depth, slope, topographic position index, northness and oxygen). The dependent data was presence or absence of *Gorgonians*. The full model was

$$y = \alpha + s(\text{depth}) + s(\text{slope}) + s(\text{TPI}) + s(\text{northness}) + s(\text{O}_2) + \sigma$$

A binomial error distribution ( $\sigma$ ) was used for the model fitting. A full model was fit initially containing all the variables with a basis degrees of freedom of 4 for each smooth. This model was reduced sequentially by removing the least significant term and comparing the AIC for the resulting reduced model following the methods of Rooper et al. (2016). This was repeated until there was a decline in model skill when removing a variable.

**2.4.5.1 Model settings** The default GAM settings in R were used (see `CobbSDM_Gorgonian.Rmd`). The only setting that was modified was the specification of the binomial error distribution and the specified number of knots for the smooth of  $k = 4$ .

**2.4.5.2 Model complexity is assessed** The results of the sequential variable reduction resulted in the retention of 2 terms; depth, TPI. The deviance explained by the model ( $D^2$ ) was 0.119.

The model complexity was assessed against simpler models with less terms during the sequential variable reduction step and the most complex model (containing these terms) was found to be the most appropriate (Table 3).

Table 3. Summary of GAM model predicting presence or absence of *Gorgonians*.

Term	edf	F	p-value
depth	1.073	4.391	0.0534
TPI	1.000	3.639	0.0565
residual	73.927		
GCV	-0.285		
Deviance explained (%)	11.900		

## 2.4.6 Model response curves are generated (where appropriate) and compared to expectations

Model response curves are shown in Figure 7. Probability of presence of *Gorgonians* was highest above 600 m depth was less when TPI values were  $< 0$  (indicating “valleys” or low points in the topography). None of the results were abnormal or unexpected.

### 2.4.6.1 Modelling method-specific term estimates or coefficients are reported (where relevant)

The model specific term estimates are provided in Table 4.

Table 4. Model coefficients, significance and standard error estimates for GAM predicting *Gorgonians* probability of presence.

	x
(Intercept)	2.406
s(depth).1	-0.058
s(depth).2	0.101
s(depth).3	0.939
s(TPI).1	0.000
s(TPI).2	0.000
s(TPI).3	0.786

**2.4.6.2 Independent variable importance is reported** The relative importance of variables in the model was measured by sequentially removing the individual variables, fitting a new model and calculating the deviance explained. The deviance explained was then scaled to the full model to determine the relative drop in model goodness-of-fit with removal of each variable. The results showed that TPI was the least important variable determining the probability of *Gorgonians* presence, and depth was the most important (Figure 8).

## 2.5 Model uncertainty

### 2.5.1 Model specific goodness of fit statistics have been checked and reported

The *Gorgonians* model AUC was 0.737, a good model according to the standards of Hosmer et al., (2013).

Using a threshold of 0.82 resulted in prediction of 54 of the 68 observed presences correctly, while predicting about 67% of the absences correctly (sensitivity = 0.794 and specificity = 0.667)

Table 5. Confusion matrix of predicted and observed presence and absence of *Gorgonians* using a probability threshold 0.82.

	Observed	
Predicted	Presence	Absence
Presence	54	3
Absence	14	6

**2.5.1.1 Multiple measures of goodness of fit have been examined** Commonly used goodness-of-fit measures for binomial models are provided in Table 5 for the GLM predicting *Gorgonians* probability of presence. These include the True Skill Statistic (Allouche et al., 2006), the root-mean-squared-error and the Spearman’s rank correlation. Other threshold dependent metrics can be calculated from the confusion matrix (Table 4).

Model diagnostics indicated some minor issues with the prediction of presence or absence (Figure 9). The predicted occurrence did not always include the 1:1 line (indicating that at some levels of probability the observed occurrences were lower than expected). For example, the model predicted lower than expected probability of presence at ~0.3-0.4 and higher than expected probability of occurrence at ~0.6-0.8.

### 2.5.2 Spatial autocorrelation in the residuals has been assessed and reported

There was not significant spatial autocorrelation in the model residuals measured by Moran’s I ( $I = 0.377$ ). This was not unexpected given the random-stratified sample design of observations in the study area.

### 2.5.3 Residuals have been tested against assumed distribution (where appropriate)

Not applicable for the binomial distribution. Figure 6 shows model residuals (on the logit scale are shown for each data point used to model *Gorgonians* and diagnostics.

**2.5.3.1 Spatial patterns in residuals** Model residuals are shown in Figure 10. This confirms the results of the Moran’s I, with little evidence of spatial patterns in the residuals.

## 2.6 Model validation

### 2.6.1 Training and testing data splitting method

Both internal model validation method and independent data was used as a validation data set. K-fold cross-validation was used here. Five (k) folds were chosen at random.

**2.6.1.1 Potential spatial biases were accounted for in splitting the data** The spatial blocking method (Valvani et al., 2019) was *not* used to split the data for the internal cross-validation.

**2.6.1.2 A standard method used for cross-validation** k-fold cross-validation is a standard method. The data was divided into 5 equal portions and a model then fit to 80% of the data and tested against the remaining 20% of the data. This was repeated for each subdivision of the data. The same maps and diagnostics were produced for each model fit on the k-folds.

The data folds appeared to show the same patterns as the full model.

The model performance was similar for all the training data sets (the full model and the individual folds). However the performance of the model on the testing folds was less impressive. For example, the True Skill Statistic and AUC for model folds 3-5 was very poor, indicating some potential issues with model performance.

## 2.6.2 Truly independent data used for model validation

The presence and absence observations from 58 transects completed in 2024 was also used to test the models developed on the 2022 survey data.

The *Gorgonians* model AUC was 0.793, an good performing model according to the standards of Hosmer et al., (2013).

Using a threshold of 0.82, 0.82 resulted in prediction of 27 of the 29 observed presences correctly, while predicting about 59% of the absences correctly (sensitivity = 0.931 and specificity = 0.586)

Table 6. Confusion matrix of predicted and observed presence and absence of *Gorgonians* using a probability threshold 0.82, 0.82 for the independently collected data set in 2024.

	Observed	
Predicted	Presence	Absence
Presence	27	12
Absence	2	17

Table 6. Model goodness of fit measures for the full model and the individual model validation folds

Fold	AIC	threshold	AUC_training	AUC_testing	TSS_training	TSS_testing
Full model	55.088	0.82	0.737	NA	0.461	NA
Fold_1	50.503	0.80	0.602	1.00	0.282	0.857
Fold_2	48.161	0.75	0.679	0.60	0.406	0.000
Fold_3	20.988	0.93	0.966	0.63	0.898	0.111
Fold_4	51.455	0.70	0.716	NaN	0.387	NaN
Fold_5	49.991	0.83	0.632	1.00	0.259	0.714

Fold	Cor_training	Cor_testing	RMSE_training	RMSE_testing
Full model	0.264	NA	0.302	NA
Fold_1	0.118	0.433	0.331	0.235
Fold_2	0.210	-0.084	0.323	0.257
Fold_3	0.347	0.220	0.173	0.605
Fold_4	0.265	NA	0.328	0.176
Fold_5	0.153	0.433	0.330	0.242

## 2.7 Model outputs

### 2.7.1 Maps of model predictions, model residuals and prediction error

Maps of model predictions are provided in Figure 12. Maps of residuals in Figure 10. Maps of prediction error in Figure 13. The model predicted that the highest probability of presence for *Gorgonians* was in a band from 600 m and deeper.

### 2.7.2 Areas of model extrapolation are clearly defined

The model was not extrapolated outside the five seamounts, although within this region, there were some areas with little or no sampling. The model was extrapolated at depths from 850 - 1250 m where no sampling occurred.

### **2.7.3 The prediction unit is clearly defined (and explained if necessary)**

The prediction unit is the probability of presence or absence of *Gorgonians*.

### **2.7.4 Thresholding methods (for dichotomising probability into presence or absence) are clearly described and appropriate**

No thresholding was done (beyond the thresholding for calculating goodness-of-fit measures). Probability of presence is presented as the result.

#### **2.7.4.1 The sensitivity of model outcomes to threshold value chosen has been explored**

Sensitivity to threshold values was not explored, but in a formal analysis of the model could be completed using the provided model outputs.

## **2.8 Conclusions**

The *Gorgonians* model fit the observations from 2022 well. The internal model validation showed robust results. The independently collected data were predicted with good accuracy.

Model response curves showed the importance of depth. At depths below 600 m, there was a high probability of *Gorgonians* presence at all seamounts on a randomly chosen transect.

PRELIMINARY

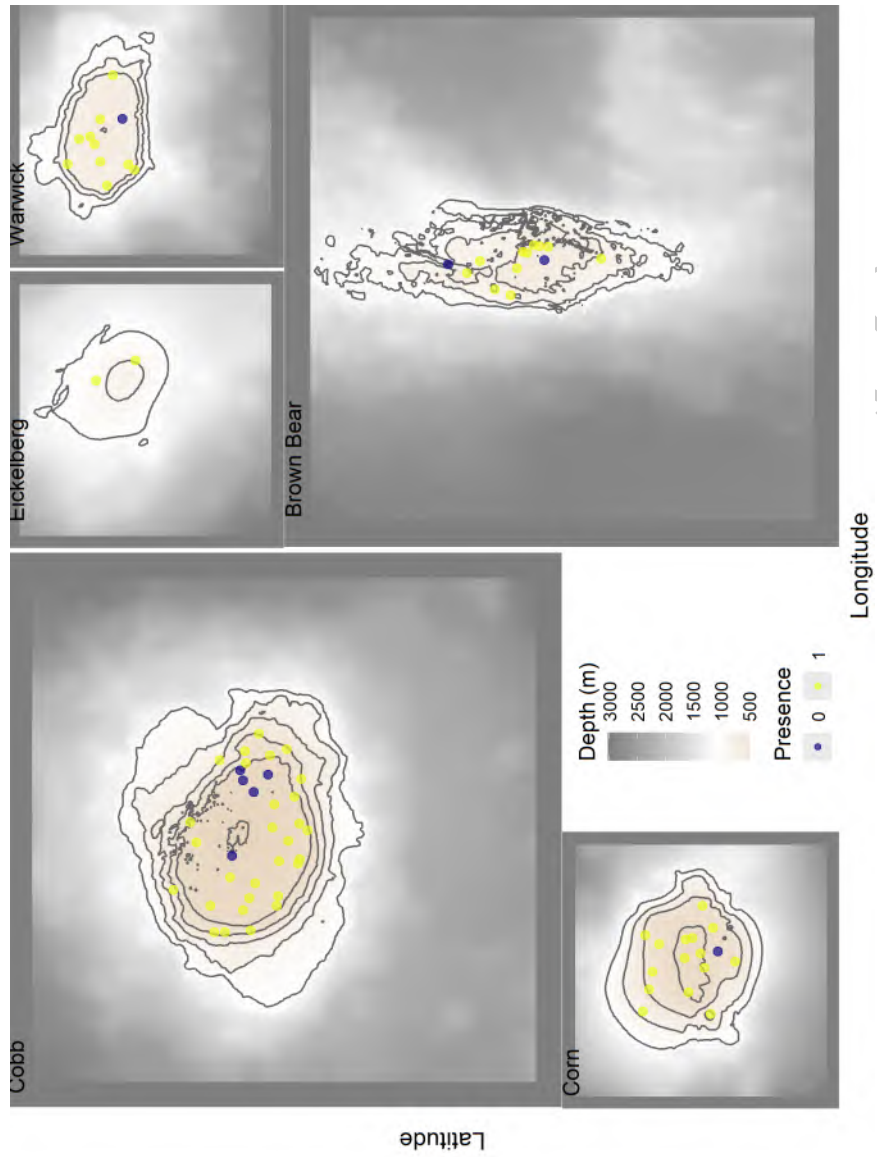


Figure 3: Locations of presence and absence transects for Gorgonians from 2022 and 2024 stereo-camera survey

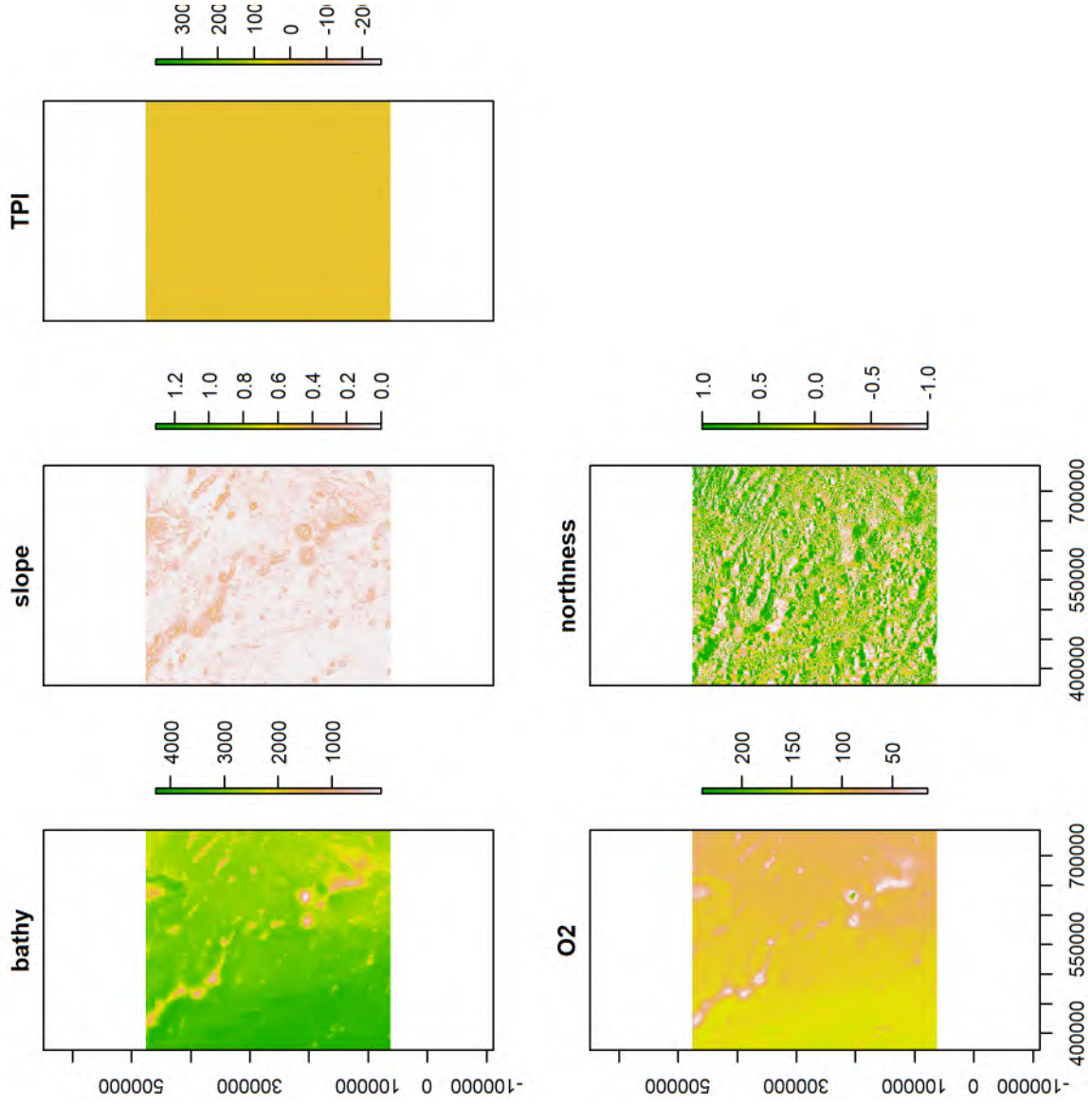


Figure 4: Map of bathymetry, slope, TPI, Oxygen and northness used as explanatory variables in this analysis of VME data

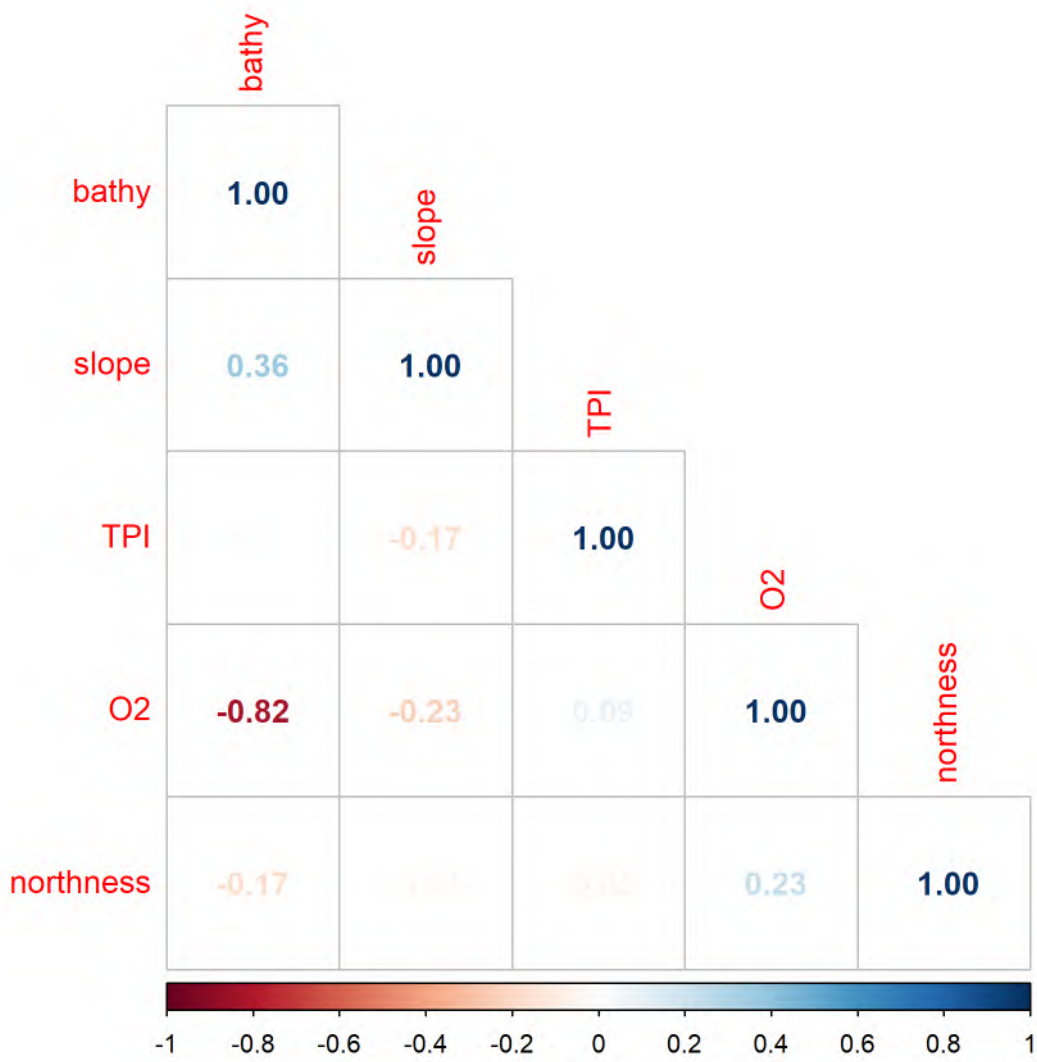


Figure 5: Correlation among independent variables used in modeling.

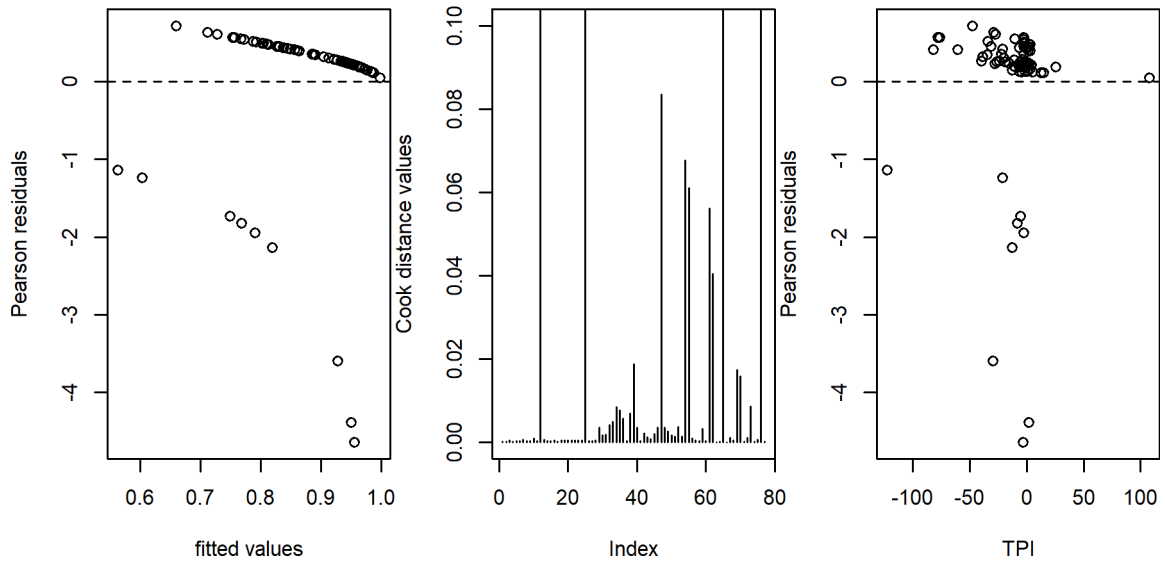


Figure 6: Diagnostic plots for GAM model assumptions.

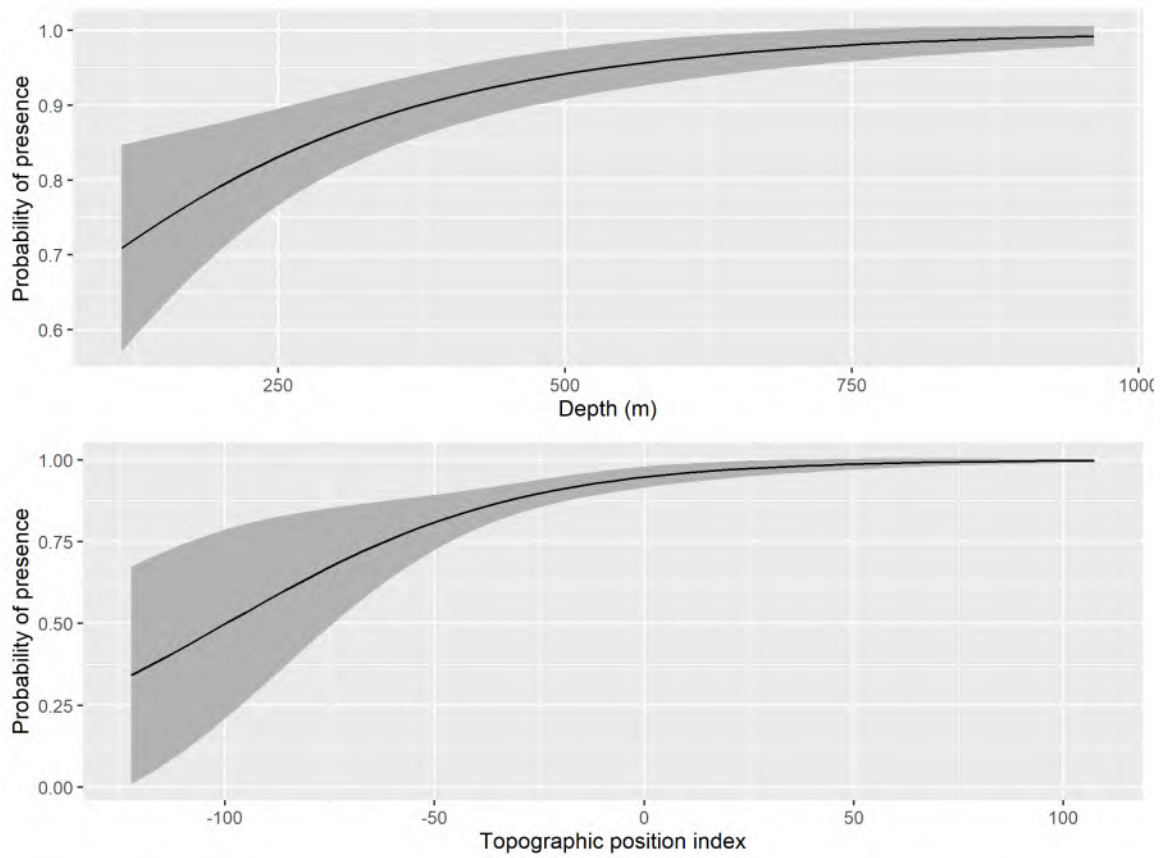


Figure 7: Response curves for independent variables used best-fitting GAM for presence or absence.

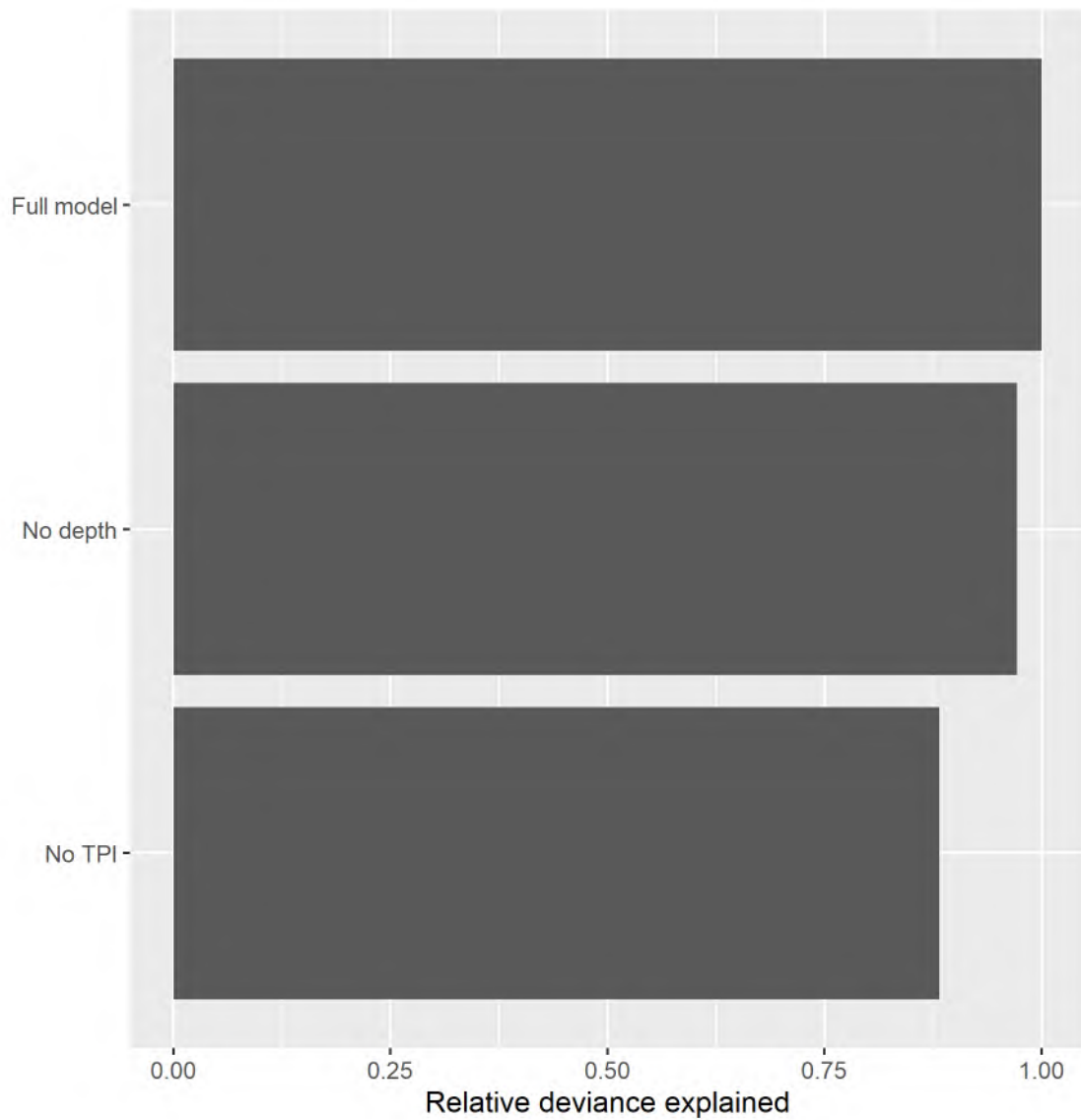


Figure 8: Relative importance of variables included in the Gorgonian presence or absence GAM measured by their contribution to deviance explained when sequentially removed from the model.

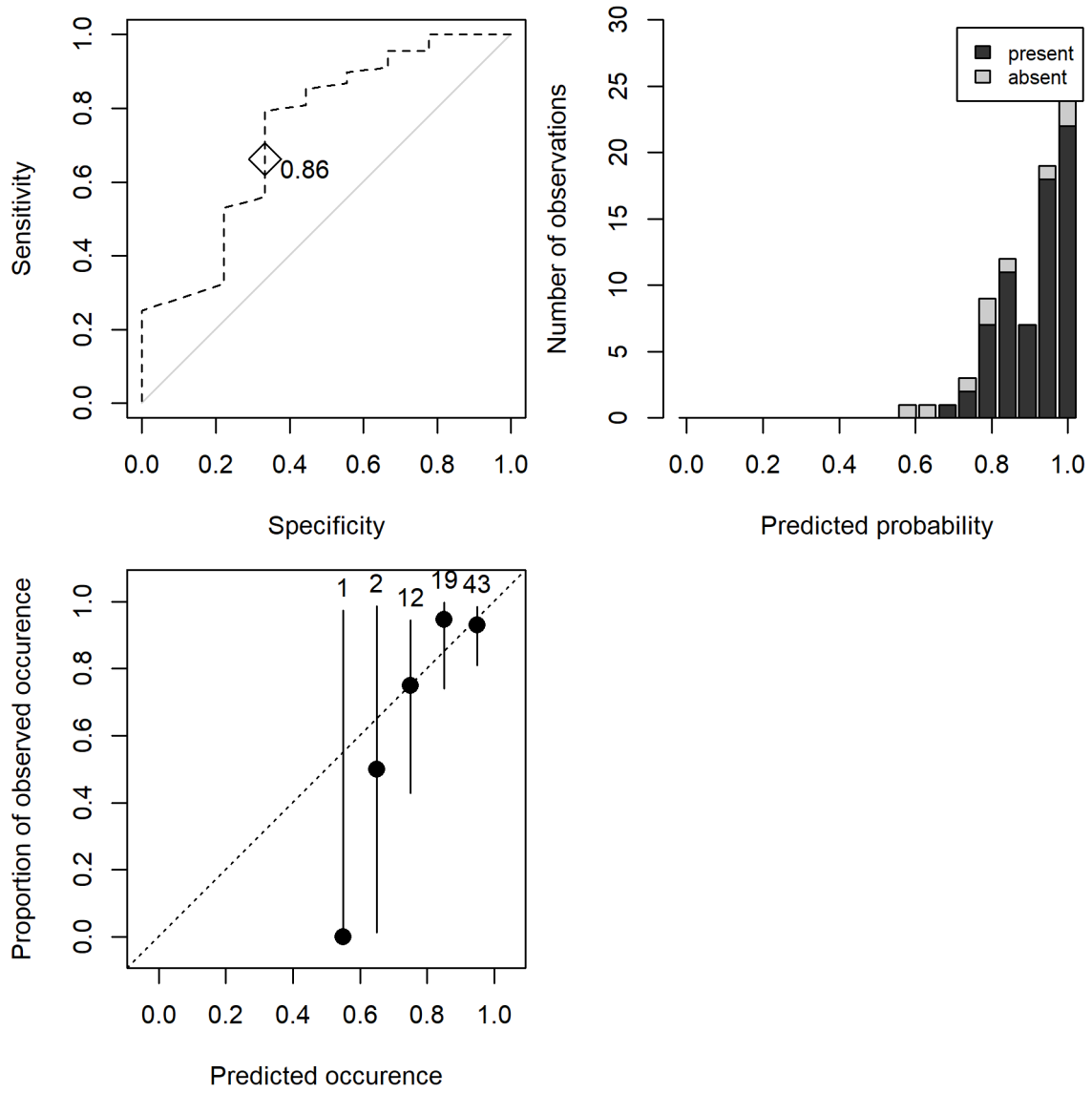


Figure 9: Model diagnostic plots for Gorgonian presence or absence GAM.

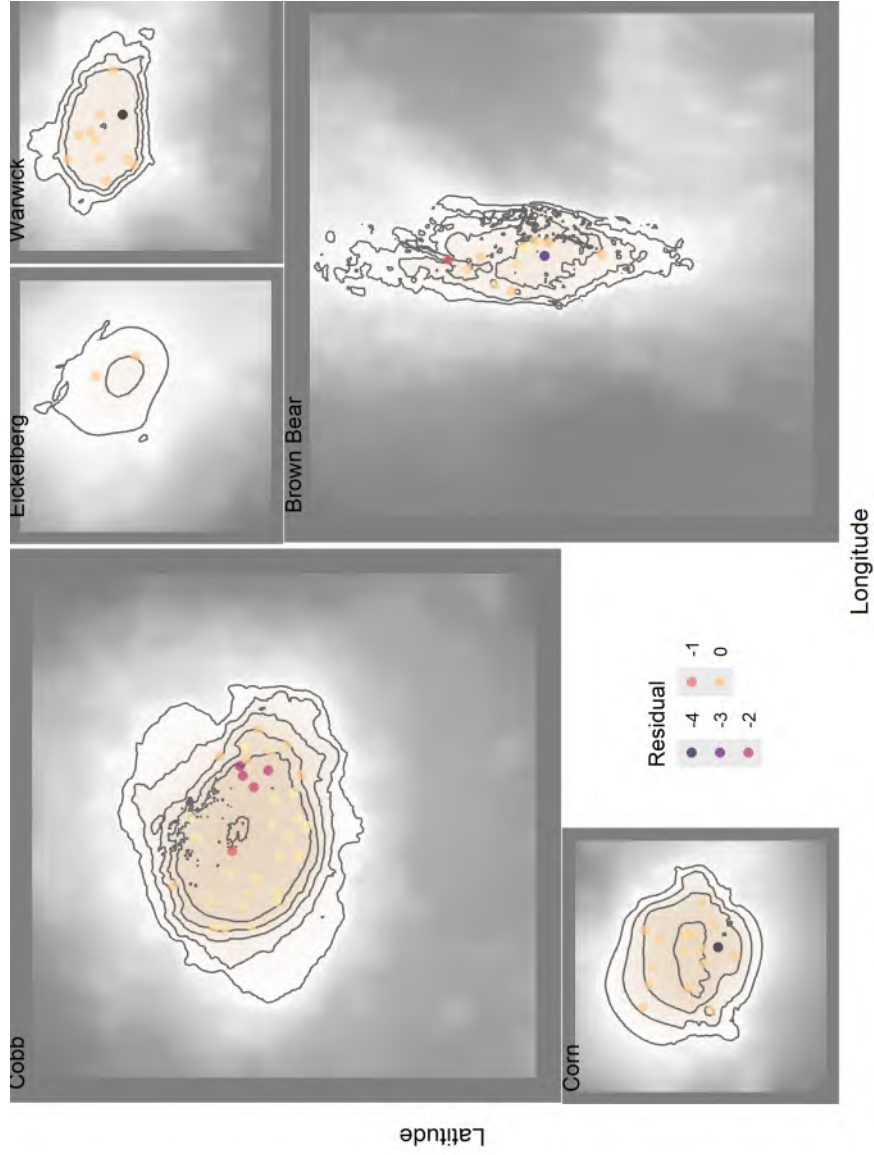


Figure 10: Spatial patterns in model Pearson residuals for G.A.M predicting probability of presence for Gorgonians.

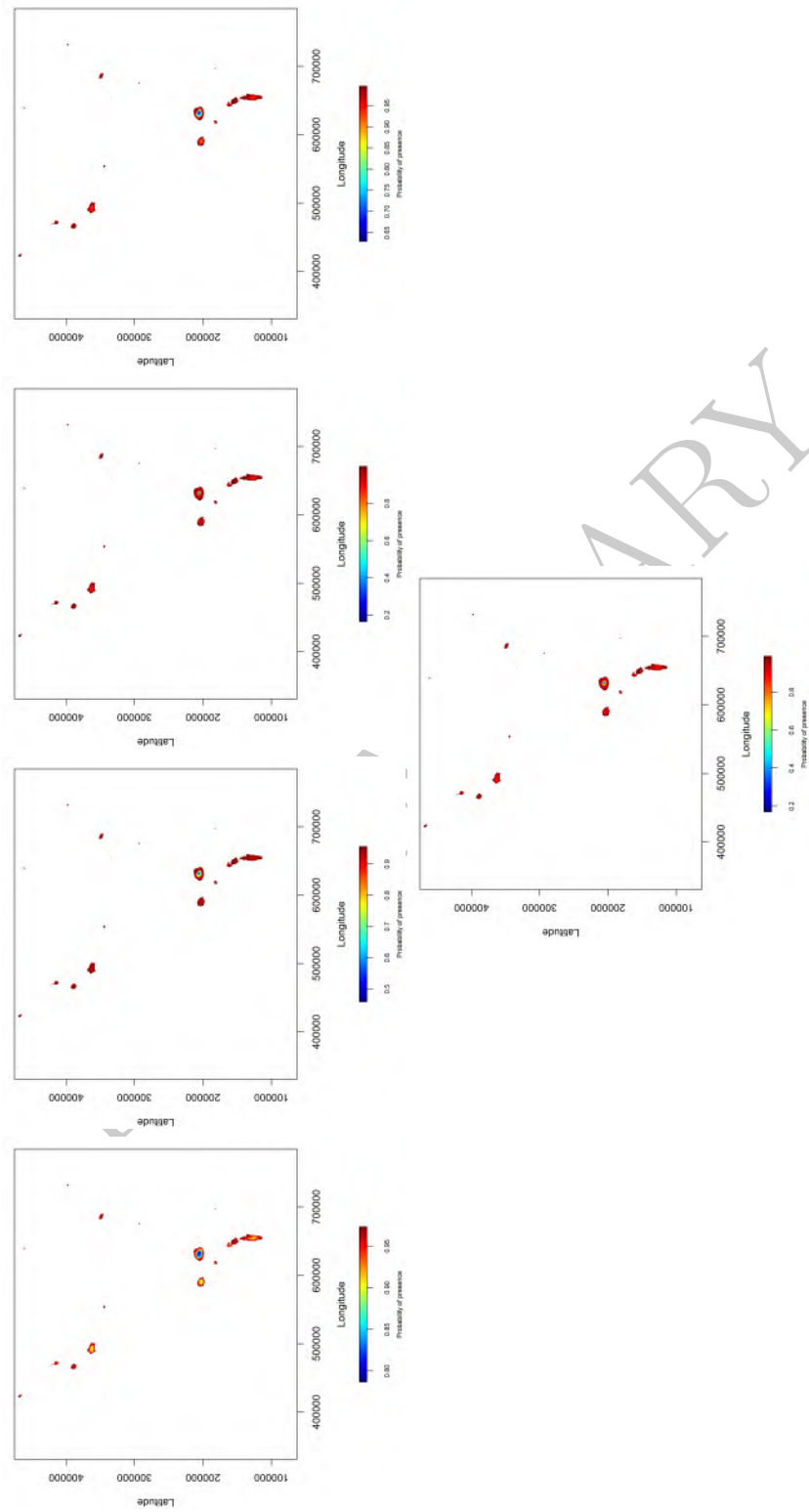


Figure 11: Maps of model predictions for 5 randomly selected folds of the data.

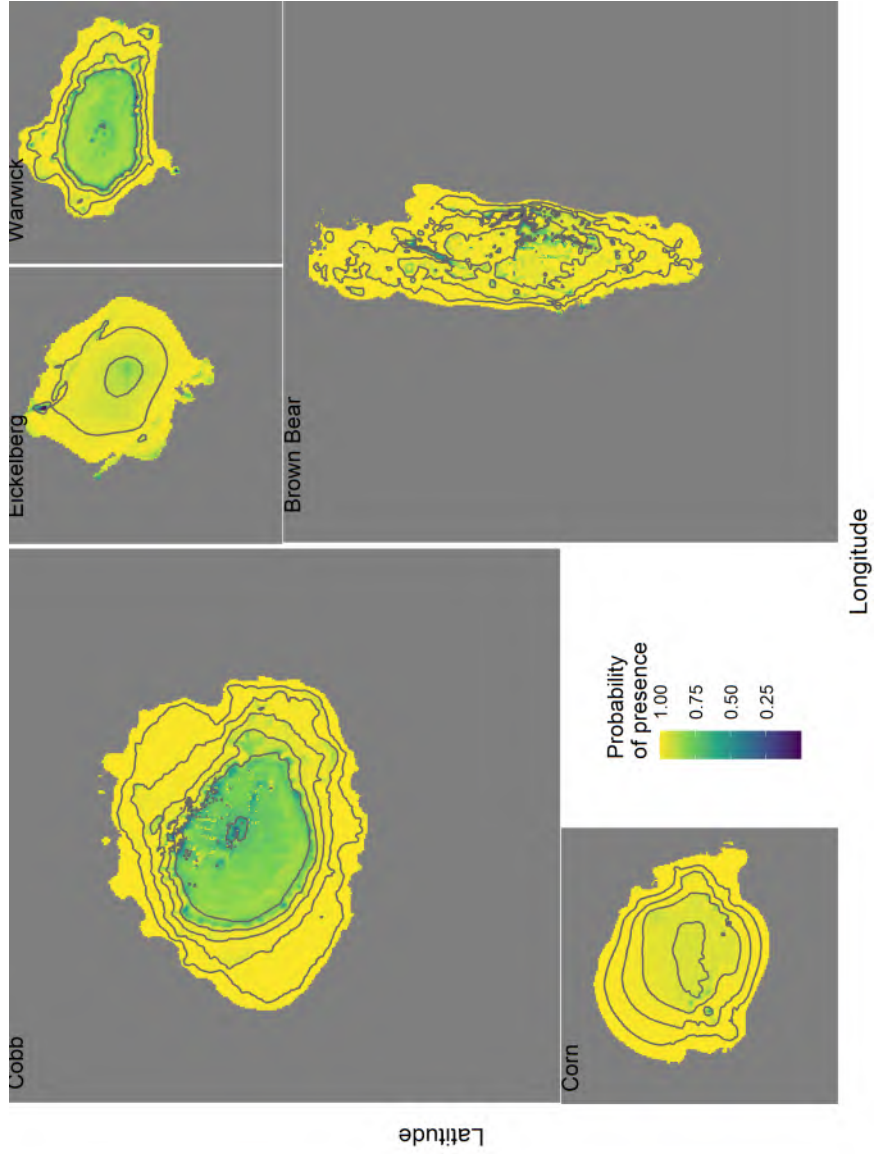


Figure 12: Predicted probability of presence for Gorgonians at seamounts in the Cobb-Eickelberg seamount chain.

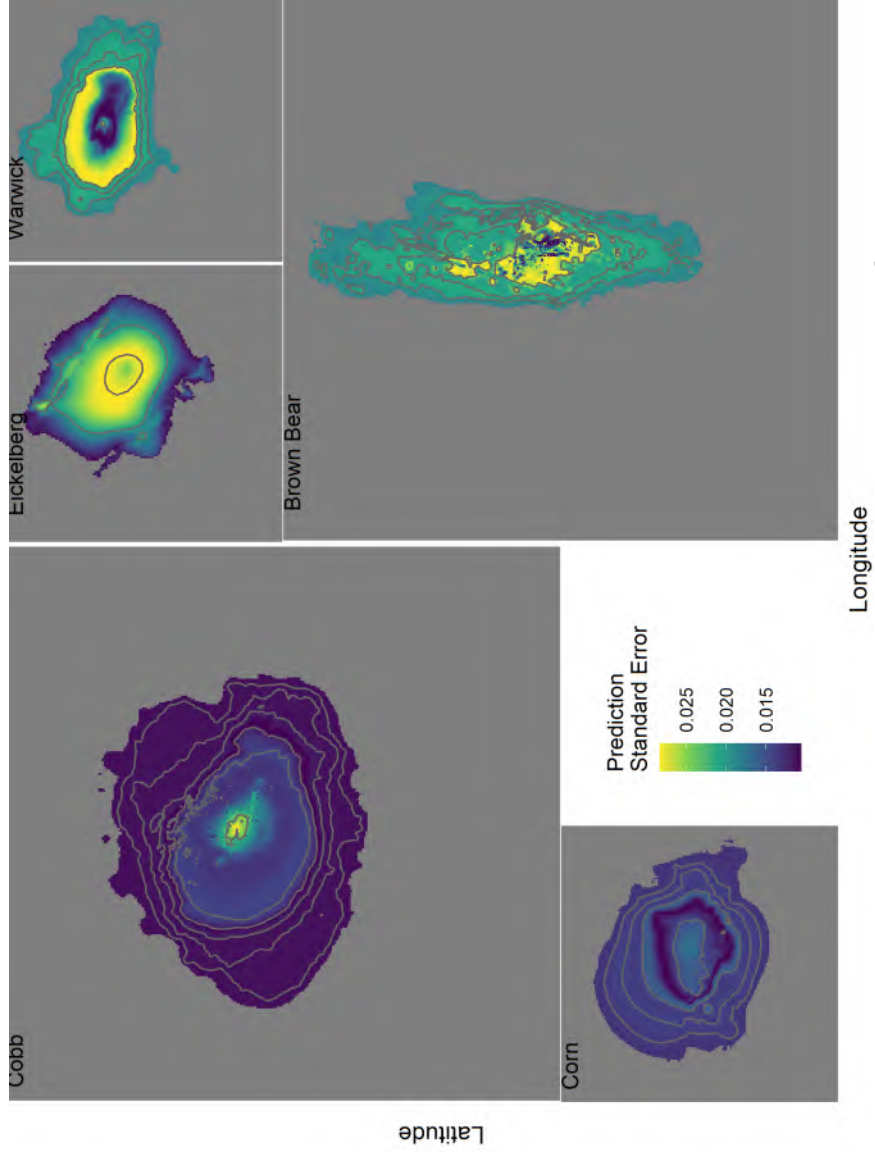


Figure 13: Spatial patterns in model prediction error for GAM predicting probability of Gorgonians at seamounts in the Cobb-Eickelberg seamount chain.

## 3 Vulnerable Marine Indicator Taxa Group: *Antipatharians*

### 3.1 Study resolution

#### 3.1.1 Location of the study area (or management region)

This modelling was carried out for five seamounts in the Northeastern Pacific Ocean where fisheries are managed by the North Pacific Fisheries Commission. The five seamounts are shown in Figure 1 and are part of the Cobb-Eickelberg seamount chain.

**3.1.1.1 Spatial extent of the modelled area** The specific seamounts modeled were five North Pacific Seamounts (Cobb, Brown Bear, Eickelberg, Warwick and Corn). Modeling was conducted from depths of 0 - 1250 m. Data was collected from 0 to ~850 m.

**3.1.1.2 Spatial resolution of the model and independent variables** The spatial resolution of the modeling was 100 m by 100 m grid cells. The all data was projected into an Albers equal area projection (proj4 description = "+proj=aea +lat\_0=45 +lon\_0=-126 +lat\_1=50 +lat\_2=58.5 +x\_0=1000000 +y\_0=0 +ellps=GRS80 +towgs84=0,0,0,0,0,0 +units=m +no\_defs").

**3.1.1.3 Spatial precision (of observations and independent variables)** The spatial precision of the observations was taken from the gps mounted on the research vessel. Based on tracking information, the camera system was towed slightly behind the vessel (~200 m typically), but along the same path as the vessel. The anticipated precision of the variation of the camera path was expected to be less than 20 m across the trackline.

**3.1.1.4 Depth resolution/range/extent (of the observations and independent variables)** The depth range of the observations of *Antipatharians* (from the depth sensor mounted on the camera) was from 61 to 808 m (mean = 442 m, SE = 206.28). The depth range of the modeled area was from 34 (the summit depth of Cobb Seamount) to 1250 m.

#### 3.1.2 Temporal extent of the data

**3.1.2.1 Dates of data extent** The dates observations used in model development were collected were September 6, 2022 to September 20, 2022. The dates for observations used for model testing were from September 3, 2024 to September 11, 2024.

**3.1.2.2 Precision of date/time** The precision of the date and the time of the data was assumed to be the closest second.

**3.1.2.3 Data/time resolution** The resolution of the date and time was fraction of a second.

**3.1.2.4 Impacts over time to consider in the data set (e.g. historical fishing effort)** Fishing occurred over the entire time frame from which these data points were collected. Fishing also has occurred historically since the 1970's. We did not attempt to account for historical fishing effort over this time. There may have been climate impacts occurring over the time frame of the data observations as well, however, these were not accounted for in the analyses.

### 3.2 Dependent data

The dependent data are shown in Figure 14.

Table 1. Number of records for each taxonomic grouping in the order *Antipatharians* from the survey database.

	Species or Taxa group	Count
1	Antipatharia	206
2	Aphanostichopathes spiessi	149
9	Schizopathidae	60
8	Parantipathes	50
4	Bathypathes sp	15
3	Bathypathes patula	10
7	Cladopathidae	2
5	Chrysopathes	1
6	Chrysopathes speciosa	1

### 3.2.1 Data type (presence, absence, abundance)

The data used for modeling *Antipatharians* distribution were observed presences ( $n = 17$ ) and absences ( $n = 60$ ) that occurred at the five seamounts.

### 3.2.2 Data source (e.g. type of survey(s) combined)

The data were entirely from random stratified surveys of the Cobb-Eickelberg seamount chain conducted in 2022.

### 3.2.3 Measure of sampling effort

Sampling effort was estimated by the distance the camera traveled along each transect multiplied by the field of view observed along the transect (Rooper et al. 2016). This provided an area observed for each transect which was used as the effort measure. Area observed ranged from 254 to 2469 m<sup>2</sup> with a median area observed of 1197 m<sup>2</sup>.

### 3.2.4 Detectability

Detectability of the width of the viewing area of the camera along the transect (area observed) was assumed to be 100% for VME indicator taxa. However, there were likely some individuals that were too small to be detected.

### 3.2.5 Taxonomic level

The taxonomic level modeled here was the taxonomic group *Antipatharians* (see Table 1 for individual families included in this grouping and refer to CMM for NPFC definitions).

### 3.2.6 Functional attributes (its ecology)

*Antipatharians* are a diverse, long-lived and fragile species. They occur in deep-water and are habitat forming structures important to many fishes, invertebrates other taxonomic groups.

### 3.2.7 Taxonomic confidence of species/assemblages

The taxonomic confidence of the assemblage was assumed to be good. Experts experienced in identification of corals and sponges from visual imagery in the North Pacific Ocean did all the identification and image analyses.

### 3.2.8 Rationale for taxonomic/assemblage level modeled

*Antipatharians* as defined here are a group that shares common habitat requirements and depth distribution. They are closely related and the order is globally distributed at deep depths. This Order has been previously modelled using Maximum entropy methods on a global extent and regional extent (Yesson et al., 2017, Chu et al. 2018, Doherty et al. 2019).

### 3.2.9 Source of absence data

Absences were observations of no individuals at transects. In total there were 60 absences in the dataset.

### 3.2.10 Other potential errors or biases in the data

There are some potential sources of error in the data, including errors in positioning of the records, errors in species identification (including both false positives and false negatives).

### 3.2.11 Data filtering steps

No data filtering was conducted.

### 3.2.12 Taxonomic aggregation steps

The records for the Order *Antipatharians* were aggregated by transect into presence or absence observations.

### 3.2.13 Method for combining dependent data sources (if done outside the modelling)

No other dependent data sources were used in this modelling.

## 3.3 Independent data

### 3.3.1 Independent data (environmental variables used)

Five independent variables were used in building a model of *Antipatharians* distribution; bathymetry, topographic position index, seafloor slope, Oxygen concentration and northness (Figure 15).

### 3.3.2 Independent data source (source of raw or derived data)

The bathymetry used here was downloaded from the NOAA website (<https://www.ncei.noaa.gov/maps/bathymetry/>). It consists of gridded bathymetry from a multibeam sources on a 3 arc-second grid for the region of interest. The details of the data sources can be found on the NOAA website. There were some gaps in the NOAA bathymetry layers. These were filled using single beam echosounder data collected during the 2022 and 2024 cruises and GEBCO bathymetry ([www.gebco.net/data\\_and\\_products/gridded\\_bathymetry\\_data](http://www.gebco.net/data_and_products/gridded_bathymetry_data)). The single beam echosounder data and GEBCO bathymetry was sampled into the missing grids in the NOAA bathymetry, with preference to the single beam echosounder data.

From the bathymetry two derived variables (slope and topographic position index) were calculated using the raster package (Hijmans 2019). Slope was calculated from the nearest 8 neighbors and TPI was calculated with a focal distance of ~300 m.

Northness was calculated as the cosine of the aspect (direction relative to 0 degrees that the slope was facing) for each grid cell based on bathymetry.

Oxygen data were based on the World Ocean Atlas data (2018 update). These data were clipped to the area of interest and resampled into the bathymetry grid using bilinear interpolation. The five explanatory variables are shown in Figure 15.

### 3.3.3 Native spatial and temporal resolution of the independent data

The native spatial resolution of the NOAA bathymetry was 3 arc-second grid. The native spatial resolution for the Oxygen data was 0.5 degrees longitude and latitude. It should be noted that the Oxygen data sources are conglomerations of data collected over varying spatial and temporal scales (e.g. the temporal scale is since ~1900's in the case of some measurements). For complete documentation of the spatial and temporal scale of the raw data the NODC respective website should be consulted ([www.gebco.net/data\\_and\\_products/gridded\\_bathymetry\\_data](http://www.gebco.net/data_and_products/gridded_bathymetry_data) and <https://www.nodc.noaa.gov/OC5/woa18/>).

All independent data layers were trimmed to include only observations and explanatory variables from this region and to depths of 1250 m.

### **3.3.4 Data processing and scaling (method for downscaling or aggregation)**

Both the bathymetry (for gap filling) and oxygen layers were downscaled to a 100 m by 100 m grid in order to match the scale of the bathymetry. This downscaling was completed using bilinear interpolation.

**3.3.4.1 Goodness of fit for downscaled aggregated data** The downscaled data at the dependent data sites for both Oxygen and bathymetry represented the lower resolution very well ( $r > 0.9$ ).

**3.3.4.2 Measurement errors and bias** Measurement errors in the data or bias in the data were not accounted for beyond the processing conducted on the raw measurements by GEBCO or NODC.

### **3.3.5 Derivation methods and calculations for derived variables**

From the bathymetry three derived variables (aspect, slope and topographic position index) were calculated using the raster package (Hijmans 2019). These variables were calculated on bathymetry aggregated (see below) to a 100 m by 100 m grid. The aspect variable was then converted to northness using a cosine function.

### **3.3.6 Rationale for inclusion of independent variables clearly stated and ecologically relevant**

These five variables (depth, slope, topographic position index, northness and oxygen) have been found in previous studies to influence the distribution of *Antipatharians* (Huff et al., 2013, Yesson et al., 2017, Etnoyer et al., 2018).

## **3.4 Modelling approach**

In this study generalized additive models (GAM) were developed to predict species distribution (Wood 2006).

### **3.4.1 Model steps**

**3.4.1.1 Code for model provided** The code and data used for this model are not currently publicly available, but can be available on request from Chris Rooper (chris.rooper@dfo-mpo.gc.ca).

**3.4.1.2 Packages used are referenced** The packages used to develop this model are referenced in the above .Rmd file. The key packages used were “sf”, “rnatualearth”, “ggplot2”, “rgdal”, “rgeos”, “gstat”, “raster”, “mgcv” and are all available for download from CRAN. The R version used here was R version 3.6.0 (2019-04-26) – “Planting of a Tree” (R Core Development Team 2019).

**3.4.1.3 Data is made available as supplementary material** The independent variables are available from Chris Rooper (chris.rooper@dfo-mpo.gc.ca).

### **3.4.2 Biases (spatial, temporal and other) acknowledged and described**

There were no inherent biases in the modeling method (although there may be biases in the dependent and independent data described above).

### **3.4.3 Methods and approaches to collinearity in independent variables**

**3.4.3.1 Collinearity in independent variables** The five explanatory variables were examined for collinearity using a pearson correlations (Figure 16). Variance inflation factors (Zuur et al. 2002) were also examined. In both cases the values were low, suggesting that the variables were fairly independent of each other.

Table 2. Variance inflation factors for independent variables using in modeling.

Variable	VIF
Depth	3.592
Slope	1.231
TPI	1.091
Oxygen	3.372
Northness	1.065

**3.4.3.2 Criteria for variable/dimension reduction provided** None of the variance inflation factors exceeded 5, indicating that dimension reduction was not warranted.

### 3.4.4 Choice of modelling method is explained and justified

The modelling method chosen was a generalized additive model (GAM). This model was primarily chosen for its simplicity of assumptions (stated below), its usefulness in fitting binomial (presence-absence) data, and the many previous applications of this method to predicting species distributions.

**3.4.4.1 Modelling assumptions are clearly stated** The basic GAM assumptions are; 1) Independence among data points, 2) The distribution of the residuals is binomially distributed, 3) homogenous variance across the fitted values, and 4) a non-linear relationship between response and predictor.

**3.4.4.2 Potential violations of model assumptions are explored** Diagnostic plots of Pearson residuals are shown in Figure 17. The residuals did not indicate any serious violations of GAM assumptions.

### 3.4.5 Model application

To build the model of *Antipatharians* a generalized additive model was constructed that contained five explanatory variables (depth, slope, topographic position index, northness and oxygen). The dependent data was presence or absence of *Antipatharians*. The full model was

$$y = \alpha + s(\text{depth}) + s(\text{slope}) + s(\text{TPI}) + s(\text{northness}) + s(O_2) + \sigma$$

A binomial error distribution ( $\sigma$ ) was used for the model fitting. A full model was fit initially containing all the variables with a basis degrees of freedom of 4 for each smooth. This model was reduced sequentially by removing the least significant term and comparing the AIC for the resulting reduced model following the methods of Rooper et al. (2016). This was repeated until there was a decline in model skill when removing a variable.

**3.4.5.1 Model settings** The default GAM settings in R were used (see `CobbSDM_Antipatharia.Rmd`). The only setting that was modified was the specification of the binomial error distribution and the specified number of knots for the smooth of  $k = 4$ .

**3.4.5.2 Model complexity is assessed** The results of the sequential variable reduction resulted in the retention of 2 terms; depth, TPI. The deviance explained by the model ( $D^2$ ) was 0.512.

The model complexity was assessed against simpler models with less terms during the sequential variable reduction step and the most complex model (containing these terms) was found to be the most appropriate (Table 3).

Table 3. Summary of GAM model predicting presence or absence of *Antipatharians*.

Term	edf	F	p-value
depth	2.893	11.984	0.0058
TPI	1.000	2.938	0.0865

Term	edf	F	p-value
residual	72.107		
GCV	-0.358		
Deviance explained (%)	51.200		

### 3.4.6 Model response curves are generated (where appropriate) and compared to expectations

Model response curves are shown in Figure 18. Probability of presence of *Antipatharians* was highest at about 350 m depth and above 600 m depth was also higher when TPI values were  $< 0$  (indicating “valleys” or low points in the topography). None of the results were abnormal or unexpected.

#### 3.4.6.1 Modelling method-specific term estimates or coefficients are reported (where relevant)

The model specific term estimates are provided in Table 4.

Table 4. Model coefficients, significance and standard error estimates for GAM predicting *Antipatharians* probability of presence.

	x
(Intercept)	-3.250
s(depth).1	-15.325
s(depth).2	9.587
s(depth).3	15.140
s(TPI).1	0.000
s(TPI).2	0.000
s(TPI).3	-0.783

**3.4.6.2 Independent variable importance is reported** The relative importance of variables in the model was measured by sequentially removing the individual variables, fitting a new model and calculating the deviance explained. The deviance explained was then scaled to the full model to determine the relative drop in model goodness-of-fit with removal of each variable. The results showed that TPI was the least important variable determining the probability of *Antipatharians* presence, and depth was the most important (Figure 19).

## 3.5 Model uncertainty

### 3.5.1 Model specific goodness of fit statistics have been checked and reported

The *Antipatharians* model AUC was 0.936, an excellent model according to the standards of Hosmer et al., (2013).

Using a threshold of 0.275 resulted in prediction of 15 of the 17 observed presences correctly, while predicting about 93% of the absences correctly (sensitivity = 0.882 and specificity = 0.933)

Table 5. Confusion matrix of predicted and observed presence and absence of *Antipatharians* using a probability threshold 0.275.

	Observed	
Predicted	Presence	Absence
Presence	15	4
Absence	2	56

**3.5.1.1 Multiple measures of goodness of fit have been examined** Commonly used goodness-of-fit measures for binomial models are provided in Table 5 for the GLM predicting *Antipatharians* probability of presence. These include the True Skill Statistic (Allouche et al., 2006), the root-mean-squared-error and the Spearman’s rank correlation. Other threshold dependent metrics can be calculated from the confusion matrix (Table 4).

Model diagnostics indicated no issues with the prediction of presence or absence (Figure 20). The predicted occurrence always included the 1:1 line.

### **3.5.2 Spatial autocorrelation in the residuals has been assessed and reported**

There was not significant spatial autocorrelation in the model residuals measured by Moran’s I ( $I = 0.702$ ). This was not unexpected given the random-stratified sample design of observations in the study area.

### **3.5.3 Residuals have been tested against assumed distribution (where appropriate)**

Not applicable for the binomial distribution. Figure 17 shows model residuals (on the logit scale are shown for each data point used to model *Antipatharians* and diagnostics.

**3.5.3.1 Spatial patterns in residuals** Model residuals are shown in Figure 21. This confirms the results of the Moran’s I, with little evidence of spatial patterns in the residuals.

## **3.6 Model validation**

### **3.6.1 Training and testing data splitting method**

Both internal model validation method and independent data was used as a validation data set. K-fold cross-validation was used here. Five (k) folds were chosen at random.

**3.6.1.1 Potential spatial biases were accounted for in splitting the data** The spatial blocking method (Valvani et al., 2019) was *not* used to split the data for the internal cross-validation.

**3.6.1.2 A standard method used for cross-validation** k-fold cross-validation is a standard method. The data was divided into 5 equal portions and a model then fit to 80% of the data and tested against the remaining 20% of the data. This was repeated for each subdivision of the data. The same maps and diagnostics were produced for each model fit on the k-folds.

The data folds appeared to show the same patterns as the full model.

The model performance was similar for all the training data sets (the full model and the individual folds). However the performance of the model on the testing folds decreased.

### **3.6.2 Truly independent data used for model validation**

The presence and absence observations from 58 transects completed in 2024 was also used to test the models developed on the 2022 survey data.

The *Antipatharians* model AUC was 0.826, a good performing model according to the standards of Hosmer et al., (2013).

Using a threshold of 0.275, 0.275 resulted in prediction of 5 of the 14 observed presences correctly, while predicting about 100% of the absences correctly (sensitivity = 0.357 and specificity = 1). The model did not predict presences in the test data set very well (predicting only ~30% correctly).

Table 6. Confusion matrix of predicted and observed presence and absence of *Antipatharians* using a probability threshold 0.275, 0.275 for the independently collected data set in 2024.

Observed		
Predicted	Presence	Absence
Presence	5	0
Absence	9	44

Table 6. Model goodness of fit measures for the full model and the individual model validation folds

Fold	AIC	threshold	AUC_training	AUC_testing	TSS_training	TSS_testing
Full model	49.464	0.275	0.936	NA	0.816	NA
Fold_1	45.228	0.245	0.915	1.000	0.667	0.818
Fold_2	35.234	0.260	0.949	0.883	0.849	0.567
Fold_3	41.724	0.140	0.959	0.932	0.857	0.659
Fold_4	33.910	0.360	0.971	0.933	0.853	0.800
Fold_5	44.830	0.310	0.935	0.808	0.782	0.423

Fold	Cor_training	Cor_testing	RMSE_training	RMSE_testing
Full model	0.627	NA	0.281	NA
Fold_1	0.586	0.768	0.310	0.234
Fold_2	0.598	0.644	0.262	0.415
Fold_3	0.648	0.663	0.294	0.394
Fold_4	0.718	0.364	0.251	0.399
Fold_5	0.645	0.363	0.304	0.261

### 3.7 Model outputs

#### 3.7.1 Maps of model predictions, model residuals and prediction error

Maps of model predictions are provided in Figure 23. Maps of residuals in Figure 21. Maps of prediction error in Figure 24. The model predicted that the highest probability of presence for *Antipatharians* was in a band from 350 m and deeper.

#### 3.7.2 Areas of model extrapolation are clearly defined

The model was not extrapolated outside the five seamounts, although within this region, there were some areas with little or no sampling. The model was extrapolated at depths from 850 - 1250 m where no sampling occurred.

#### 3.7.3 The prediction unit is clearly defined (and explained if necessary)

The prediction unit is the probability of presence or absence of *Antipatharians*.

#### 3.7.4 Thresholding methods (for dichotomising probability into presence or absence) are clearly described and appropriate

No thresholding was done (beyond the thresholding for calculating goodness-of-fit measures). Probability of presence is presented as the result.

##### 3.7.4.1 The sensitivity of model outcomes to threshold value chosen has been explored

Sensitivity to threshold values was not explored, but in a formal analysis of the model could be completed using the provided model outputs.

### 3.8 Conclusions

The *Antipatharians* model fit the observations from 2022 well. The internal model validation showed robust results. The independently collected data were predicted with good accuracy, although there were some issues with correctly identifying transects where *Antipatharians* were observed to be present.

Model response curves showed the importance of depth. At depths below about 350 m, there was a high probability of *Antipatharians* presence at all seamounts on a randomly chosen transect.

PRELIMINARY

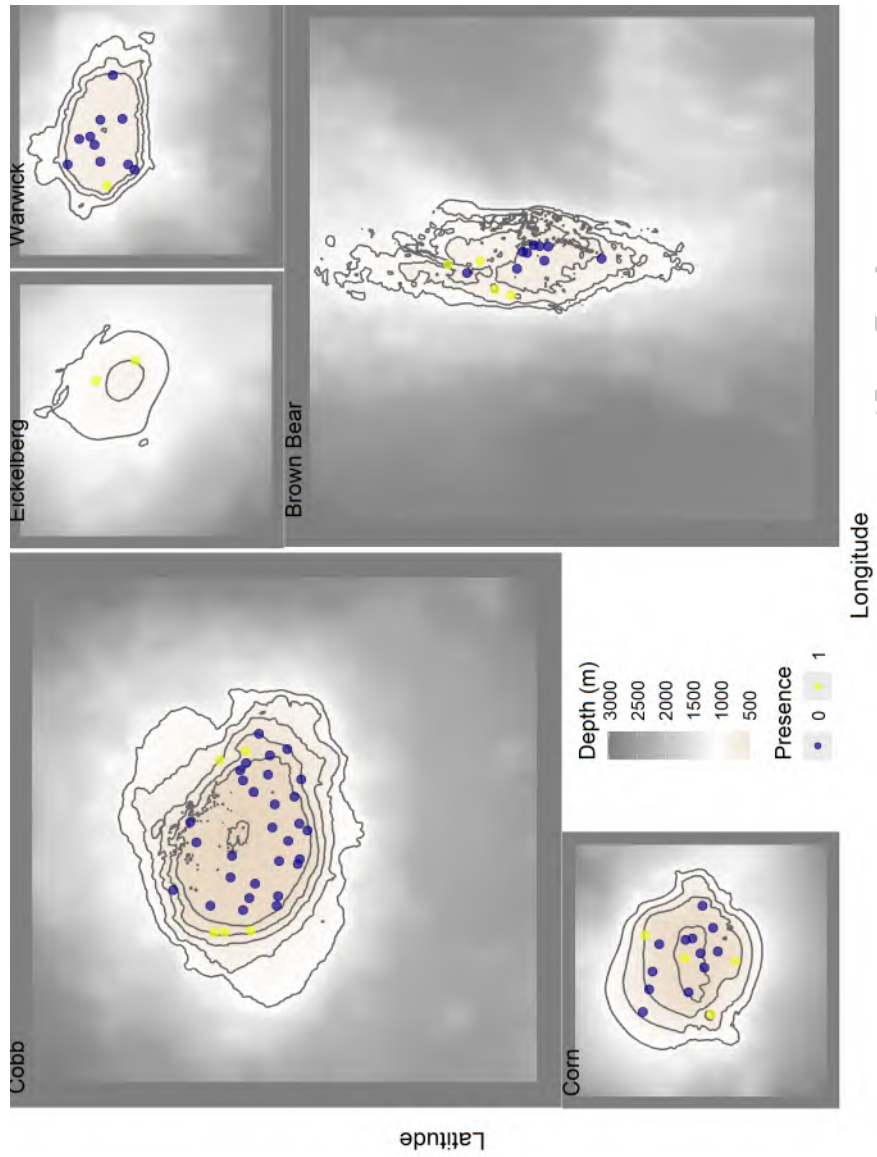


Figure 14: Locations of presence and absence transects for Antipatharians from 2022 and 2024 stereo-camera survey

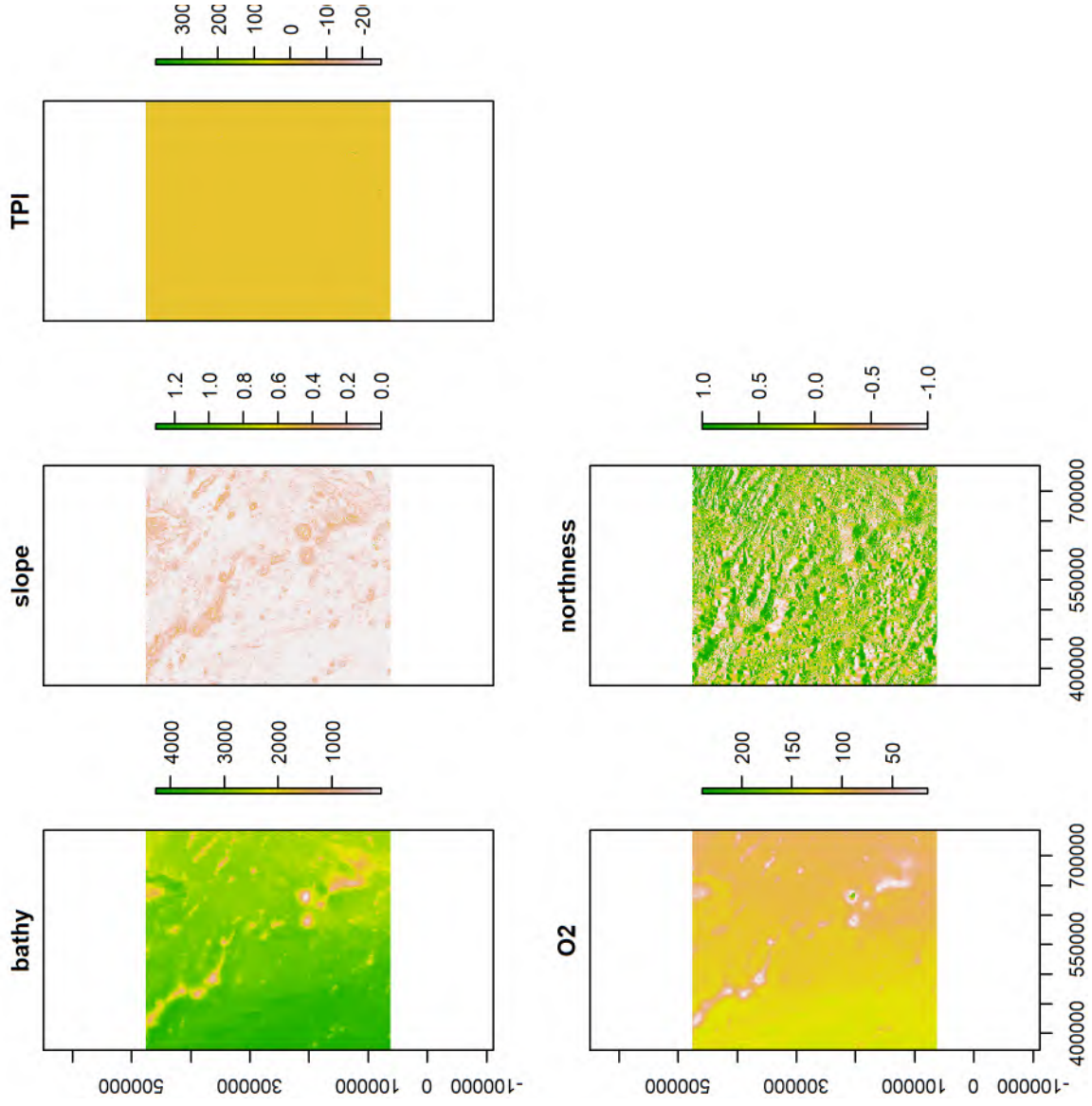


Figure 15: Map of bathymetry, slope, TPI, Oxygen and northness used as explanatory variables in this analysis of VME data

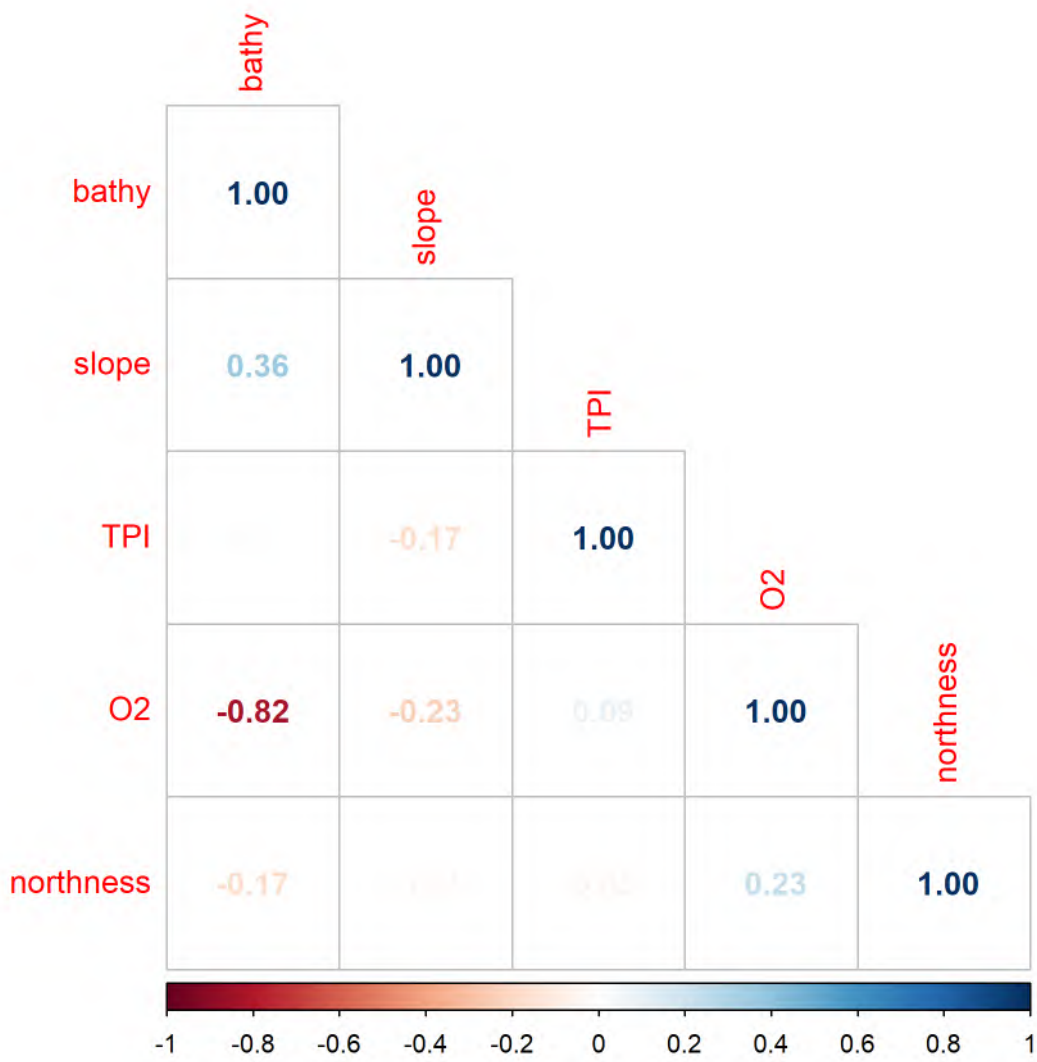


Figure 16: Correlation among independent variables used in modeling.

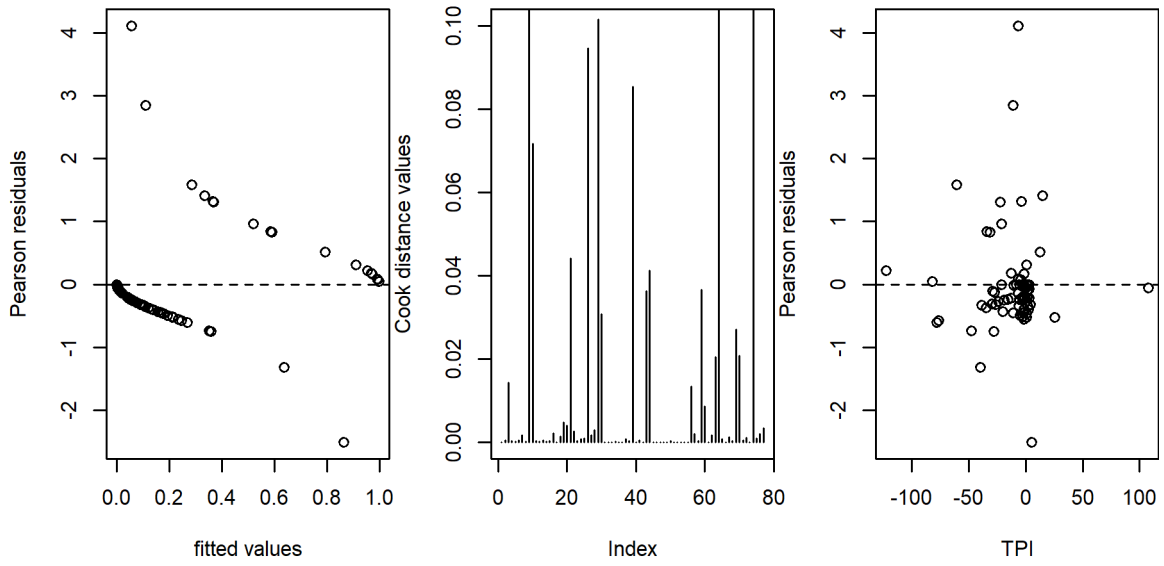


Figure 17: Diagnostic plots for GAM model assumptions.

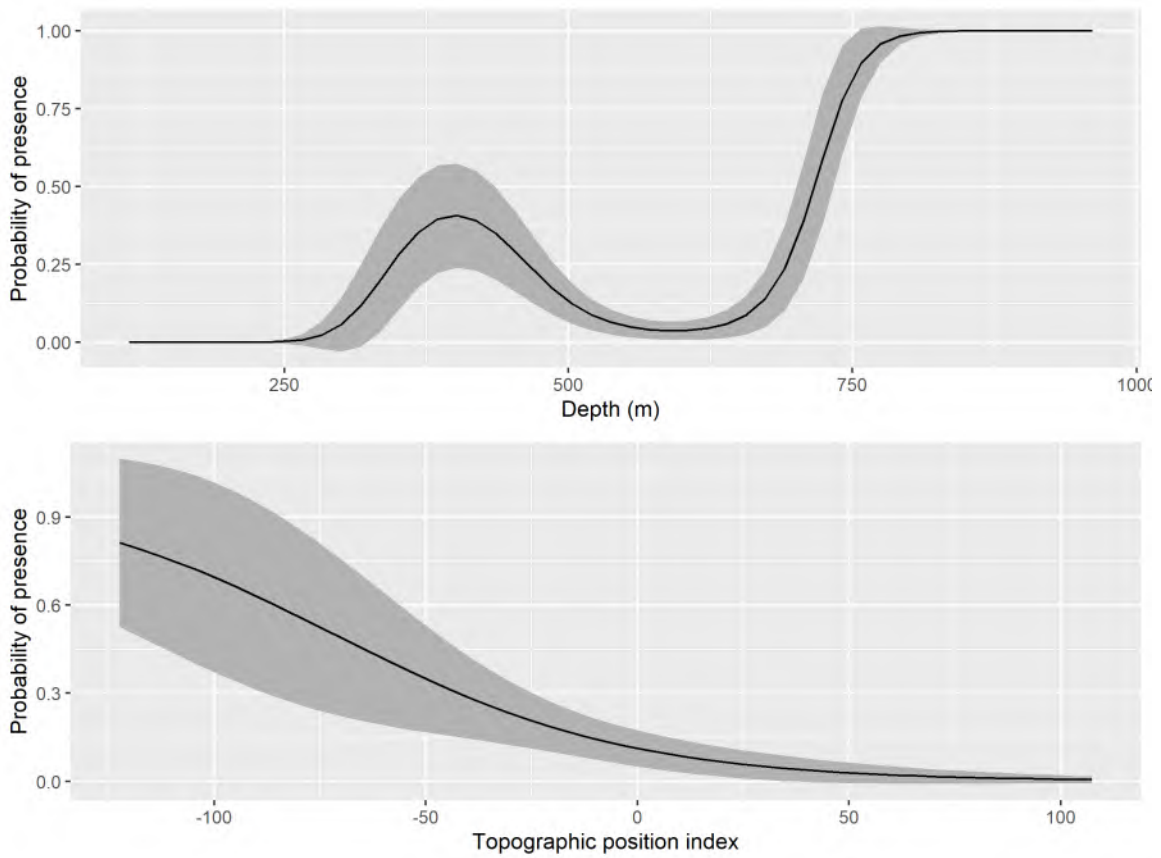


Figure 18: Response curves for independent variables used best-fitting GAM for presence or absence.

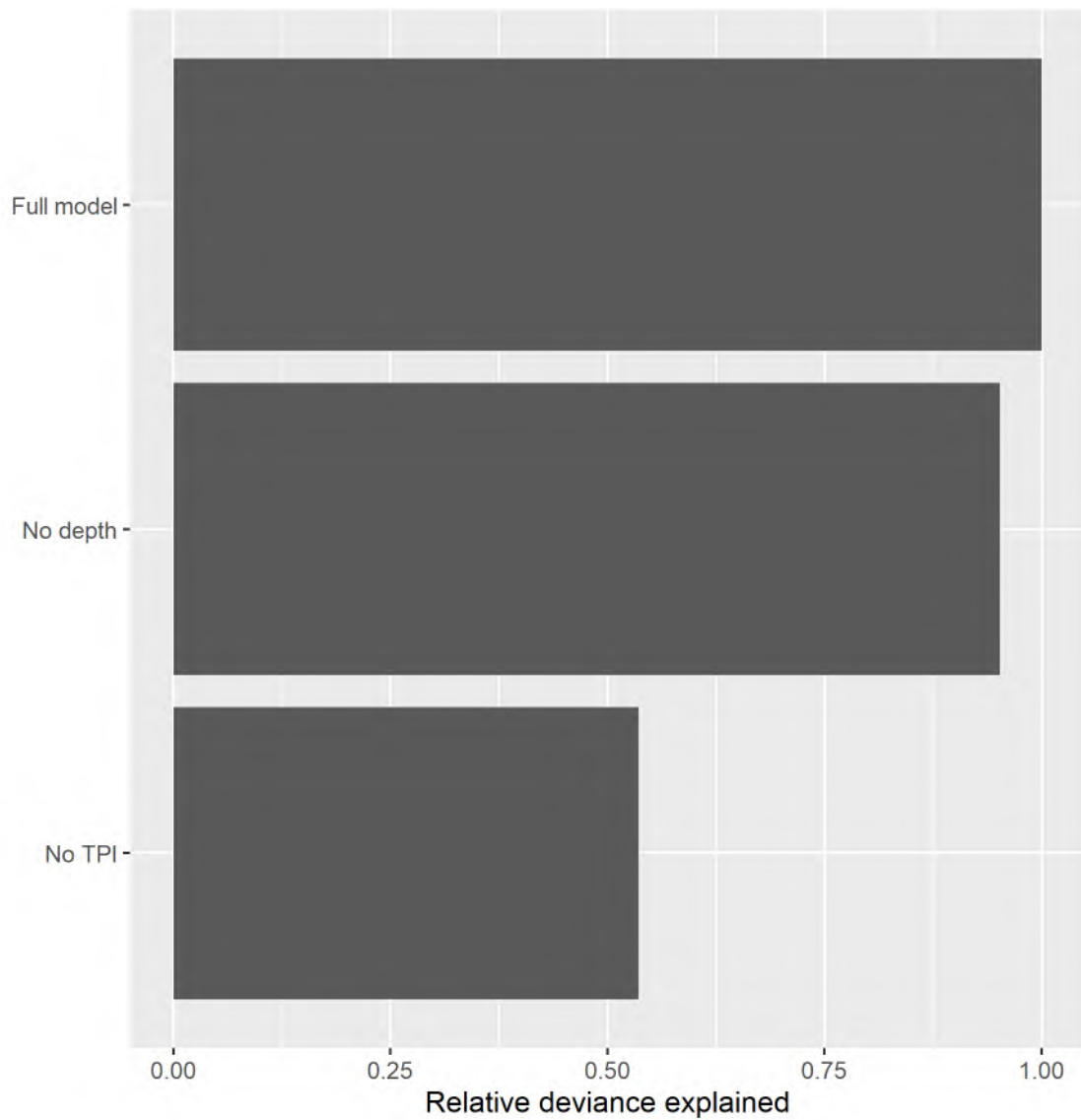


Figure 19: Relative importance of variables included in the Antipatharia presence or absence GAM measured by their contribution to deviance explained when sequentially removed from the model.

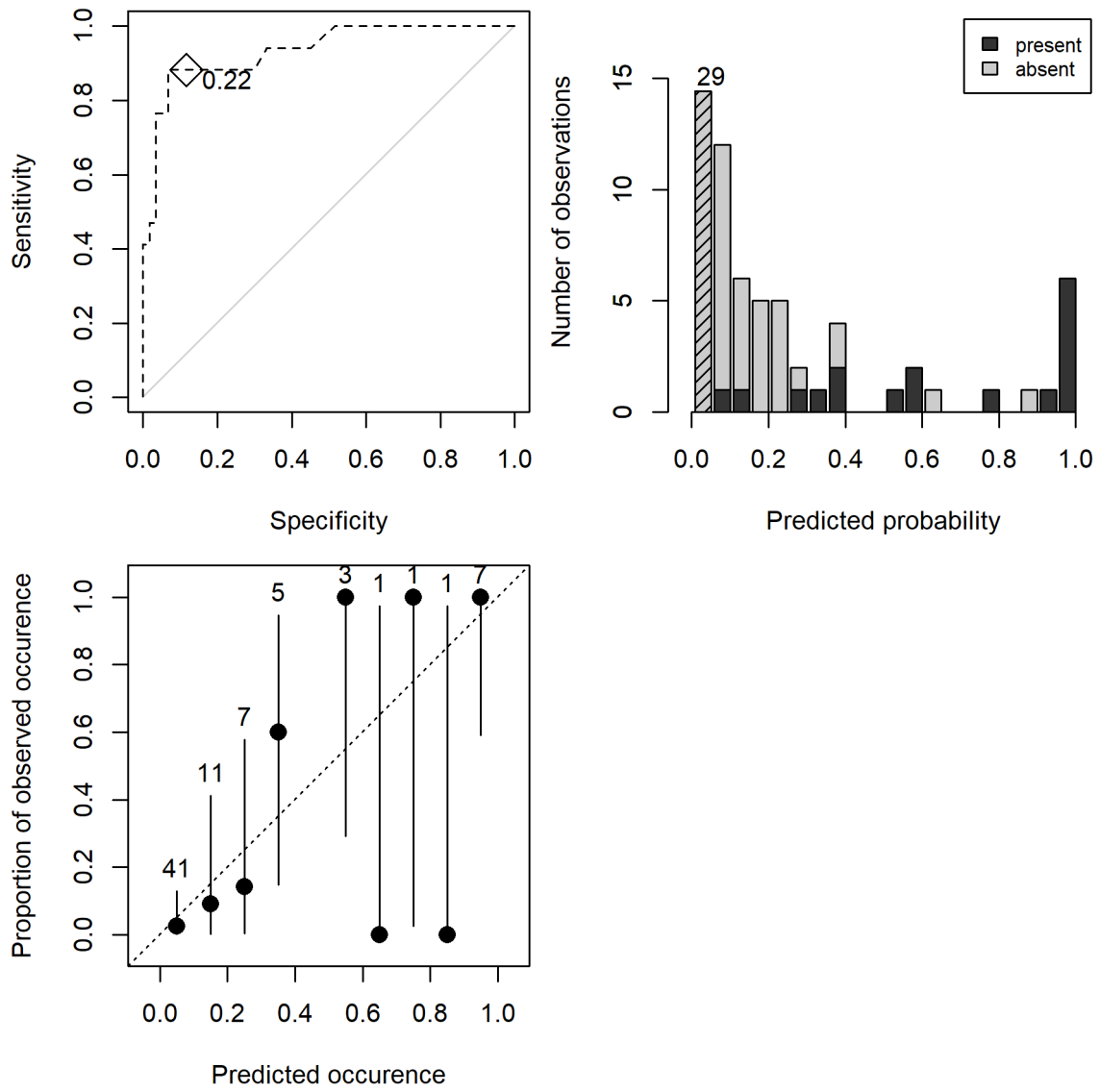


Figure 20: Model diagnostic plots for Antipatharia presence or absence GAM.

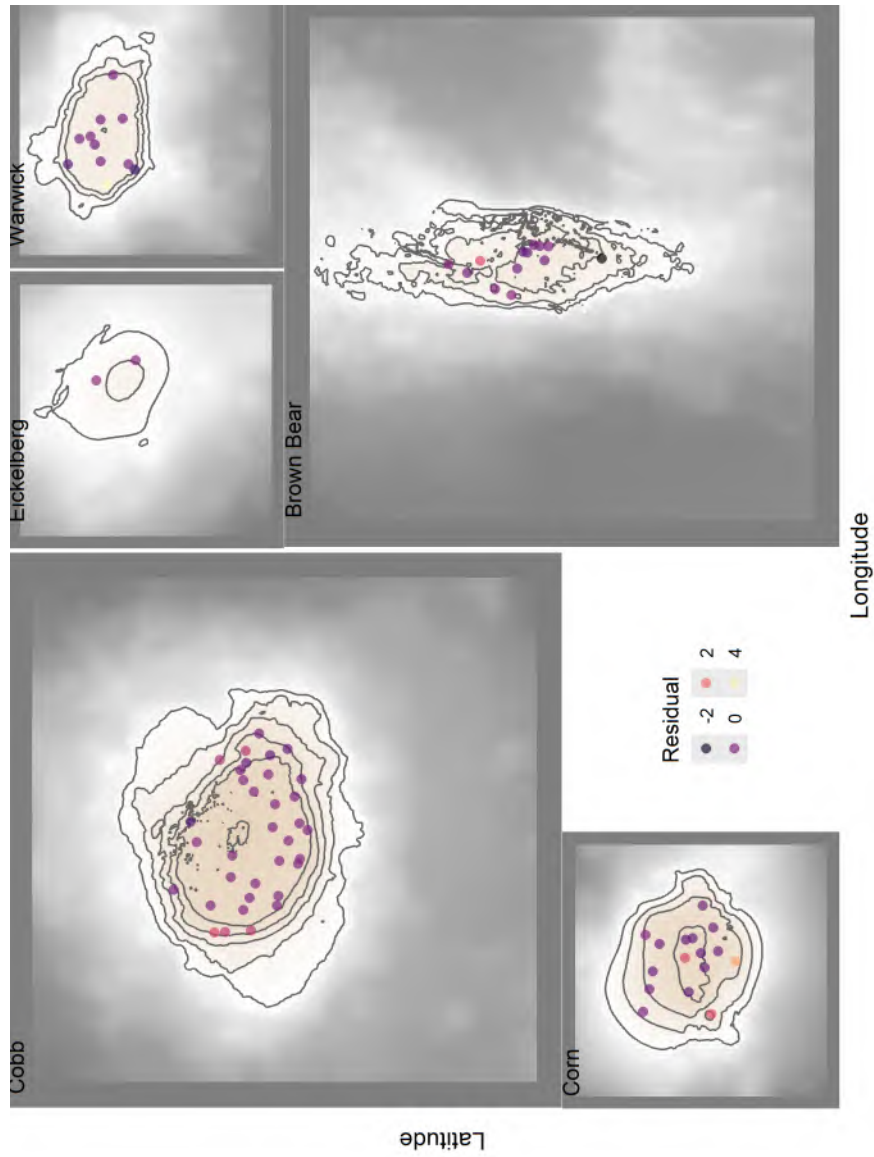


Figure 21: Spatial patterns in model Pearson residuals for GAM predicting probability of presence for Antipatharians.

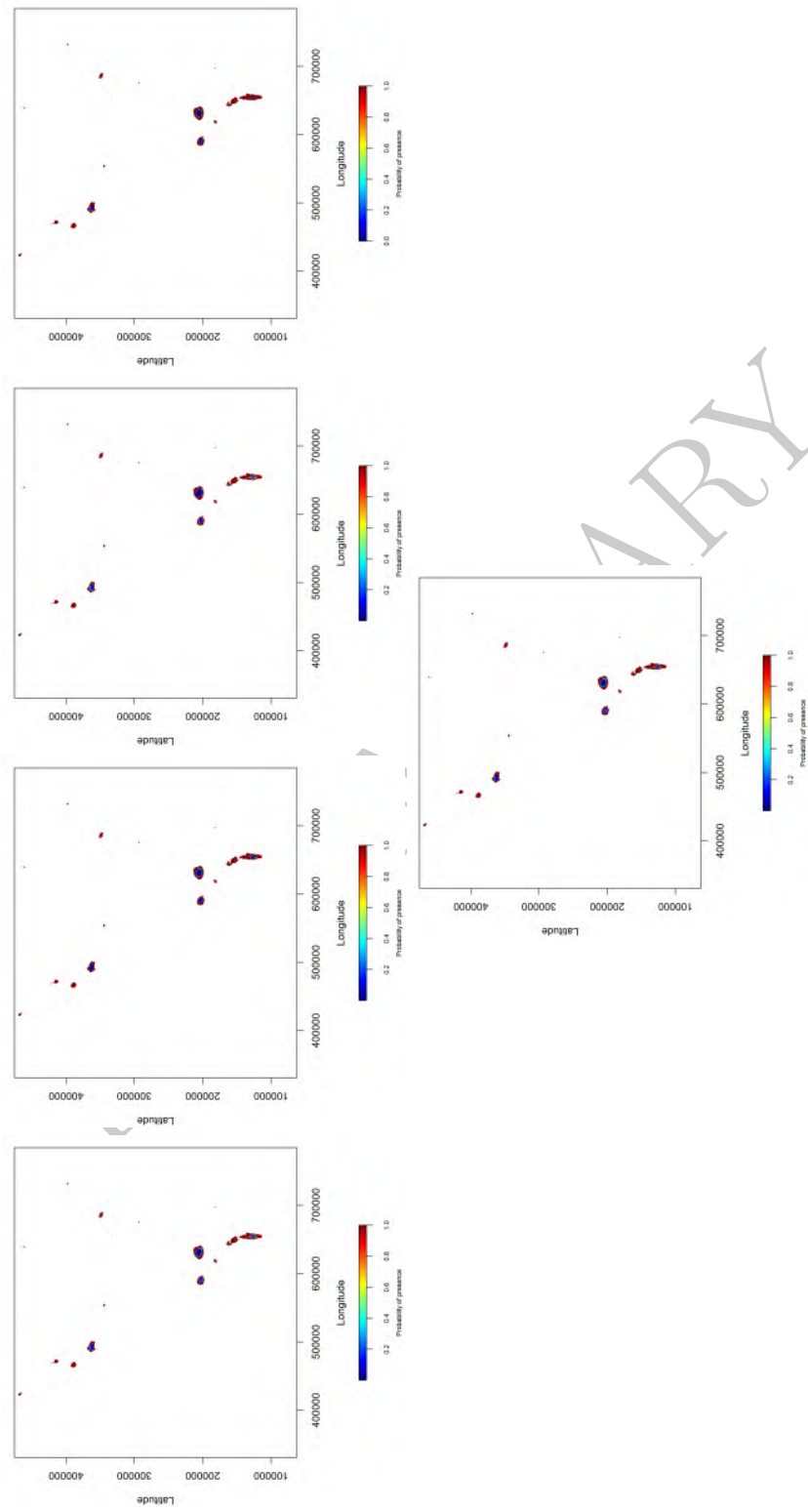


Figure 22: Maps of model predictions for 5 randomly selected folds of the data.

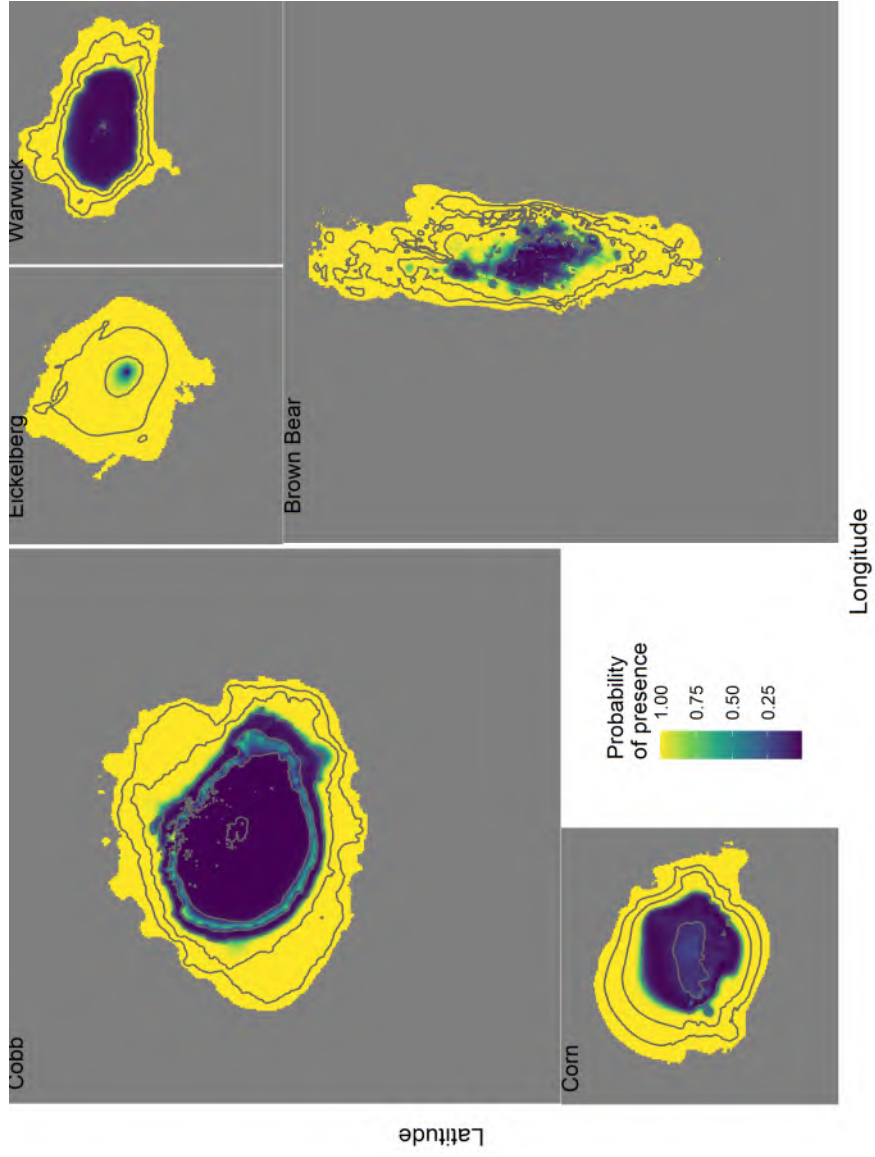


Figure 23: Predicted probability of presence for Antipatharians at seamounts in the Cobb-Eickelberg seamount chain.

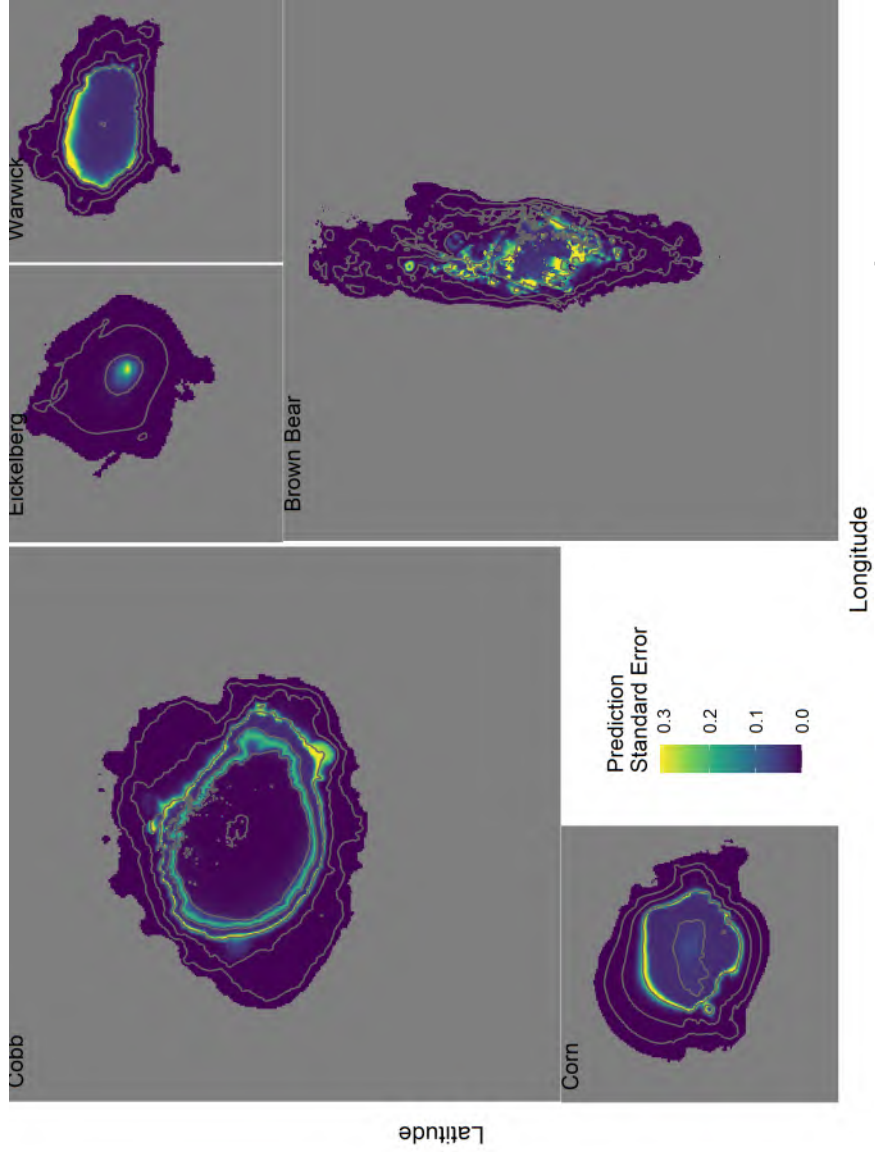


Figure 24: Spatial patterns in model prediction error for GAM predicting probability of Antipatharians at seamounts in the Cobb-Eickelberg seamount chain.

## 4 Vulnerable Marine Indicator Taxa Group: *ScleractinianReefs*

### 4.1 Study resolution

#### 4.1.1 Location of the study area (or management region)

This modelling was carried out for five seamounts in the Northeastern Pacific Ocean where fisheries are managed by the North Pacific Fisheries Commission. The five seamounts are shown in Figure 1 and are part of the Cobb-Eickelberg seamount chain.

**4.1.1.1 Spatial extent of the modelled area** The specific seamounts modeled were five North Pacific Seamounts (Cobb, Brown Bear, Eickelberg, Warwick and Corn). Modeling was conducted from depths of 0 - 1250 m. Data was collected from 0 to ~850 m.

**4.1.1.2 Spatial resolution of the model and independent variables** The spatial resolution of the modeling was 100 m by 100 m grid cells. The all data was projected into an Albers equal area projection (proj4 description = “+proj=aea +lat\_0=45 +lon\_0=-126 +lat\_1=50 +lat\_2=58.5 +x\_0=1000000 +y\_0=0 +ellps=GRS80 +towgs84=0,0,0,0,0,0 +units=m +no\_defs”).

**4.1.1.3 Spatial precision (of observations and independent variables)** The spatial precision of the observations was taken from the gps mounted on the research vessel. Based on tracking information, the camera system was towed slightly behind the vessel (~200 m typically), but along the same path as the vessel. The anticipated precision of the variation of the camera path was expected to be less than 20 m across the trackline.

**4.1.1.4 Depth resolution/range/extent (of the observations and independent variables)** The depth range of the observations of *ScleractinianReefs* (from the depth sensor mounted on the camera) was from 61 to 808 m (mean = 442 m, SE = 206.28). The depth range of the modeled area was from 34 (the summit depth of Cobb Seamount) to 1250 m.

#### 4.1.2 Temporal extent of the data

**4.1.2.1 Dates of data extent** The dates observations used in model development were collected were September 6, 2022 to September 20, 2022. The dates for observations used for model testing were from September 3, 2024 to September 11, 2024.

**4.1.2.2 Precision of date/time** The precision of the date and the time of the data was assumed to be the closest second.

**4.1.2.3 Data/time resolution** The resolution of the date and time was fraction of a second.

**4.1.2.4 Impacts over time to consider in the data set (e.g. historical fishing effort)** Fishing occurred over the entire time frame from which these data points were collected. Fishing also has occurred historically since the 1970's. We did not attempt to account for historical fishing effort over this time. There may have been climate impacts occurring over the time frame of the data observations as well, however, these were not accounted for in the analyses.

### 4.2 Dependent data

The dependent data are shown in Figure 25.

Table 1. Number of records for each taxonomic grouping in the order *ScleractinianReefs* from the survey database.

Species or Taxa group	Count
Desmophyllum pertusum	3

#### 4.2.1 Data type (presence, absence, abundance)

The data used for modeling *ScleractinianReefs* distribution were observed presences ( $n = 7$ ) and absences ( $n = 70$ ) that occurred at the five seamounts.

#### 4.2.2 Data source (e.g. type of survey(s) combined)

The data were entirely from random stratified surveys of the Cobb-Eickelberg seamount chain conducted in 2022.

#### 4.2.3 Measure of sampling effort

Sampling effort was estimated by the distance the camera traveled along each transect multiplied by the field of view observed along the transect (Rooper et al. 2016). This provided an area observed for each transect which was used as the effort measure. Area observed ranged from 254 to 2469 m<sup>2</sup> with a median area observed of 1197 m<sup>2</sup>.

#### 4.2.4 Detectability

Detectability of the width of the viewing area of the camera along the transect (area observed) was assumed to be 100% for VME indicator taxa. However, there were likely some individuals that were too small to be detected.

#### 4.2.5 Taxonomic level

The taxonomic level modeled here was the taxonomic group *ScleractinianReefs* (see Table 1 for individual families included in this grouping and refer to CMM for NPFC definitions).

#### 4.2.6 Functional attributes (its ecology)

*ScleractinianReefs* are a diverse, long-lived and fragile species. They occur in deep-water and are habitat forming structures important to many fishes, invertebrates other taxonomic groups.

#### 4.2.7 Taxonomic confidence of species/assemblages

The taxonomic confidence of the assemblage was assumed to be good. Experts experienced in identification of corals and sponges from visual imagery in the North Pacific Ocean did all the identification and image analyses.

#### 4.2.8 Rationale for taxonomic/assemblage level modeled

*ScleractinianReefs* as defined here are a group that shares common habitat requirements and depth distribution. They are closely related and the order is globally distributed at deep depths. This Order has been previously modelled using Maximum entropy methods on a global extent and regional extent (Yesson et al., 2017, Chu et al. 2018, Doherty et al. 2019).

#### 4.2.9 Source of absence data

Absences were observations of no individuals at transects. In total there were 70 absences in the dataset.

#### 4.2.10 Other potential errors or biases in the data

There are some potential sources of error in the data, including errors in positioning of the records, errors in species identification (including both false positives and false negatives).

#### 4.2.11 Data filtering steps

No data filtering was conducted.

#### 4.2.12 Taxonomic aggregation steps

The records for the Order *ScleractinianReefs* were aggregated by transect into presence or absence observations.

#### 4.2.13 Method for combining dependent data sources (if done outside the modelling)

No other dependent data sources were used in this modelling.

### 4.3 Independent data

#### 4.3.1 Independent data (environmental variables used)

Five independent variables were used in building a model of *ScleractinianReefs* distribution; bathymetry, topographic position index, seafloor slope, Oxygen concentration and northness (Figure 26).

#### 4.3.2 Independent data source (source of raw or derived data)

The bathymetry used here was downloaded from the NOAA website (<https://www.ncei.noaa.gov/maps/bathymetry/>). It consists of gridded bathymetry from a multibeam sources on a 3 arc-second grid for the region of interest. The details of the data sources can be found on the NOAA website. There were some gaps in the NOAA bathymetry layers. These were filled using single beam echosounder data collected during the 2022 and 2024 cruises and GEBCO bathymetry ([www.gebco.net/data\\_and\\_products/gridded\\_bathymetry\\_data](http://www.gebco.net/data_and_products/gridded_bathymetry_data)). The single beam echosounder data and GEBCO bathymetry was sampled into the missing grids in the NOAA bathymetry, with preference to the single beam echosounder data.

From the bathymetry two derived variables (slope and topographic position index) were calculated using the raster package (Hijmans 2019). Slope was calculated from the nearest 8 neighbors and TPI was calculated with a focal distance of ~300 m.

Northness was calculated as the cosine of the aspect (direction relative to 0 degrees that the slope was facing) for each grid cell based on bathymetry.

Oxygen data were based on the World Ocean Atlas data (2018 update). These data were clipped to the area of interest and resampled into the bathymetry grid using bilinear interpolation. The five explanatory variables are shown in Figure 26.

#### 4.3.3 Native spatial and temporal resolution of the independent data

The native spatial resolution of the NOAA bathymetry was 3 arc-second grid. The native spatial resolution for the Oxygen data was 0.5 degrees longitude and latitude. It should be noted that the Oxygen data sources are conglomerations of data collected over varying spatial and temporal scales (e.g. the temporal scale is since ~1900's in the case of some measurements). For complete documentation of the spatial and temporal scale of the raw data the NODC respective website should be consulted ([www.gebco.net/data\\_and\\_products/gridded\\_bathymetry\\_data](http://www.gebco.net/data_and_products/gridded_bathymetry_data) and <https://www.nodc.noaa.gov/OC5/woa18/>).

All independent data layers were trimmed to include only observations and explanatory variables from this region and to depths of 1250 m.

#### 4.3.4 Data processing and scaling (method for downscaling or aggregation)

Both the bathymetry (for gap filling) and oxygen layers were downscaled to a 100 m by 100 m grid in order to match the scale of the bathymetry. This downscaling was completed using bilinear interpolation.

**4.3.4.1 Goodness of fit for downscaled aggregated data** The downscaled data at the dependent data sites for both Oxygen and bathymetry represented the lower resolution very well ( $r > 0.9$ ).

**4.3.4.2 Measurement errors and bias** Measurement errors in the data or bias in the data were not accounted for beyond the processing conducted on the raw measurements by GEBCO or NODC.

#### 4.3.5 Derivation methods and calculations for derived variables

From the bathymetry three derived variables (aspect, slope and topographic position index) were calculated using the raster package (Hijmans 2019). These variables were calculated on bathymetry aggregated (see below) to a 100 m by 100 m grid. The aspect variable was then converted to northness using a cosine function.

#### 4.3.6 Rationale for inclusion of independent variables clearly stated and ecologically relevant

These five variables (depth, slope, topographic position index, northness and oxygen) have been found in previous studies to influence the distribution of *ScleractinianReefs* (Huff et al., 2013, Yesson et al., 2017, Etnoyer et al., 2018).

### 4.4 Modelling approach

In this study generalized additive models (GAM) were developed to predict species distribution (Wood 2006).

#### 4.4.1 Model steps

**4.4.1.1 Code for model provided** The code and data used for this model are not currently publicly available, but can be available on request from Chris Rooper (chris.rooper@dfo-mpo.gc.ca).

**4.4.1.2 Packages used are referenced** The packages used to develop this model are referenced in the above .Rmd file. The key packages used were “sf”, “rnatrualearth”, “ggplot2”, “rgdal”, “rgeos”, “gstat”, “raster”, “mgcv” and are all available for download from CRAN. The R version used here was R version 3.6.0 (2019-04-26) – “Planting of a Tree” (R Core Development Team 2019).

**4.4.1.3 Data is made available as supplementary material** The independent variables are available from Chris Rooper (chris.rooper@dfo-mpo.gc.ca).

#### 4.4.2 Biases (spatial, temporal and other) acknowledged and described

There were no inherent biases in the modeling method (although there may be biases in the dependent and independent data described above).

#### 4.4.3 Methods and approaches to collinearity in independent variables

**4.4.3.1 Collinearity in independent variables** The five explanatory variables were examined for collinearity using a pearson correlations (Figure 27). Variance inflation factors (Zuur et al. 2002) were also examined. In both cases the values were low, suggesting that the variables were fairly independent of each other.

Table 2. Variance inflation factors for independent variables using in modeling.

Variable	VIF
Depth	3.592
Slope	1.231
TPI	1.091
Oxygen	3.372
Northness	1.065

**4.4.3.2 Criteria for variable/dimension reduction provided** None of the variance inflation factors exceeded 5, indicating that dimension reduction was not warranted.

#### 4.4.4 Choice of modelling method is explained and justified

The modelling method chosen was a generalized additive model (GAM). This model was primarily chosen for its simplicity of assumptions (stated below), its usefulness in fitting binomial (presence-absence) data, and the many previous applications of this method to predicting species distributions.

**4.4.4.1 Modelling assumptions are clearly stated** The basic GAM assumptions are; 1) Independence among data points, 2) The distribution of the residuals is binomially distributed, 3) homogenous variance across the fitted values, and 4) a non-linear relationship between response and predictor.

**4.4.4.2 Potential violations of model assumptions are explored** Diagnostic plots of Pearson residuals are shown in Figure 28. The residuals did not indicate any serious violations of GAM assumptions.

#### 4.4.5 Model application

To build the model of *ScleractinianReefs* a generalized additive model was constructed that contained five explanatory variables (depth, slope, topographic position index, northness and oxygen). The dependent data was presence or absence of *ScleractinianReefs*. The full model was

$$y = \alpha + s(\text{depth}) + s(\text{slope}) + s(\text{TPI}) + s(\text{northness}) + s(\text{O}_2) + \sigma$$

A binomial error distribution ( $\sigma$ ) was used for the model fitting. A full model was fit initially containing all the variables with a basis degrees of freedom of 4 for each smooth. This model was reduced sequentially by removing the least significant term and comparing the AIC for the resulting reduced model following the methods of Rooper et al. (2016). This was repeated until there was a decline in model skill when removing a variable.

**4.4.5.1 Model settings** The default GAM settings in R were used (see `CobbSDM_ScleractinianReef.Rmd`). The only setting that was modified was the specification of the binomial error distribution and the specified number of knots for the smooth of  $k = 4$ .

**4.4.5.2 Model complexity is assessed** The results of the sequential variable reduction resulted in the retention of 5 terms; depth, TPI, slope, O<sub>2</sub>, northness. The deviance explained by the model ( $D^2$ ) was 0.523.

The model complexity was assessed against simpler models with less terms during the sequential variable reduction step and the most complex model (containing these terms) was found to be the most appropriate (Table 3).

Table 3. Summary of GAM model predicting presence or absence of *ScleractinianReefs*.

Term	edf	F	p-value
depth	1.845	2.625	0.3208
TPI	2.020	3.864	0.267

Term	edf	F	p-value
slope	2.915	7.453	0.0609
O2	2.313	1.783	0.5163
northness	1.000	0.792	0.3734
residual	65.906		
GCV	-0.421		
Deviance explained (%)	52.300		

#### 4.4.6 Model response curves are generated (where appropriate) and compared to expectations

Model response curves are shown in Figure 29. Probability of presence of *ScleractinianReefs* was flat through most of the depth range. The probability of presence was highest at moderate oxygen concentrations and on lower and north facing slopes. The probability of presence was also highest when TPI values were  $< 0$  (indicating “valleys” or low points in the topography). None of the results were abnormal or unexpected.

##### 4.4.6.1 Modelling method-specific term estimates or coefficients are reported (where relevant)

The model specific term estimates are provided in Table 4.

Table 4. Model coefficients, significance and standard error estimates for GAM predicting *ScleractinianReefs* probability of presence.

	x
(Intercept)	-5.998
s(depth).1	1.452
s(depth).2	-4.982
s(depth).3	2.313
s(TPI).1	-4.387
s(TPI).2	15.374
s(TPI).3	2.704
s(slope).1	-14.520
s(slope).2	30.294
s(slope).3	-20.494
s(O2).1	-3.245
s(O2).2	12.469
s(O2).3	-2.124
s(northness).1	0.000
s(northness).2	0.000
s(northness).3	0.642

**4.4.6.2 Independent variable importance is reported** The relative importance of variables in the model was measured by sequentially removing the individual variables, fitting a new model and calculating the deviance explained. The deviance explained was then scaled to the full model to determine the relative drop in model goodness-of-fit with removal of each variable. The results showed that depth was the least important variable determining the probability of *ScleractinianReefs* presence, and Oxygen and TPI were the most important (Figure 30).

## 4.5 Model uncertainty

### 4.5.1 Model specific goodness of fit statistics have been checked and reported

The *ScleractinianReefs* model AUC was 0.953, an excellent model according to the standards of Hosmer et al., (2013).

Using a threshold of 0.21 resulted in prediction of 6 of the 7 observed presences correctly, while predicting about 96% of the absences correctly (sensitivity = 0.857 and specificity = 0.957).

Table 5. Confusion matrix of predicted and observed presence and absence of *ScleractinianReefs* using a probability threshold 0.21.

	Observed	
Predicted	Presence	Absence
Presence	6	3
Absence	1	67

**4.5.1.1 Multiple measures of goodness of fit have been examined** Commonly used goodness-of-fit measures for binomial models are provided in Table 5 for the GLM predicting *ScleractinianReefs* probability of presence. These include the True Skill Statistic (Allouche et al., 2006), the root-mean-squared-error and the Spearman’s rank correlation. Other threshold dependent metrics can be calculated from the confusion matrix (Table 4).

Model diagnostics indicated no issues with the prediction of presence or absence (Figure 31).

#### 4.5.2 Spatial autocorrelation in the residuals has been assessed and reported

There was not significant spatial autocorrelation in the model residuals measured by Moran’s I ( $I = 0.826$ ). This was not unexpected given the random-stratified sample design of observations in the study area.

#### 4.5.3 Residuals have been tested against assumed distribution (where appropriate)

Not applicable for the binomial distribution. Figure 28 shows model residuals (on the logit scale are shown for each data point used to model *ScleractinianReefs* and diagnostics.

**4.5.3.1 Spatial patterns in residuals** Model residuals are shown in Figure 32. This confirms the results of the Moran’s I, with little evidence of spatial patterns in the residuals.

### 4.6 Model validation

#### 4.6.1 Training and testing data splitting method

Both internal model validation method and independent data was used as a validation data set. K-fold cross-validation was used here. Five (k) folds were chosen at random.

**4.6.1.1 Potential spatial biases were accounted for in splitting the data** The spatial blocking method (Valvani et al., 2019) was *not* used to split the data for the internal cross-validation.

**4.6.1.2 A standard method used for cross-validation** k-fold cross-validation is a standard method. The data was divided into 5 equal portions and a model then fit to 80% of the data and tested against the remaining 20% of the data. This was repeated for each subdivision of the data. The same maps and diagnostics were produced for each model fit on the k-folds.

The data folds appeared to show the same patterns as the full model.

The model performance was similar for all the training data sets (the full model and the individual folds). However the performance of the model on the testing folds was less impressive. For example, the True Skill Statistic and AUC for model folds 1 and 3-5 was very poor, indicating some potential issues with model performance. In particular, the low number of presences may have resulted in poor fits when the data was divided into folds.

#### 4.6.2 Truly independent data used for model validation

The presence and absence observations from 58 transects completed in 2024 was also used to test the models developed on the 2022 survey data.

The *ScleractinianReefs* model AUC was 0.509, a poor performing model according to the standards of Hosmer et al., (2013).

Using a threshold of 0.21, 0.21 resulted in prediction of 1 of the 4 observed presences correctly, while predicting about 81% of the absences correctly (sensitivity = 0.25 and specificity = 0.815)

Table 6. Confusion matrix of predicted and observed presence and absence of *ScleractinianReefs* using a probability threshold 0.21, 0.21 for the independently collected data set in 2024.

	Observed	
Predicted	Presence	Absence
Presence	1	10
Absence	3	44

Table 6. Model goodness of fit measures for the full model and the individual model validation folds

Fold	AIC	threshold	AUC_training	AUC_testing	TSS_training	TSS_testing
Full model	44.579	0.210	0.953	NA	0.814	NA
Fold_1	16.472	0.490	1.000	0.500	1.000	0.000
Fold_2	39.834	0.350	0.936	0.800	0.815	0.000
Fold_3	43.432	0.105	0.827	0.643	0.565	-0.357
Fold_4	21.746	0.495	1.000	0.518	1.000	-0.357
Fold_5	42.078	0.210	0.951	NaN	0.784	NaN

Fold	Cor_training	Cor_testing	RMSE_training	RMSE_testing
Full model	0.451	NA	0.207	NA
Fold_1	0.665	NA	0.007	0.447
Fold_2	0.450	0.252	0.209	0.251
Fold_3	0.335	-0.124	0.274	0.278
Fold_4	0.664	-0.024	0.002	0.661
Fold_5	0.494	NA	0.223	0.260

## 4.7 Model outputs

### 4.7.1 Maps of model predictions, model residuals and prediction error

Maps of model predictions are provided in Figure 34. Maps of residuals in Figure 32. Maps of prediction error in Figure 35. The model predicted that the highest probability of presence for *ScleractinianReefs* was at deep depths and in some areas near the summit depths of seamounts. It is likely that the model misfit the deeper portions of the data, as there were only two instances where *ScleractinianReefs* were observed below ~400 m. So this may be an artifact of the low number of presence observations.

### 4.7.2 Areas of model extrapolation are clearly defined

The model was not extrapolated outside the five seamounts, although within this region, there were some areas with little or no sampling. The model was extrapolated at depths from 850 - 1250 m where no sampling occurred.

#### **4.7.3 The prediction unit is clearly defined (and explained if necessary)**

The prediction unit is the probability of presence or absence of *ScleractinianReefs*.

#### **4.7.4 Thresholding methods (for dichotomising probability into presence or absence) are clearly described and appropriate**

No thresholding was done (beyond the thresholding for calculating goodness-of-fit measures). Probability of presence is presented as the result.

##### **4.7.4.1 The sensitivity of model outcomes to threshold value chosen has been explored**

Sensitivity to threshold values was not explored, but in a formal analysis of the model could be completed using the provided model outputs.

## **4.8 Conclusions**

The *ScleractinianReefs* model fit the observations from 2022 well. The internal model validation showed less robust and even poor results. The independently collected data were not predicted with good accuracy. This is likely due to the small number of observed presences in the dataset.

PRELIMINARY

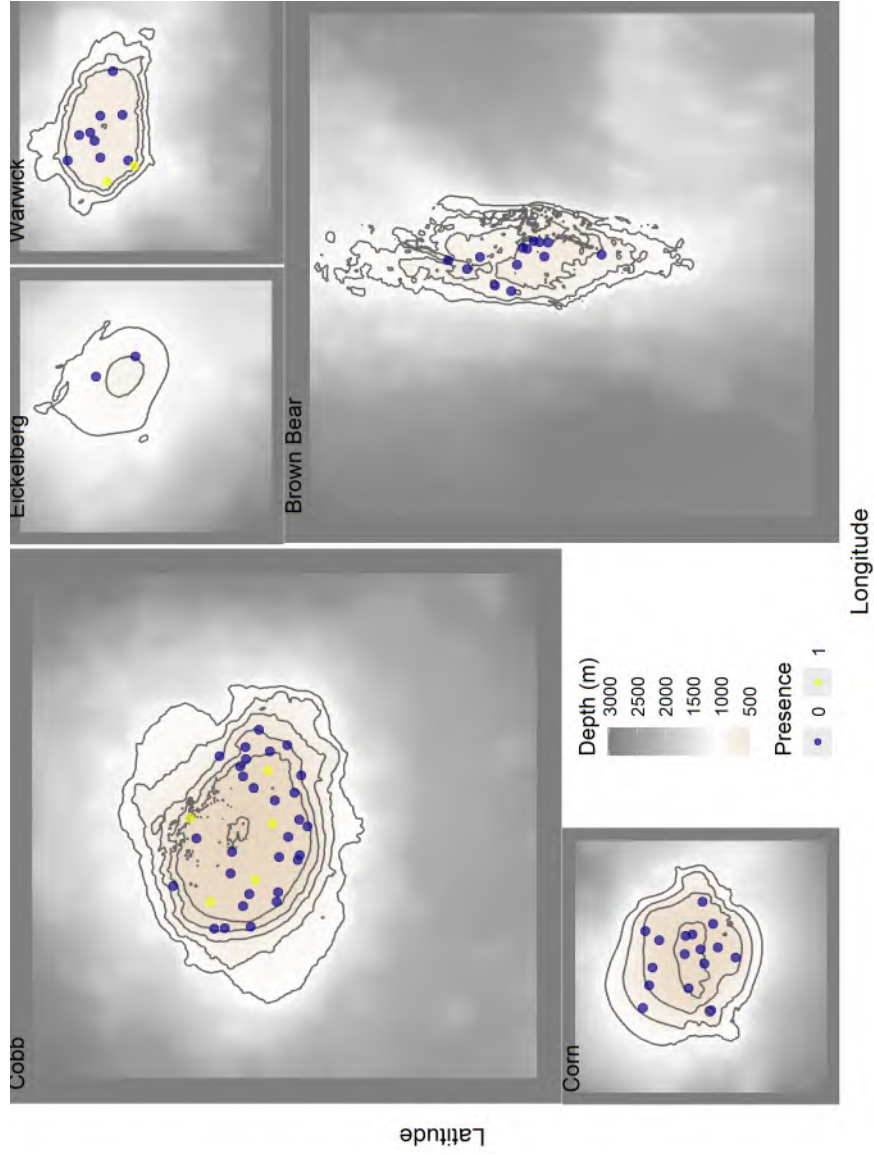


Figure 25: Locations of presence and absence transects for Scleractinian Reefs from 2022 and 2024 stereo-camera survey

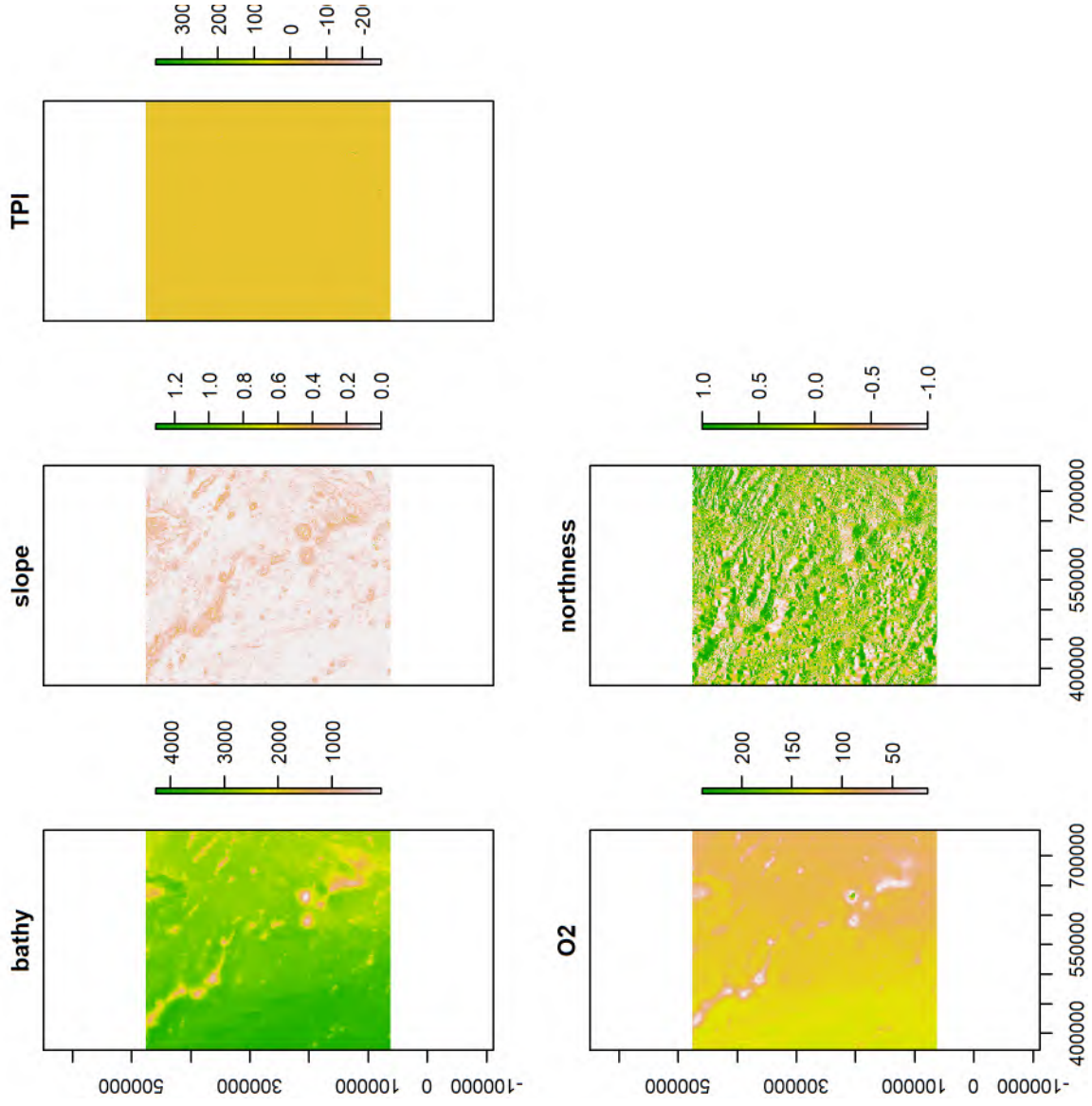


Figure 26: Map of bathymetry, slope, TPI, Oxygen and northness used as explanatory variables in this analysis of VME data

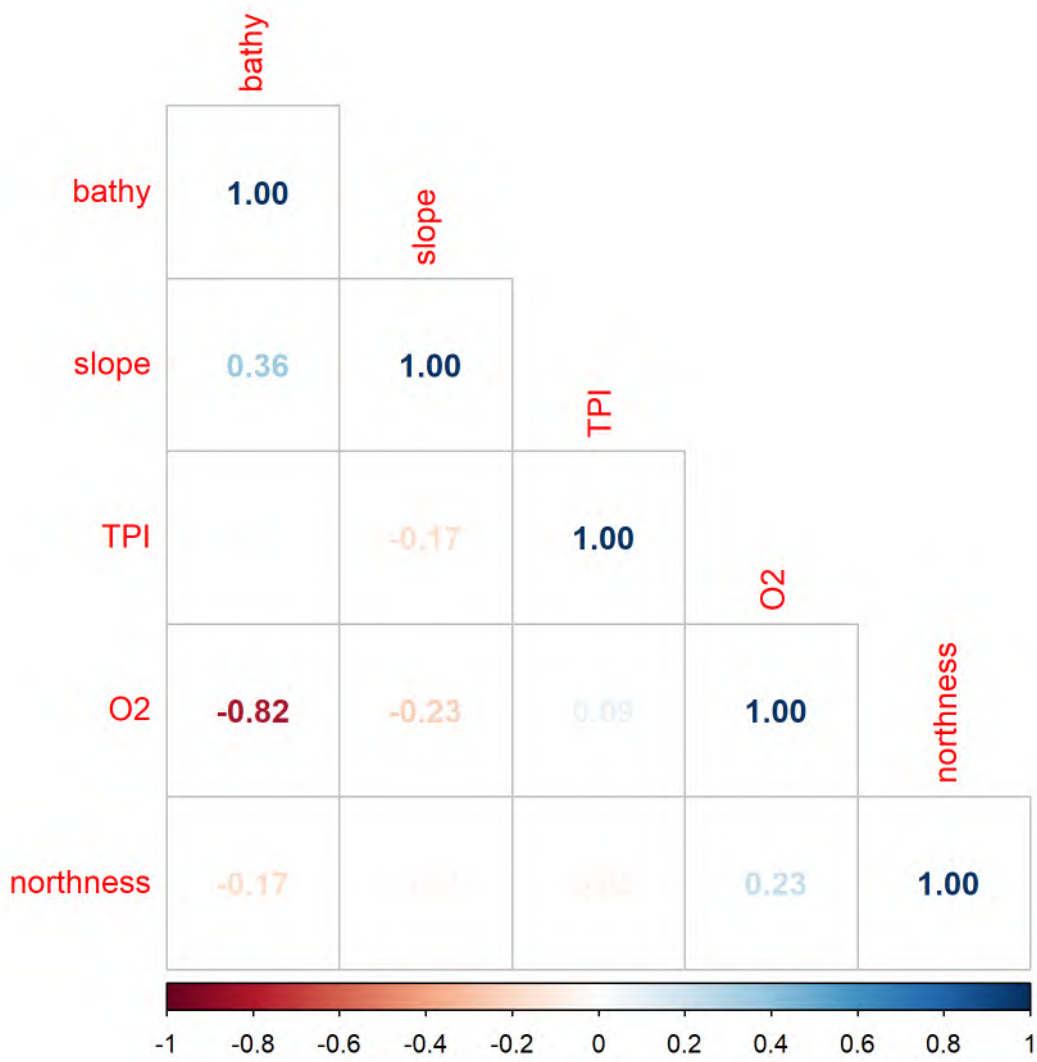


Figure 27: Correlation among independent variables used in modeling.

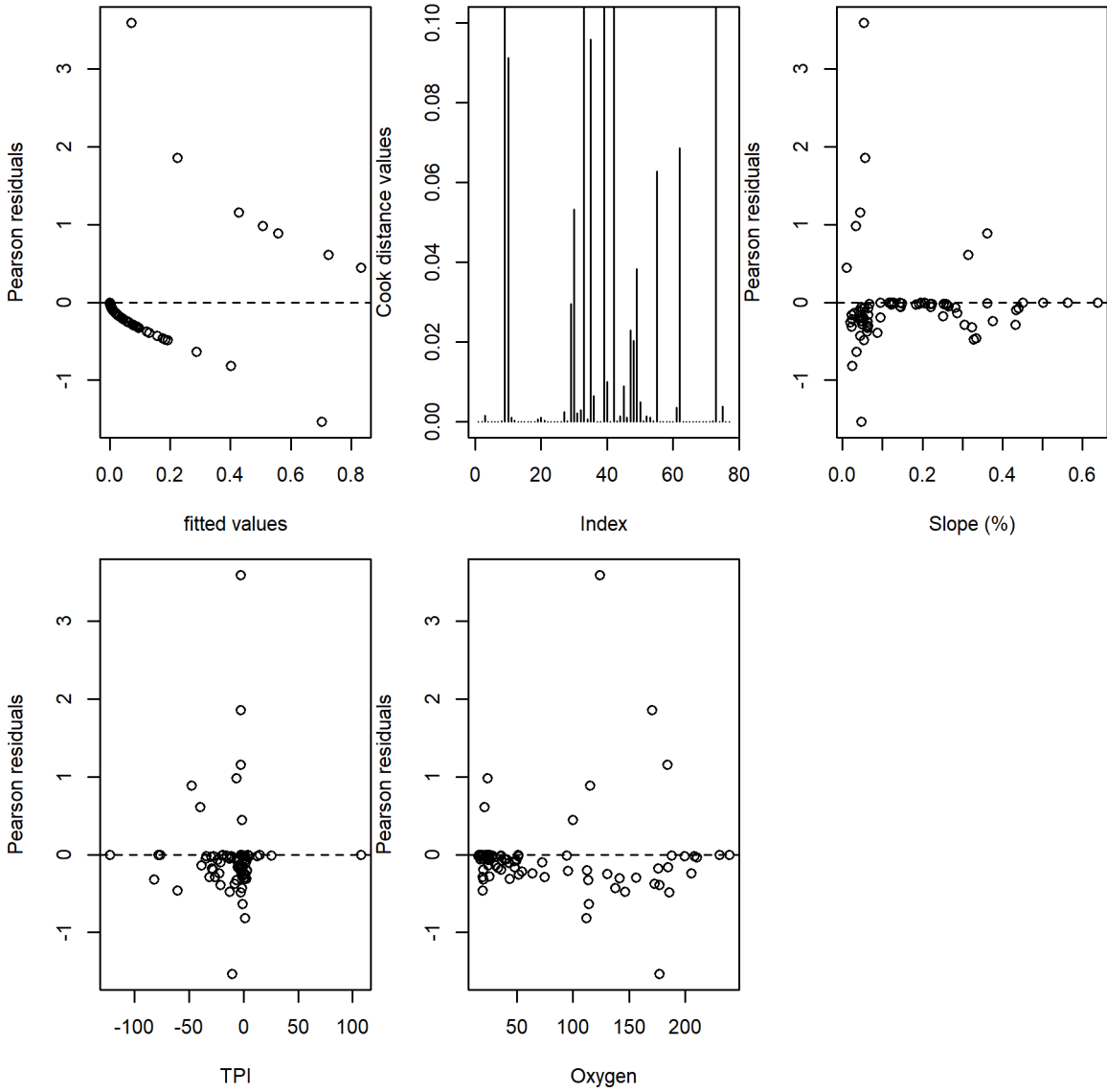


Figure 28: Diagnostic plots for GAM model assumptions.

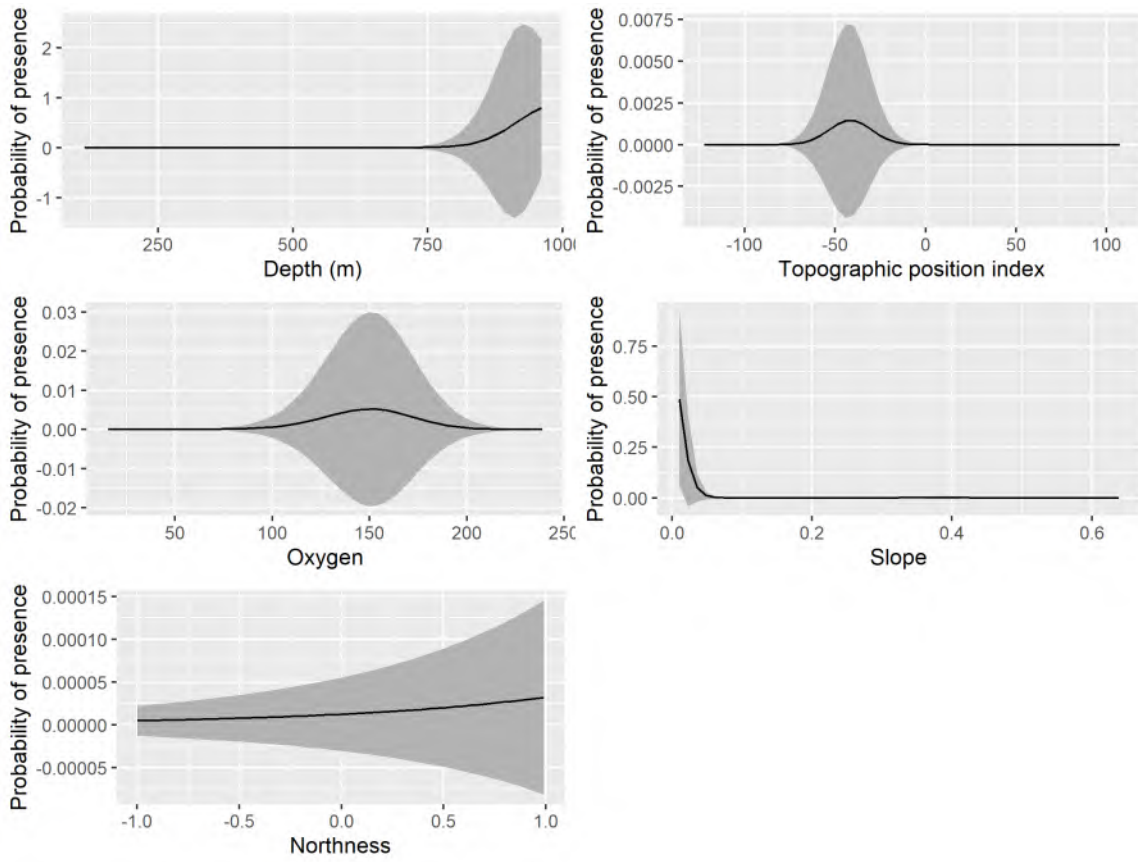


Figure 29: Response curves for independent variables used best-fitting GAM for presence or absence.

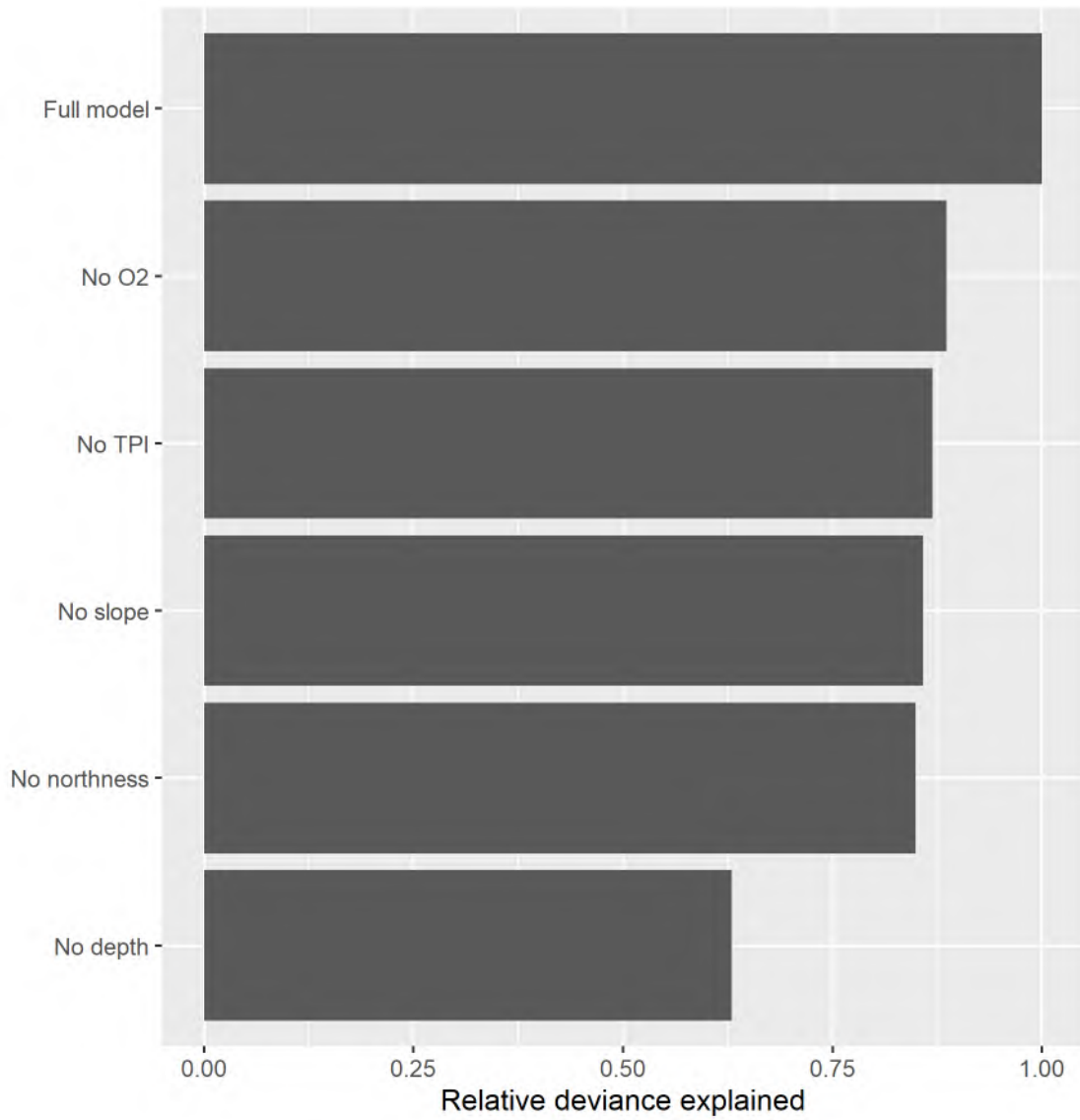


Figure 30: Relative importance of variables included in the ScleractinianReef presence or absence GAM measured by their contribution to deviance explained when sequentially removed from the model.

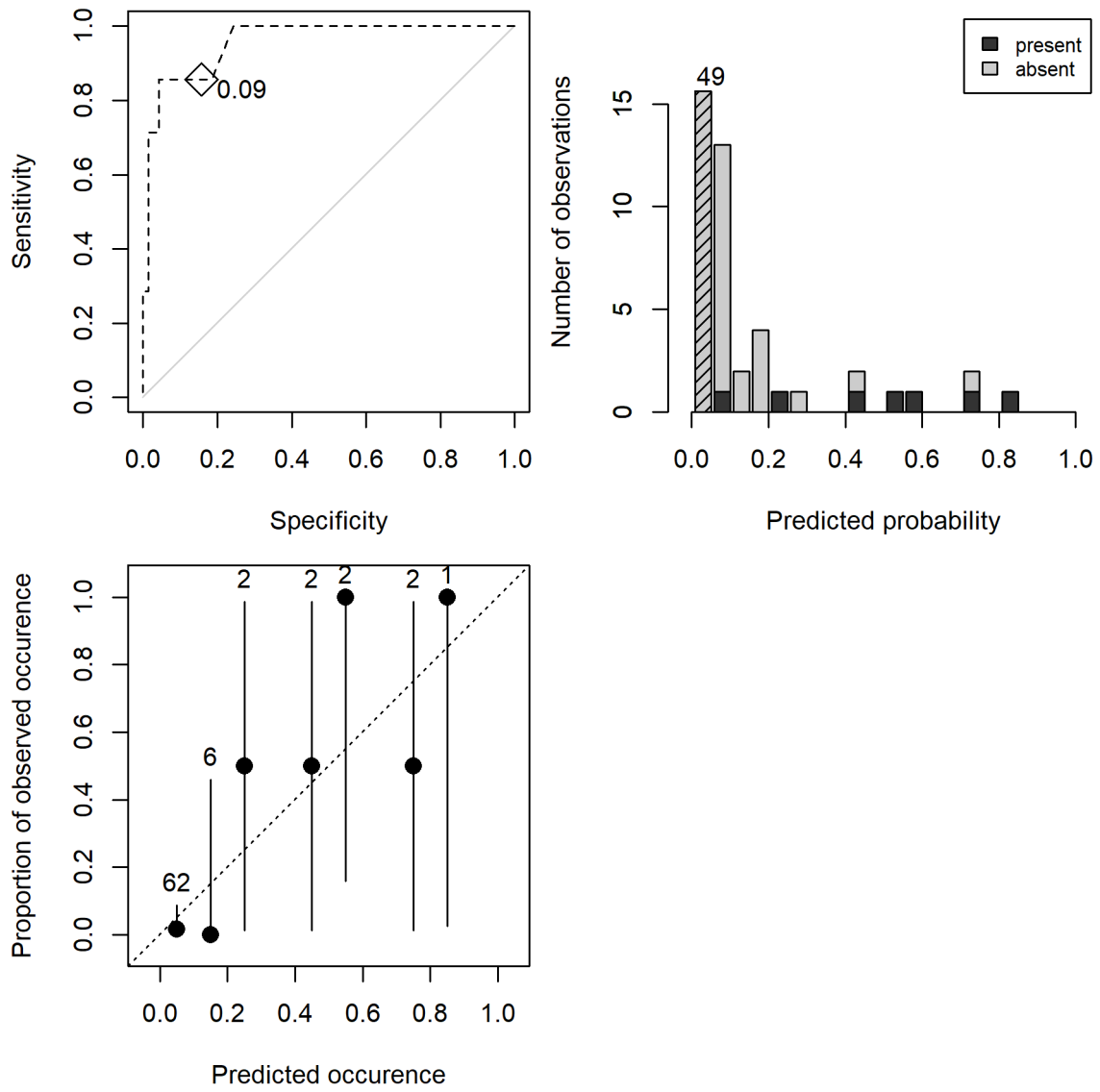


Figure 31: Model diagnostic plots for ScleractinianReef presence or absence GAM.

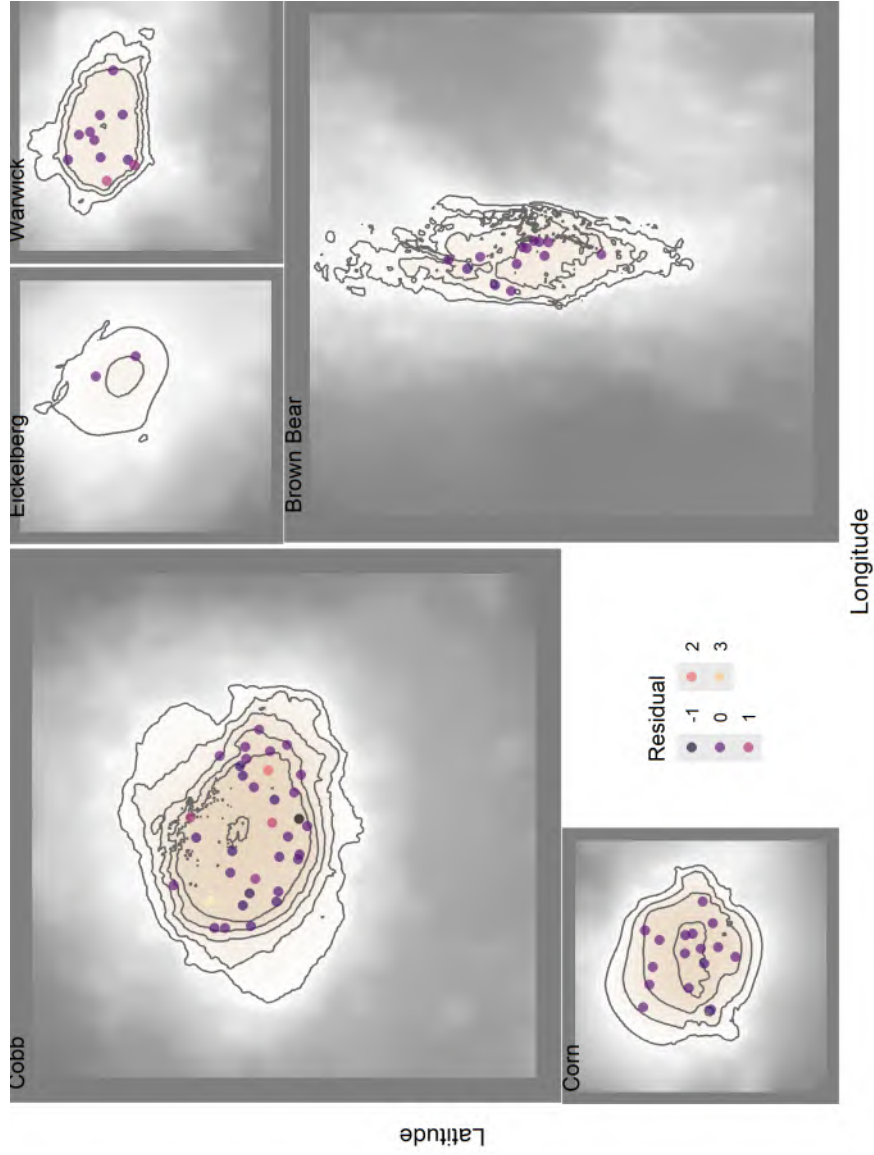


Figure 32: Spatial patterns in model Pearson residuals for GAM predicting probability of presence for Scleractinian Reefs.

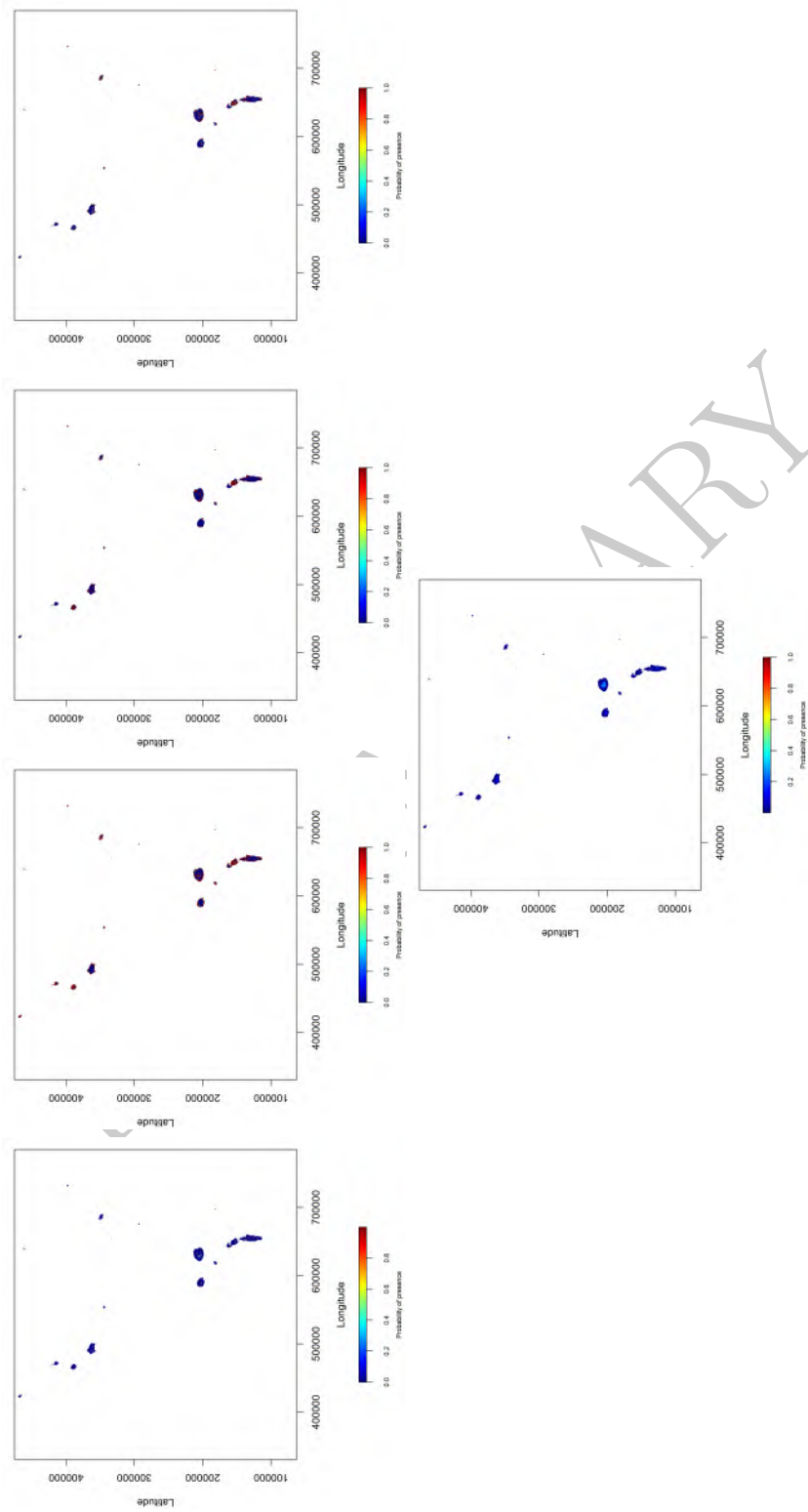


Figure 33: Maps of model predictions for 5 randomly selected folds of the data.

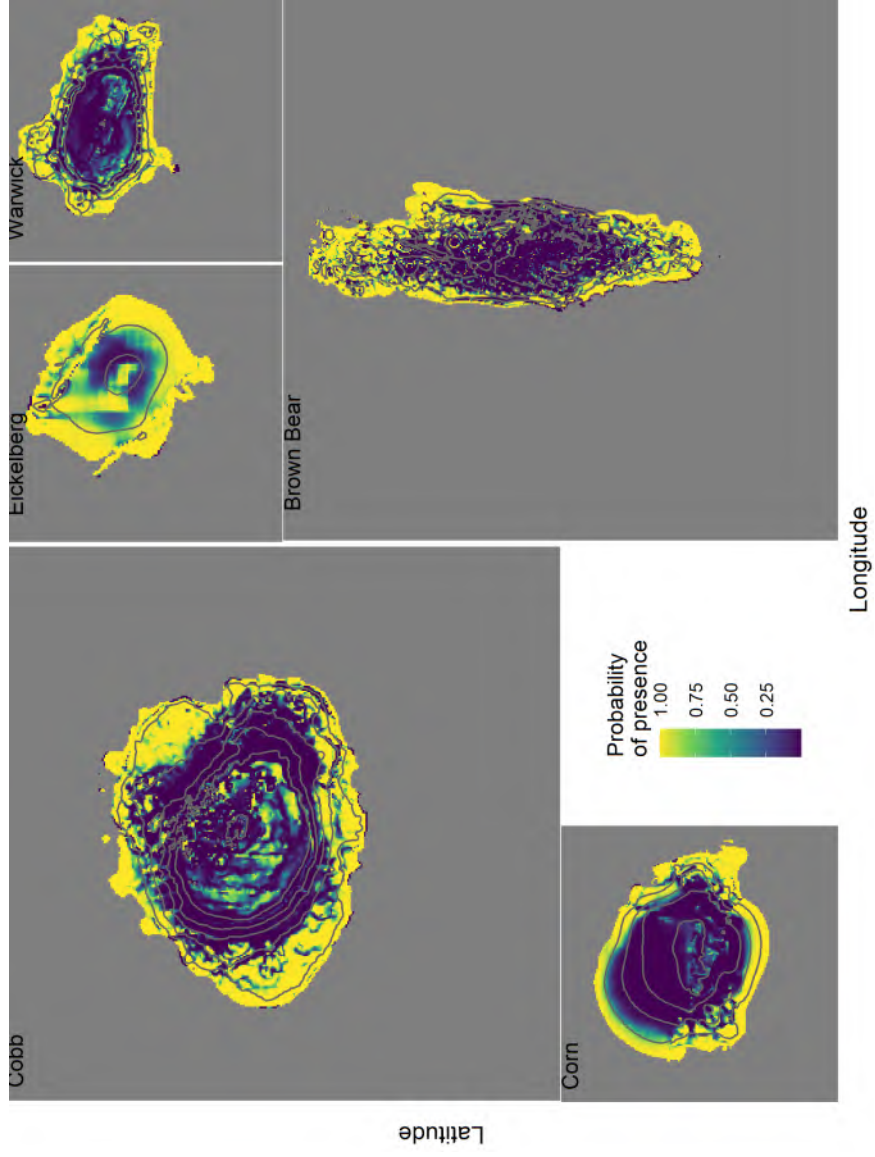


Figure 34: Predicted probability of presence for ScleractinianReefs at seamounts in the Cobb-Eickelberg seamount chain.

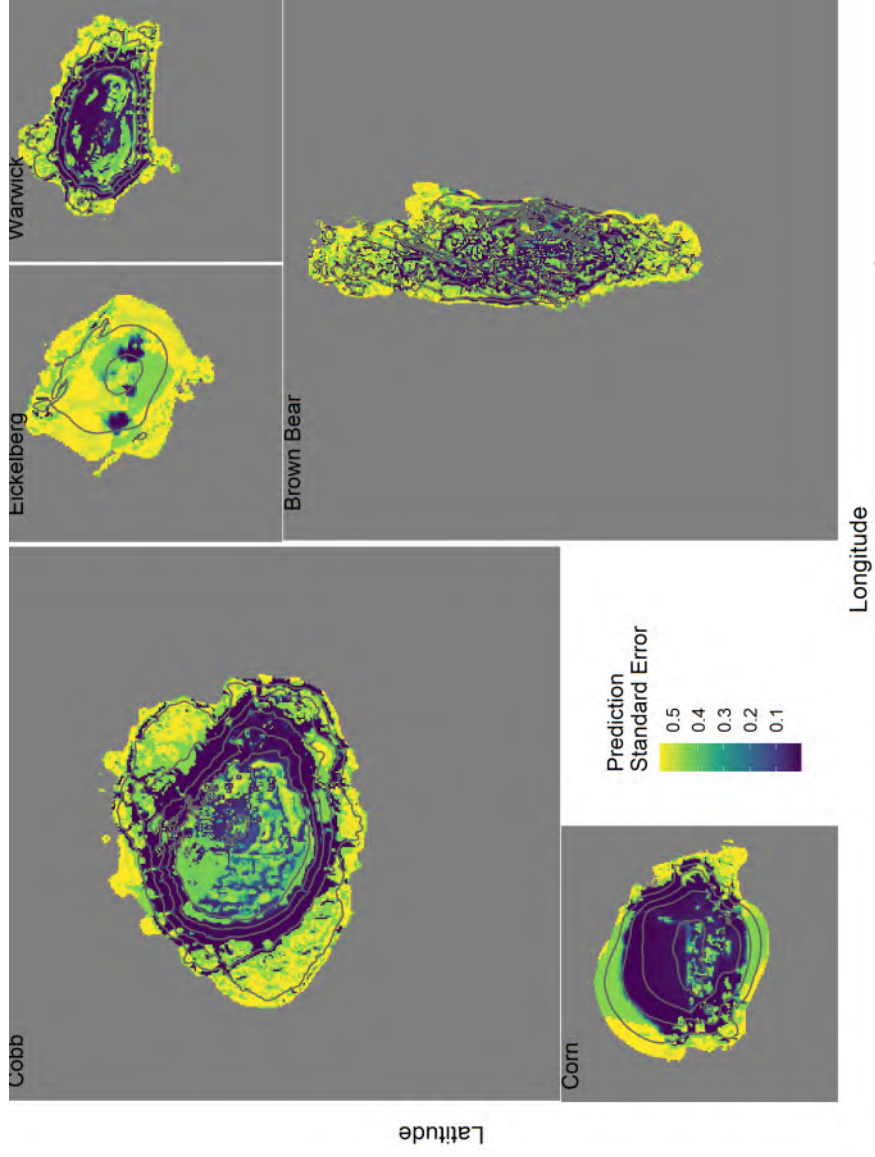


Figure 35: Spatial patterns in model prediction error for GAM predicting probability of ScleractinianReefs at seamounts in the Cobb-Eickelberg seamount chain.

## 5 Vulnerable Marine Indicator Taxa Group: *Hexactinellids*

### 5.1 Study resolution

#### 5.1.1 Location of the study area (or management region)

This modelling was carried out for five seamounts in the Northeastern Pacific Ocean where fisheries are managed by the North Pacific Fisheries Commission. The five seamounts are shown in Figure 1 and are part of the Cobb-Eickelberg seamount chain.

**5.1.1.1 Spatial extent of the modelled area** The specific seamounts modeled were five North Pacific Seamounts (Cobb, Brown Bear, Eickelberg, Warwick and Corn). Modeling was conducted from depths of 0 - 1250 m. Data was collected from 0 to ~850 m.

**5.1.1.2 Spatial resolution of the model and independent variables** The spatial resolution of the modeling was 100 m by 100 m grid cells. The all data was projected into an Albers equal area projection (proj4 description = “+proj=aea +lat\_0=45 +lon\_0=-126 +lat\_1=50 +lat\_2=58.5 +x\_0=1000000 +y\_0=0 +ellps=GRS80 +towgs84=0,0,0,0,0,0 +units=m +no\_defs”).

**5.1.1.3 Spatial precision (of observations and independent variables)** The spatial precision of the observations was taken from the gps mounted on the research vessel. Based on tracking information, the camera system was towed slightly behind the vessel (~200 m typically), but along the same path as the vessel. The anticipated precision of the variation of the camera path was expected to be less than 20 m across the trackline.

**5.1.1.4 Depth resolution/range/extent (of the observations and independent variables)** The depth range of the observations of *Hexactinellids* (from the depth sensor mounted on the camera) was from 61 to 808 m (mean = 442 m, SE = 206.28). The depth range of the modeled area was from 34 (the summit depth of Cobb Seamount) to 1250 m.

#### 5.1.2 Temporal extent of the data

**5.1.2.1 Dates of data extent** The dates observations used in model development were collected were September 6, 2022 to September 20, 2022. The dates for observations used for model testing were from September 3, 2024 to September 11, 2024.

**5.1.2.2 Precision of date/time** The precision of the date and the time of the data was assumed to be the closest second.

**5.1.2.3 Data/time resolution** The resolution of the date and time was fraction of a second.

**5.1.2.4 Impacts over time to consider in the data set (e.g. historical fishing effort)** Fishing occurred over the entire time frame from which these data points were collected. Fishing also has occurred historically since the 1970's. We did not attempt to account for historical fishing effort over this time. There may have been climate impacts occurring over the time frame of the data observations as well, however, these were not accounted for in the analyses.

### 5.2 Dependent data

The dependent data are shown in Figure 36.

Table 1. Number of records for each taxonomic grouping in the order *Hexactinellids* from the survey database.

	Species or Taxa group	Count
2	Hexactinellida	617
1	Farrea	25

### 5.2.1 Data type (presence, absence, abundance)

The data used for modeling *Hexactinellids* distribution were observed presences (n = 40) and absences (n = 37) that occurred at the five seamounts.

### 5.2.2 Data source (e.g. type of survey(s) combined)

The data were entirely from random stratified surveys of the Cobb-Eickelberg seamount chain conducted in 2022.

### 5.2.3 Measure of sampling effort

Sampling effort was estimated by the distance the camera traveled along each transect multiplied by the field of view observed along the transect (Rooper et al. 2016). This provided an area observed for each transect which was used as the effort measure. Area observed ranged from 254 to 2469 m<sup>2</sup> with a median area observed of 1197 m<sup>2</sup>.

### 5.2.4 Detectability

Detectability of the width of the viewing area of the camera along the transect (area observed) was assumed to be 100% for VME indicator taxa. However, there were likely some individuals that were too small to be detected.

### 5.2.5 Taxonomic level

The taxonomic level modeled here was the taxonomic group *Hexactinellids* (see Table 1 for individual families included in this grouping and refer to CMM for NPFC definitions).

### 5.2.6 Functional attributes (its ecology)

*Hexactinellids* are a diverse, long-lived and fragile species. They occur in deep-water and are habitat forming structures important to many fishes, invertebrates other taxonomic groups.

### 5.2.7 Taxonomic confidence of species/assemblages

The taxonomic confidence of the assemblage was assumed to be good. Experts experienced in identification of corals and sponges from visual imagery in the North Pacific Ocean did all the identification and image analyses.

### 5.2.8 Rationale for taxonomic/assemblage level modeled

*Hexactinellids* as defined here are a group that shares common habitat requirements and depth distribution. They are closely related and the order is globally distributed at deep depths. This Order has been previously modelled using Maximum entropy methods on a global extent and regional extent (Yesson et al., 2017, Chu et al. 2018, Doherty et al. 2019).

### 5.2.9 Source of absence data

Absences were observations of no individuals at transects. In total there were 37 absences in the dataset.

### 5.2.10 Other potential errors or biases in the data

There are some potential sources of error in the data, including errors in positioning of the records, errors in species identification (including both false positives and false negatives).

### 5.2.11 Data filtering steps

No data filtering was conducted.

### 5.2.12 Taxonomic aggregation steps

The records for the Order *Hexactinellids* were aggregated by transect into presence or absence observations.

### 5.2.13 Method for combining dependent data sources (if done outside the modelling)

No other dependent data sources were used in this modelling.

## 5.3 Independent data

### 5.3.1 Independent data (environmental variables used)

Five independent variables were used in building a model of *Hexactinellids* distribution; bathymetry, topographic position index, seafloor slope, Oxygen concentration and northness (Figure 37).

### 5.3.2 Independent data source (source of raw or derived data)

The bathymetry used here was downloaded from the NOAA website (<https://www.ncei.noaa.gov/maps/bathymetry/>). It consists of gridded bathymetry from a multibeam sources on a 3 arc-second grid for the region of interest. The details of the data sources can be found on the NOAA website. There were some gaps in the NOAA bathymetry layers. These were filled using single beam echosounder data collected during the 2022 and 2024 cruises and GEBCO bathymetry ([www.gebco.net/data\\_and\\_products/gridded\\_bathymetry\\_data](http://www.gebco.net/data_and_products/gridded_bathymetry_data)). The single beam echosounder data and GEBCO bathymetry was sampled into the missing grids in the NOAA bathymetry, with preference to the single beam echosounder data.

From the bathymetry two derived variables (slope and topographic position index) were calculated using the raster package (Hijmans 2019). Slope was calculated from the nearest 8 neighbors and TPI was calculated with a focal distance of ~300 m.

Northness was calculated as the cosine of the aspect (direction relative to 0 degrees that the slope was facing) for each grid cell based on bathymetry.

Oxygen data were based on the World Ocean Atlas data (2018 update). These data were clipped to the area of interest and resampled into the bathymetry grid using bilinear interpolation. The five explanatory variables are shown in Figure 37.

### 5.3.3 Native spatial and temporal resolution of the independent data

The native spatial resolution of the NOAA bathymetry was 3 arc-second grid. The native spatial resolution for the Oxygen data was 0.5 degrees longitude and latitude. It should be noted that the Oxygen data sources are conglomerations of data collected over varying spatial and temporal scales (e.g. the temporal scale is since ~1900's in the case of some measurements). For complete documentation of the spatial and temporal scale of the raw data the NODC respective website should be consulted ([www.gebco.net/data\\_and\\_products/gridded\\_bathymetry\\_data](http://www.gebco.net/data_and_products/gridded_bathymetry_data) and <https://www.nodc.noaa.gov/OC5/woa18/>).

All independent data layers were trimmed to include only observations and explanatory variables from this region and to depths of 1250 m.

### 5.3.4 Data processing and scaling (method for downscaling or aggregation)

Both the bathymetry (for gap filling) and oxygen layers were downscaled to a 100 m by 100 m grid in order to match the scale of the bathymetry. This downscaling was completed using bilinear interpolation.

**5.3.4.1 Goodness of fit for downscaled aggregated data** The downscaled data at the dependent data sites for both Oxygen and bathymetry represented the lower resolution very well ( $r > 0.9$ ).

**5.3.4.2 Measurement errors and bias** Measurement errors in the data or bias in the data were not accounted for beyond the processing conducted on the raw measurements by GEBCO or NODC.

### 5.3.5 Derivation methods and calculations for derived variables

From the bathymetry three derived variables (aspect, slope and topographic position index) were calculated using the raster package (Hijmans 2019). These variables were calculated on bathymetry aggregated (see below) to a 100 m by 100 m grid. The aspect variable was then converted to northness using a cosine function.

### 5.3.6 Rationale for inclusion of independent variables clearly stated and ecologically relevant

These five variables (depth, slope, topographic position index, northness and oxygen) have been found in previous studies to influence the distribution of *Hexactinellids* (Huff et al., 2013, Yesson et al., 2017, Etnoyer et al., 2018).

## 5.4 Modelling approach

In this study generalized additive models (GAM) were developed to predict species distribution (Wood 2006).

### 5.4.1 Model steps

**5.4.1.1 Code for model provided** The code and data used for this model are not currently publicly available, but can be available on request from Chris Rooper (chris.rooper@dfo-mpo.gc.ca).

**5.4.1.2 Packages used are referenced** The packages used to develop this model are referenced in the above .Rmd file. The key packages used were “sf”, “rnatuarearth”, “ggplot2”, “rgdal”, “rgeos”, “gstat”, “raster”, “mgcv” and are all available for download from CRAN. The R version used here was R version 3.6.0 (2019-04-26) – “Planting of a Tree” (R Core Development Team 2019).

**5.4.1.3 Data is made available as supplementary material** The independent variables are available from Chris Rooper (chris.rooper@dfo-mpo.gc.ca).

### 5.4.2 Biases (spatial, temporal and other) acknowledged and described

There were no inherent biases in the modeling method (although there may be biases in the dependent and independent data described above).

### 5.4.3 Methods and approaches to collinearity in independent variables

**5.4.3.1 Collinearity in independent variables** The five explanatory variables were examined for collinearity using a pearson correlations (Figure 38). Variance inflation factors (Zuur et al. 2002) were also examined. In both cases the values were low, suggesting that the variables were fairly independent of each other.

Table 2. Variance inflation factors for independent variables using in modeling.

Variable	VIF
Depth	3.592
Slope	1.231
TPI	1.091
Oxygen	3.372
Northness	1.065

**5.4.3.2 Criteria for variable/dimension reduction provided** None of the variance inflation factors exceeded 5, indicating that dimension reduction was not warranted.

#### 5.4.4 Choice of modelling method is explained and justified

The modelling method chosen was a generalized additive model (GAM). This model was primarily chosen for its simplicity of assumptions (stated below), its usefulness in fitting binomial (presence-absence) data, and the many previous applications of this method to predicting species distributions.

**5.4.4.1 Modelling assumptions are clearly stated** The basic GAM assumptions are; 1) Independence among data points, 2) The distribution of the residuals is binomially distributed, 3) homogenous variance across the fitted values, and 4) a non-linear relationship between response and predictor.

**5.4.4.2 Potential violations of model assumptions are explored** Diagnostic plots of Pearson residuals are shown in Figure 39. The residuals did not indicate any serious violations of GAM assumptions.

#### 5.4.5 Model application

To build the model of *Hexactinellids* a generalized additive model was constructed that contained five explanatory variables (depth, slope, topographic position index, northness and oxygen). The dependent data was presence or absence of *Hexactinellids*. The full model was

$$y = \alpha + s(\text{depth}) + s(\text{slope}) + s(\text{TPI}) + s(\text{northness}) + s(O_2) + \sigma$$

A binomial error distribution ( $\sigma$ ) was used for the model fitting. A full model was fit initially containing all the variables with a basis degrees of freedom of 4 for each smooth. This model was reduced sequentially by removing the least significant term and comparing the AIC for the resulting reduced model following the methods of Rooper et al. (2016). This was repeated until there was a decline in model skill when removing a variable.

**5.4.5.1 Model settings** The default GAM settings in R were used (see `CobbSDM_Hexactinellid.Rmd`). The only setting that was modified was the specification of the binomial error distribution and the specified number of knots for the smooth of  $k = 4$ .

**5.4.5.2 Model complexity is assessed** The results of the sequential variable reduction resulted in the retention of 3 terms; depth, TPI, slope. The deviance explained by the model ( $D^2$ ) was 0.691.

The model complexity was assessed against simpler models with less terms during the sequential variable reduction step and the most complex model (containing these terms) was found to be the most appropriate (Table 3).

Table 3. Summary of GAM model predicting presence or absence of *Hexactinellids*.

Term	edf	F	p-value
depth	1.000	13.486	0.0002
TPI	2.854	9.034	0.0267

Term	edf	F	p-value
slope	2.708	2.276	0.4972
residual	69.438		
GCV	-0.376		
Deviance explained (%)	69.100		

#### 5.4.6 Model response curves are generated (where appropriate) and compared to expectations

Model response curves are shown in Figure 40. Probability of presence of *Hexactinellids* was highest above 500 m depth was higher when TPI values were  $< 0$  (indicating “valleys” or low points in the topography). Hexactinellid probability of presence was also higher at steeper slopes. None of the results were abnormal or unexpected.

##### 5.4.6.1 Modelling method-specific term estimates or coefficients are reported (where relevant)

The model specific term estimates are provided in Table 4.

Table 4. Model coefficients, significance and standard error estimates for GAM predicting *Hexactinellids* probability of presence.

	x
(Intercept)	0.429
s(depth).1	0.000
s(depth).2	0.000
s(depth).3	4.230
s(TPI).1	14.809
s(TPI).2	39.478
s(TPI).3	-17.633
s(slope).1	7.659
s(slope).2	-49.073
s(slope).3	19.652

**5.4.6.2 Independent variable importance is reported** The relative importance of variables in the model was measured by sequentially removing the individual variables, fitting a new model and calculating the deviance explained. The deviance explained was then scaled to the full model to determine the relative drop in model goodness-of-fit with removal of each variable. The results showed that slope was the least important variable determining the probability of *Hexactinellids* presence, and TPI and depth were the most important (Figure 41).

## 5.5 Model uncertainty

### 5.5.1 Model specific goodness of fit statistics have been checked and reported

The *Hexactinellids* model AUC was 0.968, an excellent model according to the standards of Hosmer et al., (2013).

Using a threshold of 0.665 resulted in prediction of 34 of the 40 observed presences correctly, while predicting about 97% of the absences correctly (sensitivity = 0.85 and specificity = 0.973).

Table 5. Confusion matrix of predicted and observed presence and absence of *Hexactinellids* using a probability threshold 0.665.

	Observed	
Predicted	Presence	Absence
Presence	34	1
Absence	6	36

**5.5.1.1 Multiple measures of goodness of fit have been examined** Commonly used goodness-of-fit measures for binomial models are provided in Table 5 for the GAM predicting *Hexactinellids* probability of presence. These include the True Skill Statistic (Allouche et al., 2006), the root-mean-squared-error and the Spearman’s rank correlation. Other threshold dependent metrics can be calculated from the confusion matrix (Table 4).

Model diagnostics indicated no issues with the prediction of presence or absence (Figure 42). The predicted occurrence always included the 1:1 line.

### 5.5.2 Spatial autocorrelation in the residuals has been assessed and reported

There was not significant spatial autocorrelation in the model residuals measured by Moran’s I ( $I = 0.052$ ), although the value was almost significant. This was not unexpected given the random-stratified sample design of observations in the study area.

### 5.5.3 Residuals have been tested against assumed distribution (where appropriate)

Not applicable for the binomial distribution. Figure 39 shows model residuals (on the logit scale are shown for each data point used to model *Hexactinellids* and diagnostics.

**5.5.3.1 Spatial patterns in residuals** Model residuals are shown in Figure 43. This confirms the results of the Moran’s I, with little evidence of spatial patterns in the residuals.

## 5.6 Model validation

### 5.6.1 Training and testing data splitting method

Both internal model validation method and independent data was used as a validation data set. K-fold cross-validation was used here. Five (k) folds were chosen at random.

**5.6.1.1 Potential spatial biases were accounted for in splitting the data** The spatial blocking method (Valvani et al., 2019) was *not* used to split the data for the internal cross-validation.

**5.6.1.2 A standard method used for cross-validation** k-fold cross-validation is a standard method. The data was divided into 5 equal portions and a model then fit to 80% of the data and tested against the remaining 20% of the data. This was repeated for each subdivision of the data. The same maps and diagnostics were produced for each model fit on the k-folds.

The data folds appeared to show the same patterns as the full model.

The model performance was similar for all the training and testing data sets (the full model and the individual folds).

### 5.6.2 Truly independent data used for model validation

The presence and absence observations from 58 transects completed in 2024 was also used to test the models developed on the 2022 survey data.

The *Hexactinellids* model AUC was 0.754, a good performing model according to the standards of Hosmer et al., (2013).

Using a threshold of 0.665, 0.665 resulted in prediction of 12 of the 22 observed presences correctly, while predicting about 78% of the absences correctly (sensitivity = 0.545 and specificity = 0.778).

Table 6. Confusion matrix of predicted and observed presence and absence of *Hexactinellids* using a probability threshold 0.665, 0.665 for the independently collected data set in 2024.

	Observed	
Predicted	Presence	Absence
Presence	12	8
Absence	10	28

Table 6. Model goodness of fit measures for the full model and the individual model validation folds

Fold	AIC	threshold	AUC_training	AUC_testing	TSS_training	TSS_testing
Full model	48.086	0.665	0.968	NA	0.823	NA
Fold_1	37.432	0.545	0.977	0.852	0.839	0.611
Fold_2	37.228	0.670	0.973	0.953	0.809	0.875
Fold_3	45.402	0.435	0.957	1.000	0.797	0.875
Fold_4	41.625	0.355	0.963	0.968	0.857	0.857
Fold_5	37.296	0.547	0.971	0.833	0.839	0.222

Fold	Cor_training	Cor_testing	RMSE_training	RMSE_testing
Full model	0.810	NA	0.256	NA
Fold_1	0.826	0.598	0.237	0.421
Fold_2	0.819	0.786	0.247	0.275
Fold_3	0.790	0.866	0.274	0.160
Fold_4	0.800	0.806	0.265	0.282
Fold_5	0.816	0.567	0.246	0.417

## 5.7 Model outputs

### 5.7.1 Maps of model predictions, model residuals and prediction error

Maps of model predictions are provided in Figure 45. Maps of residuals in Figure 43. Maps of prediction error in Figure 46. The model predicted that the highest probability of presence for *Hexactinellids* was in a band from 500 m and deeper.

### 5.7.2 Areas of model extrapolation are clearly defined

The model was not extrapolated outside the five seamounts, although within this region, there were some areas with little or no sampling. The model was extrapolated at depths from 850 - 1250 m where no sampling occurred.

### 5.7.3 The prediction unit is clearly defined (and explained if necessary)

The prediction unit is the probability of presence or absence of *Hexactinellids*.

### 5.7.4 Thresholding methods (for dichotomising probability into presence or absence) are clearly described and appropriate

No thresholding was done (beyond the thresholding for calculating goodness-of-fit measures). Probability of presence is presented as the result.

**5.7.4.1 The sensitivity of model outcomes to threshold value chosen has been explored**  
Sensitivity to threshold values was not explored, but in a formal analysis of the model could be completed using the provided model outputs.

## 5.8 Conclusions

The *Hexactinellids* model fit the observations from 2022 well. The internal model validation showed robust results. The independently collected data were predicted with good accuracy.

Model response curves showed the importance of depth. At depths below 500 m, there was a high probability of *Hexactinellids* presence at all seamounts on a randomly chosen transect.

PRELIMINARY

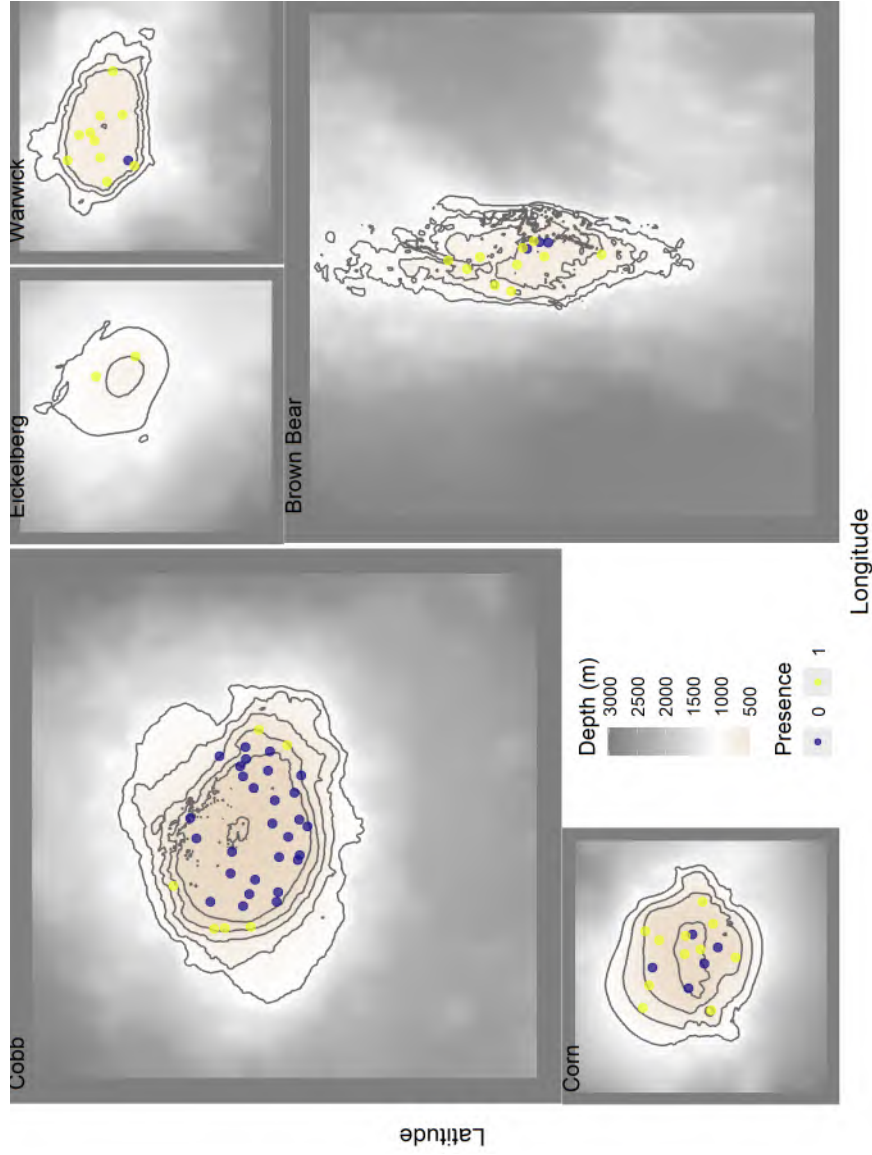


Figure 36: Locations of presence and absence transects for Hexactinellids from 2022 and 2024 stereo-camera survey

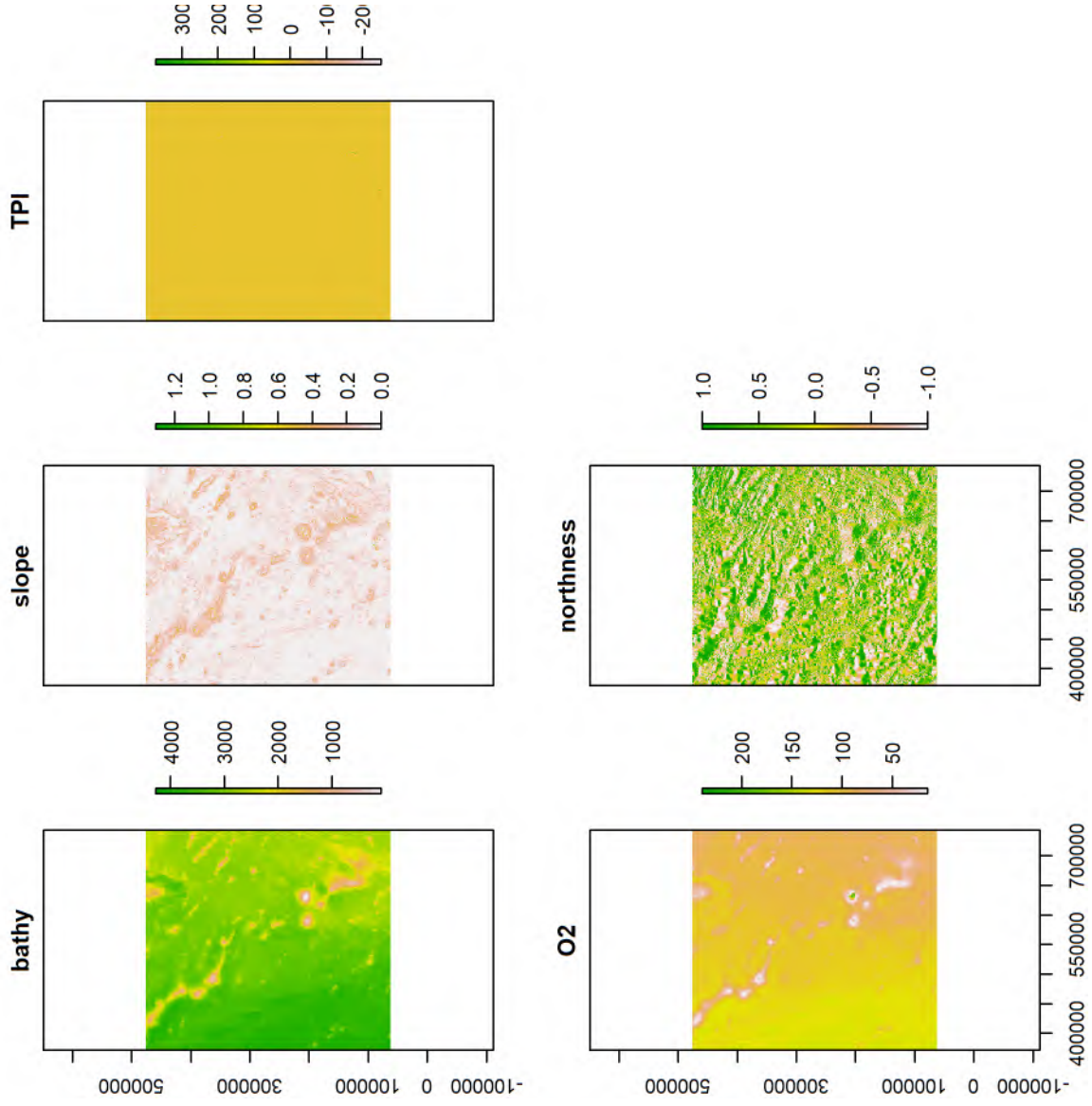


Figure 37: Map of bathymetry, slope, TPI, Oxygen and northness used as explanatory variables in this analysis of VME data

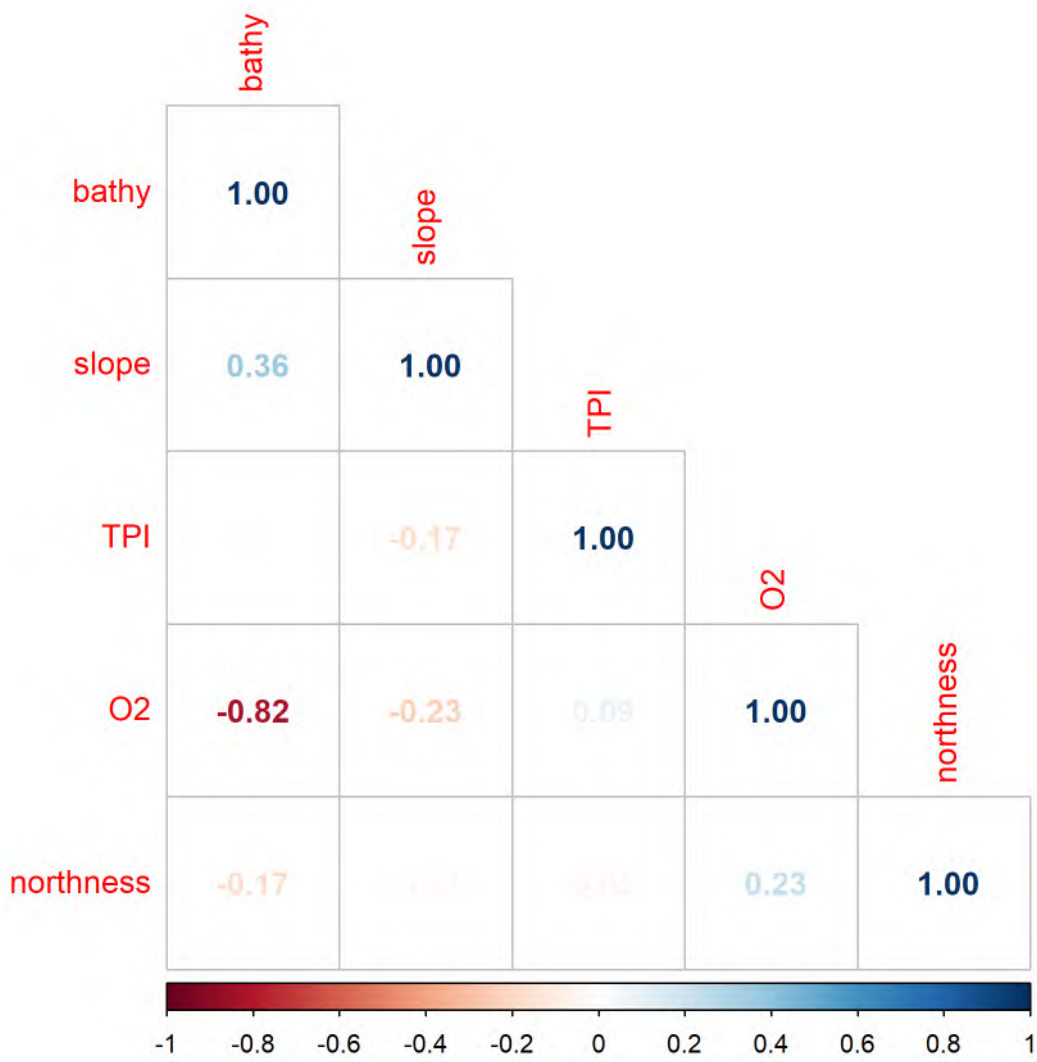


Figure 38: Correlation among independent variables used in modeling.

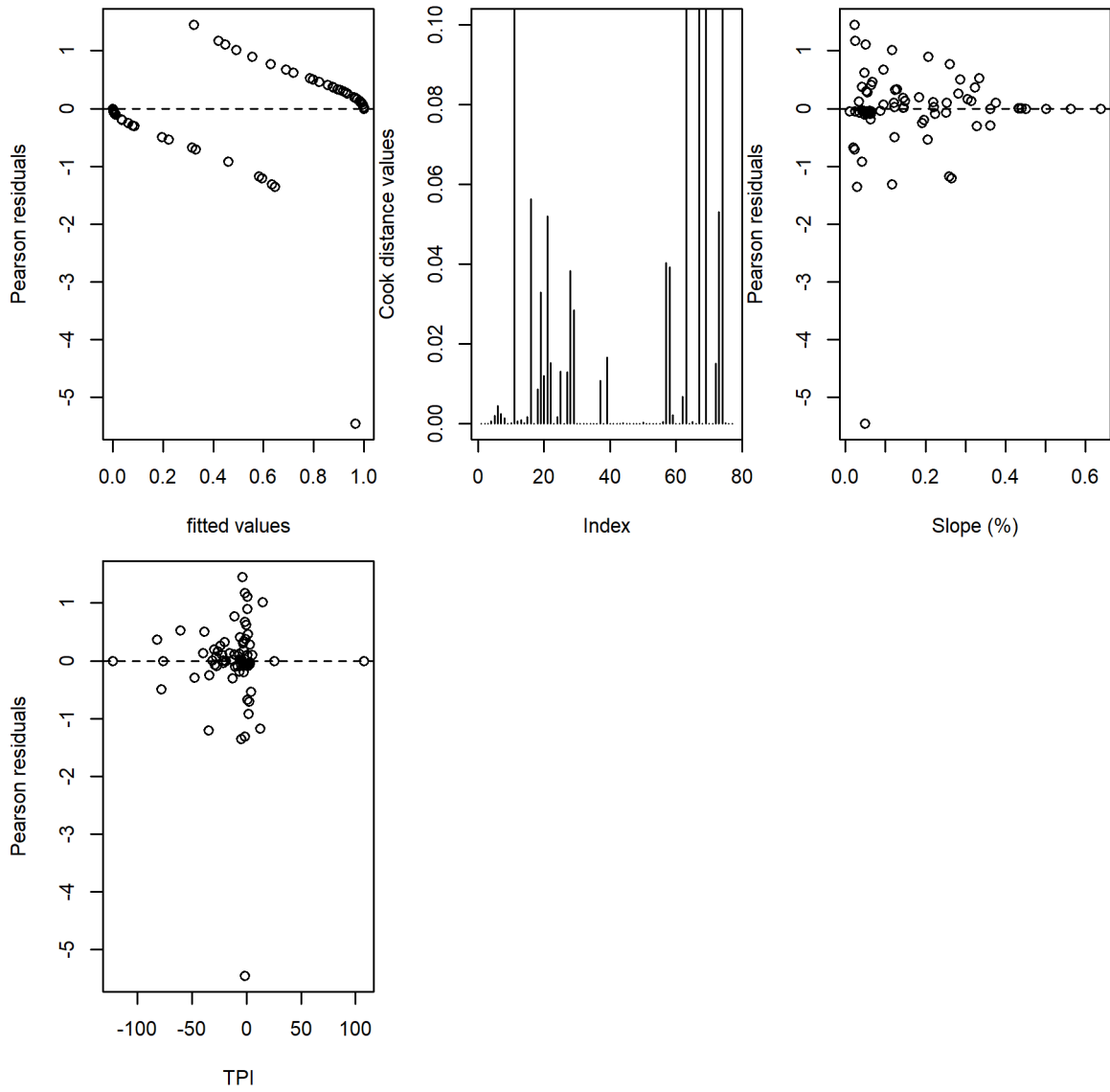


Figure 39: Diagnostic plots for GAM model assumptions.

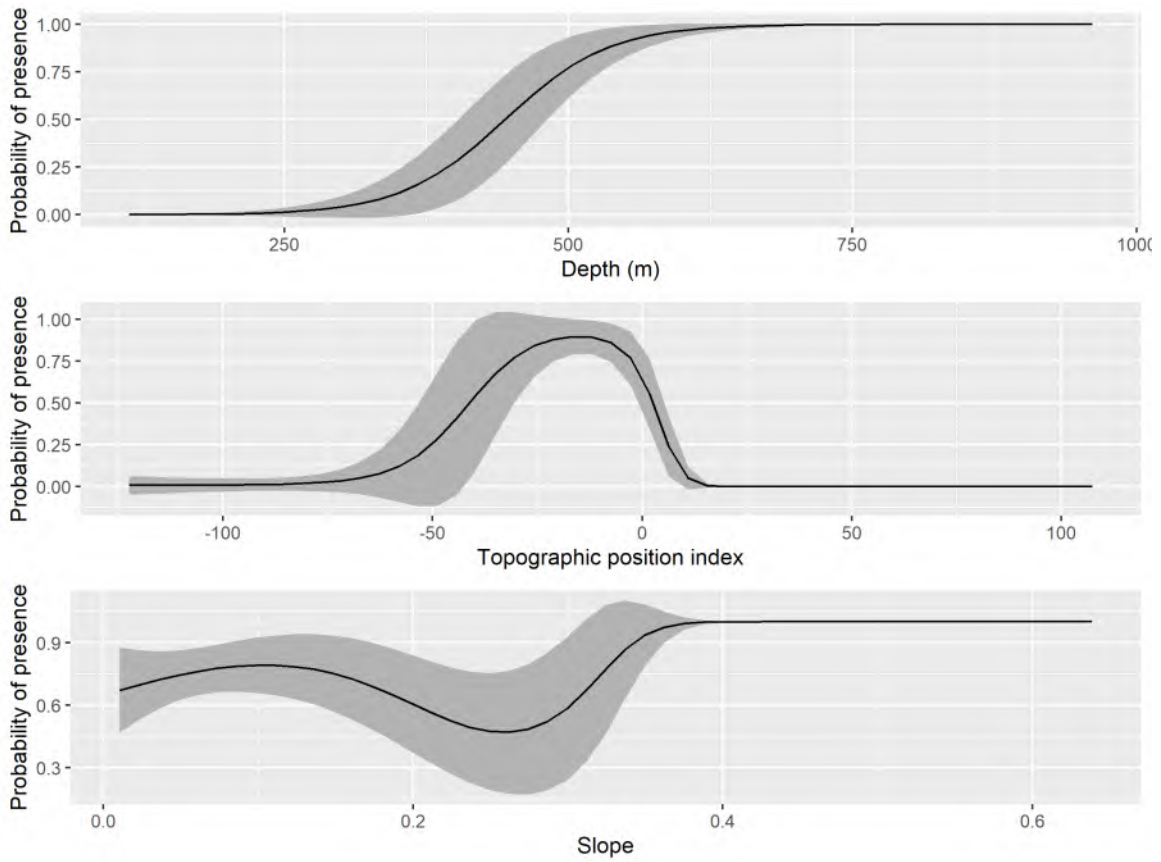


Figure 40: Response curves for independent variables used best-fitting GAM for presence or absence.

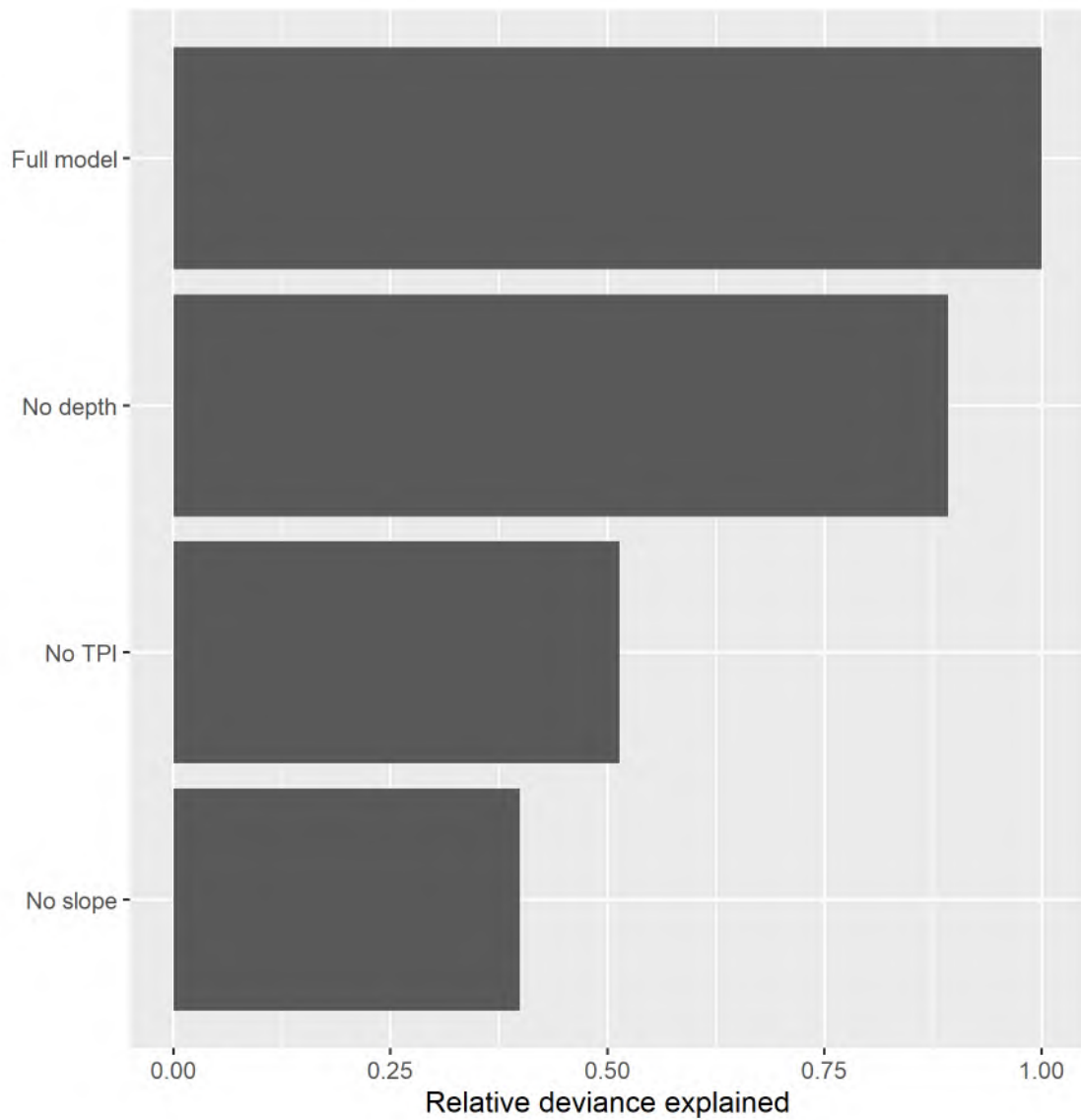


Figure 41: Relative importance of variables included in the Hexactinellid presence or absence GAM measured by their contribution to deviance explained when sequentially removed from the model.

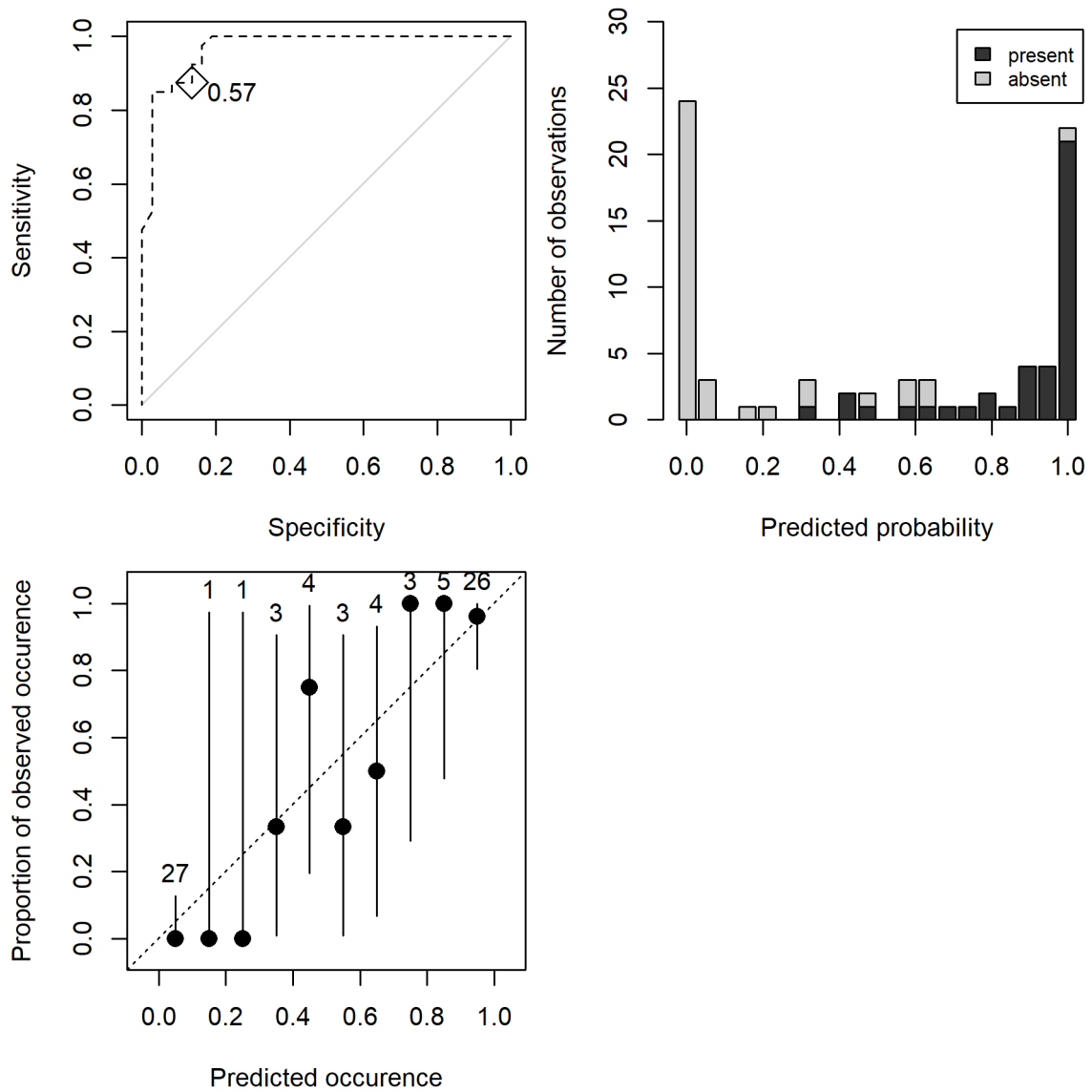


Figure 42: Model diagnostic plots for Hexactinellid presence or absence GAM.

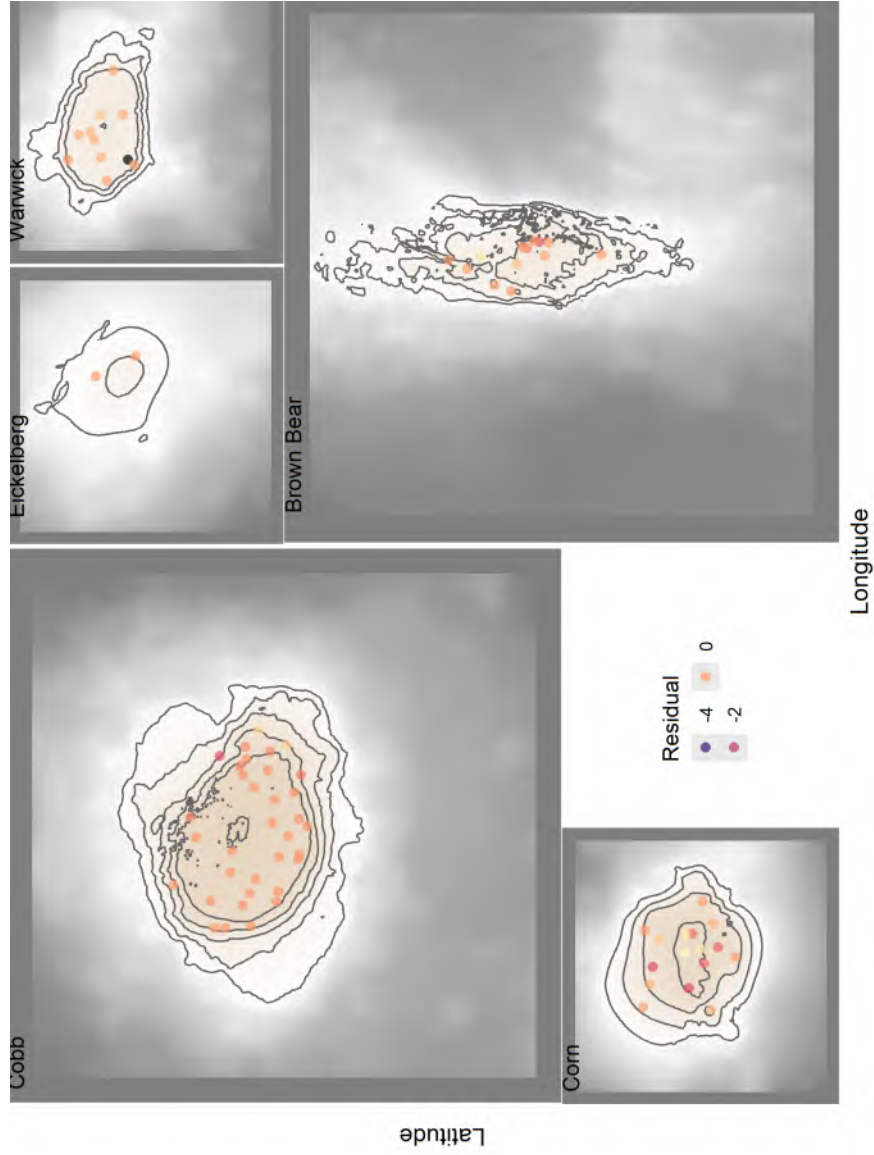


Figure 43: Spatial patterns in model Pearson residuals for G<sub>AM</sub> predicting probability of presence for Hexactinellids.

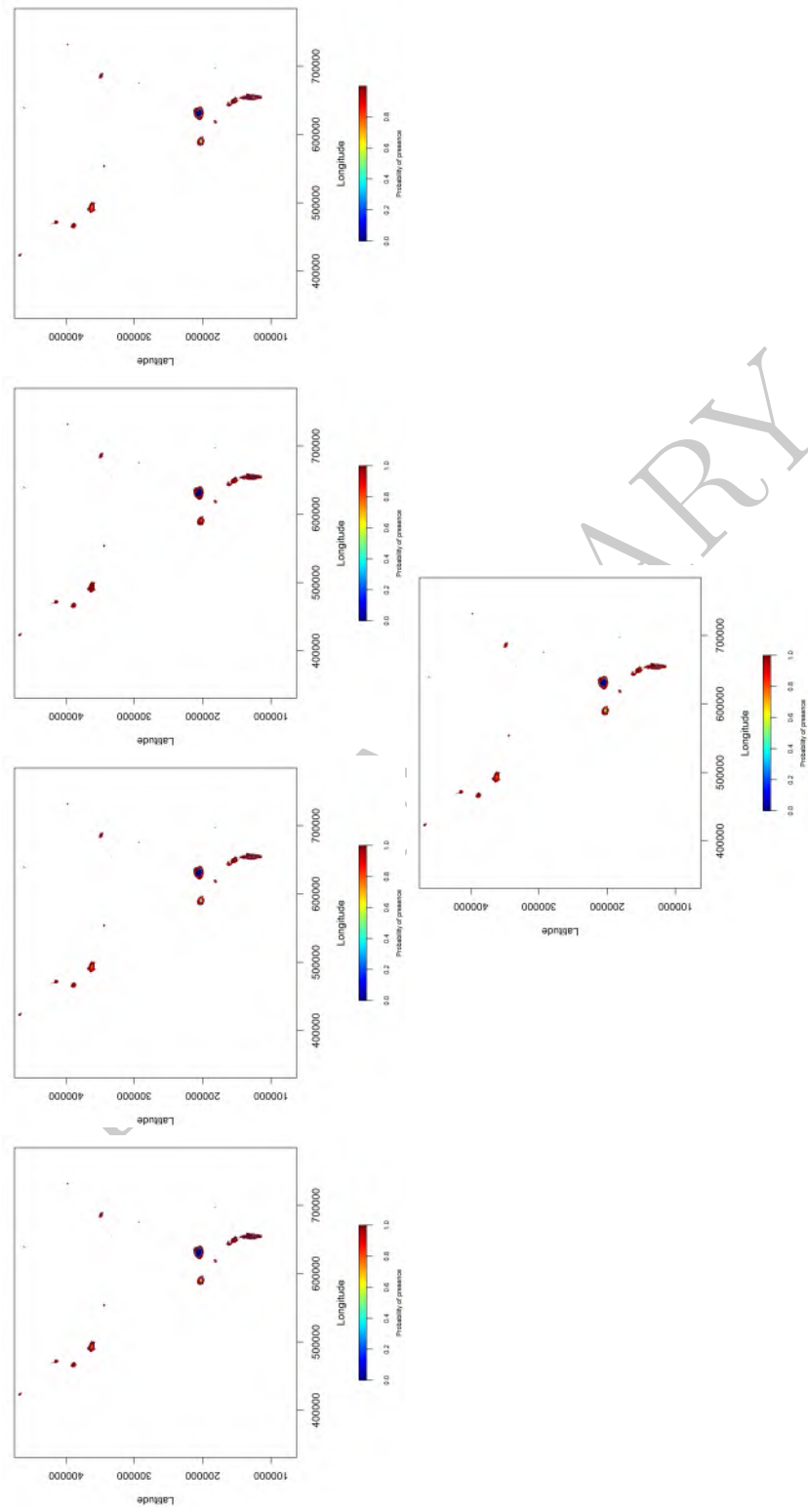


Figure 44: Maps of model predictions for 5 randomly selected folds of the data.

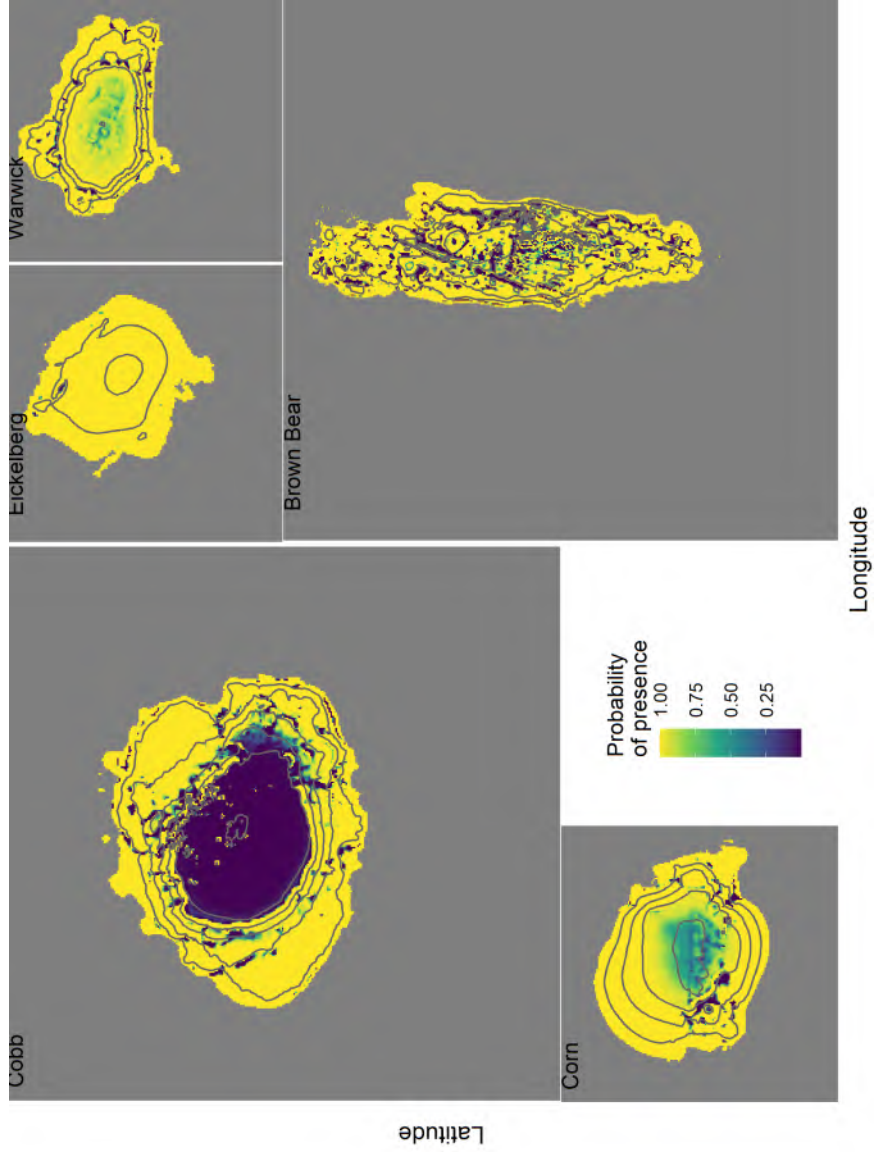


Figure 45: Predicted probability of presence for Hexactinellids at seamounts in the Cobb-Eickelberg seamount chain.

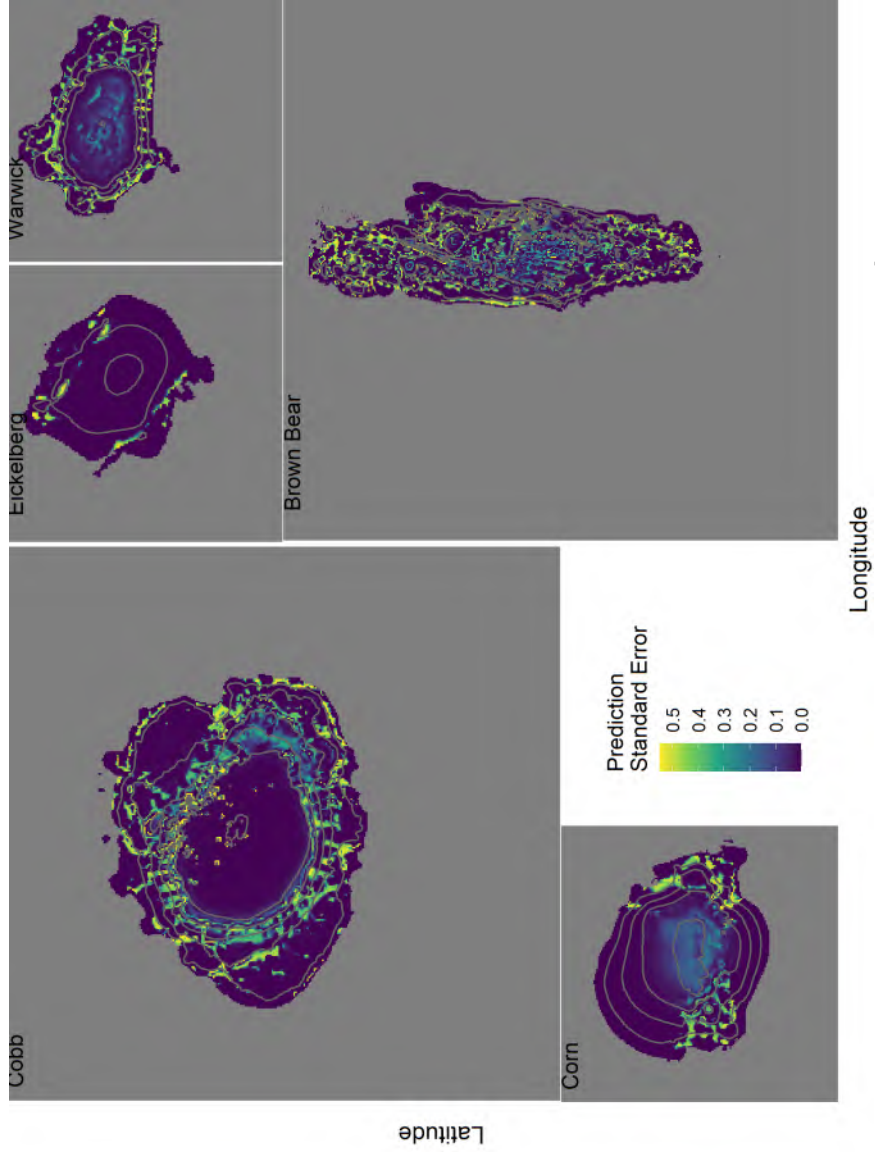


Figure 46: Spatial patterns in model prediction error for GAM predicting probability of Hexactinellids at seamounts in the Cobb-Eickelberg seamount chain.

## 6 Vulnerable Marine Indicator Taxa Group: *Demosponges*

### 6.1 Study resolution

#### 6.1.1 Location of the study area (or management region)

This modelling was carried out for five seamounts in the Northeastern Pacific Ocean where fisheries are managed by the North Pacific Fisheries Commission. The five seamounts are shown in Figure 1 and are part of the Cobb-Eickelberg seamount chain.

**6.1.1.1 Spatial extent of the modelled area** The specific seamounts modeled were five North Pacific Seamounts (Cobb, Brown Bear, Eickelberg, Warwick and Corn). Modeling was conducted from depths of 0 - 1250 m. Data was collected from 0 to ~850 m.

**6.1.1.2 Spatial resolution of the model and independent variables** The spatial resolution of the modeling was 100 m by 100 m grid cells. The all data was projected into an Albers equal area projection (proj4 description = “+proj=aea +lat\_0=45 +lon\_0=-126 +lat\_1=50 +lat\_2=58.5 +x\_0=1000000 +y\_0=0 +ellps=GRS80 +towgs84=0,0,0,0,0,0 +units=m +no\_defs”).

**6.1.1.3 Spatial precision (of observations and independent variables)** The spatial precision of the observations was taken from the gps mounted on the research vessel. Based on tracking information, the camera system was towed slightly behind the vessel (~200 m typically), but along the same path as the vessel. The anticipated precision of the variation of the camera path was expected to be less than 20 m across the trackline.

**6.1.1.4 Depth resolution/range/extent (of the observations and independent variables)** The depth range of the observations of *Demosponges* (from the depth sensor mounted on the camera) was from 61 to 808 m (mean = 442 m, SE = 206.28). The depth range of the modeled area was from 34 (the summit depth of Cobb Seamount) to 1250 m.

#### 6.1.2 Temporal extent of the data

**6.1.2.1 Dates of data extent** The dates observations used in model development were collected were September 6, 2022 to September 20, 2022. The dates for observations used for model testing were from September 3, 2024 to September 11, 2024.

**6.1.2.2 Precision of date/time** The precision of the date and the time of the data was assumed to be the closest second.

**6.1.2.3 Data/time resolution** The resolution of the date and time was fraction of a second.

**6.1.2.4 Impacts over time to consider in the data set (e.g. historical fishing effort)** Fishing occurred over the entire time frame from which these data points were collected. Fishing also has occurred historically since the 1970's. We did not attempt to account for historical fishing effort over this time. There may have been climate impacts occurring over the time frame of the data observations as well, however, these were not accounted for in the analyses.

### 6.2 Dependent data

The dependent data are shown in Figure 47.

Table 1. Number of records for each taxonomic grouping in the order *Demosponges* from the survey database.

Species or Taxa group	Count
Demospongiae	61

### 6.2.1 Data type (presence, absence, abundance)

The data used for modeling *Demosponges* distribution were observed presences (n = 12) and absences (n = 65) that occurred at the five seamounts.

### 6.2.2 Data source (e.g. type of survey(s) combined)

The data were entirely from random stratified surveys of the Cobb-Eickelberg seamount chain conducted in 2022.

### 6.2.3 Measure of sampling effort

Sampling effort was estimated by the distance the camera traveled along each transect multiplied by the field of view observed along the transect (Rooper et al. 2016). This provided an area observed for each transect which was used as the effort measure. Area observed ranged from 254 m<sup>2</sup> to 2469 with a median area observed of 1197 m<sup>2</sup>.

### 6.2.4 Detectability

Detectability of the width of the viewing area of the camera along the transect (area observed) was assumed to be 100% for VME indicator taxa. However, there were likely some individuals that were too small to be detected.

### 6.2.5 Taxonomic level

The taxonomic level modeled here was the taxonomic group *Demosponges* (see Table 1 for individual families included in this grouping and refer to CMM for NPFC definitions).

### 6.2.6 Functional attributes (its ecology)

*Demosponges* are a diverse, long-lived and fragile species. They occur in deep-water and are habitat forming structures important to many fishes, invertebrates other taxonomic groups.

### 6.2.7 Taxonomic confidence of species/assemblages

The taxonomic confidence of the assemblage was assumed to be good. Experts experienced in identification of corals and sponges from visual imagery in the North Pacific Ocean did all the identification and image analyses.

### 6.2.8 Rationale for taxonomic/assemblage level modeled

*Demosponges* as defined here are a group that shares common habitat requirements and depth distribution. They are closely related and the order is globally distributed at deep depths. This Order has been previously modelled using Maximum entropy methods on a global extent and regional extent (Yesson et al., 2017, Chu et al. 2018, Doherty et al. 2019).

### 6.2.9 Source of absence data

Absences were observations of no individuals at transects. In total there were 65 absences in the dataset.

### 6.2.10 Other potential errors or biases in the data

There are some potential sources of error in the data, including errors in positioning of the records, errors in species identification (including both false positives and false negatives).

### 6.2.11 Data filtering steps

No data filtering was conducted.

### 6.2.12 Taxonomic aggregation steps

The records for the Order *Demosponges* were aggregated by transect into presence or absence observations.

### 6.2.13 Method for combining dependent data sources (if done outside the modelling)

No other dependent data sources were used in this modelling.

## 6.3 Independent data

### 6.3.1 Independent data (environmental variables used)

Five independent variables were used in building a model of *Demosponges* distribution; bathymetry, topographic position index, seafloor slope, Oxygen concentration and northness (Figure 48).

### 6.3.2 Independent data source (source of raw or derived data)

The bathymetry used here was downloaded from the NOAA website (<https://www.ncei.noaa.gov/maps/bathymetry/>). It consists of gridded bathymetry from a multibeam sources on a 3 arc-second grid for the region of interest. The details of the data sources can be found on the NOAA website. There were some gaps in the NOAA bathymetry layers. These were filled using single beam echosounder data collected during the 2022 and 2024 cruises and GEBCO bathymetry ([www.gebco.net/data\\_and\\_products/gridded\\_bathymetry\\_data](http://www.gebco.net/data_and_products/gridded_bathymetry_data)). The single beam echosounder data and GEBCO bathymetry was sampled into the missing grids in the NOAA bathymetry, with preference to the single beam echosounder data.

From the bathymetry two derived variables (slope and topographic position index) were calculated using the raster package (Hijmans 2019). Slope was calculated from the nearest 8 neighbors and TPI was calculated with a focal distance of ~300 m.

Northness was calculated as the cosine of the aspect (direction relative to 0 degrees that the slope was facing) for each grid cell based on bathymetry.

Oxygen data were based on the World Ocean Atlas data (2018 update). These data were clipped to the area of interest and resampled into the bathymetry grid using bilinear interpolation. The five explanatory variables are shown in Figure 48.

### 6.3.3 Native spatial and temporal resolution of the independent data

The native spatial resolution of the NOAA bathymetry was 3 arc-second grid. The native spatial resolution for the Oxygen data was 0.5 degrees longitude and latitude. It should be noted that the Oxygen data sources are conglomerations of data collected over varying spatial and temporal scales (e.g. the temporal scale is since ~1900's in the case of some measurements). For complete documentation of the spatial and temporal scale of the raw data the NODC respective website should be consulted ([www.gebco.net/data\\_and\\_products/gridded\\_bathymetry\\_data](http://www.gebco.net/data_and_products/gridded_bathymetry_data) and <https://www.nodc.noaa.gov/OC5/woa18/>).

All independent data layers were trimmed to include only observations and explanatory variables from this region and to depths of 1250 m.

### 6.3.4 Data processing and scaling (method for downscaling or aggregation)

Both the bathymetry (for gap filling) and oxygen layers were downscaled to a 100 m by 100 m grid in order to match the scale of the bathymetry. This downscaling was completed using bilinear interpolation.

**6.3.4.1 Goodness of fit for downscaled aggregated data** The downscaled data at the dependent data sites for both Oxygen and bathymetry represented the lower resolution very well ( $r > 0.9$ ).

**6.3.4.2 Measurement errors and bias** Measurement errors in the data or bias in the data were not accounted for beyond the processing conducted on the raw measurements by GEBCO or NODC.

### 6.3.5 Derivation methods and calculations for derived variables

From the bathymetry three derived variables (aspect, slope and topographic position index) were calculated using the raster package (Hijmans 2019). These variables were calculated on bathymetry aggregated (see below) to a 100 m by 100 m grid. The aspect variable was then converted to northness using a cosine function.

### 6.3.6 Rationale for inclusion of independent variables clearly stated and ecologically relevant

These five variables (depth, slope, topographic position index, northness and oxygen) have been found in previous studies to influence the distribution of *Demosponges* (Huff et al., 2013, Yesson et al., 2017, Etnoyer et al., 2018).

## 6.4 Modelling approach

In this study generalized additive models (GAM) were developed to predict species distribution (Wood 2006).

### 6.4.1 Model steps

**6.4.1.1 Code for model provided** The code and data used for this model are not currently publicly available, but can be available on request from Chris Rooper (chris.rooper@dfo-mpo.gc.ca).

**6.4.1.2 Packages used are referenced** The packages used to develop this model are referenced in the above .Rmd file. The key packages used were “sf”, “rnaturalearth”, “ggplot2”, “rgdal”, “rgeos”, “gstat”, “raster”, “mgcv” and are all available for download from CRAN. The R version used here was R version 3.6.0 (2019-04-26) – “Planting of a Tree” (R Core Development Team 2019).

**6.4.1.3 Data is made available as supplementary material** The independent variables are available from Chris Rooper (chris.rooper@dfo-mpo.gc.ca).

### 6.4.2 Biases (spatial, temporal and other) acknowledged and described

There were no inherent biases in the modeling method (although there may be biases in the dependent and independent data described above).

### 6.4.3 Methods and approaches to collinearity in independent variables

**6.4.3.1 Collinearity in independent variables** The five explanatory variables were examined for collinearity using a pearson correlations (Figure 49). Variance inflation factors (Zuur et al. 2002) were also examined. In both cases the values were low, suggesting that the variables were fairly independent of each other.

Table 2. Variance inflation factors for independent variables using in modeling.

Variable	VIF
Depth	3.592
Slope	1.231
TPI	1.091
Oxygen	3.372
Northness	1.065

**6.4.3.2 Criteria for variable/dimension reduction provided** None of the variance inflation factors exceeded 5, indicating that dimension reduction was not warranted.

#### 6.4.4 Choice of modelling method is explained and justified

The modelling method chosen was a generalized additive model (GAM). This model was primarily chosen for its simplicity of assumptions (stated below), its usefulness in fitting binomial (presence-absence) data, and the many previous applications of this method to predicting species distributions.

**6.4.4.1 Modelling assumptions are clearly stated** The basic GAM assumptions are; 1) Independence among data points, 2) The distribution of the residuals is binomially distributed, 3) homogenous variance across the fitted values, and 4) a non-linear relationship between response and predictor.

**6.4.4.2 Potential violations of model assumptions are explored** Diagnostic plots of Pearson residuals are shown in Figure 50. The residuals did not indicate any serious violations of GAM assumptions.

#### 6.4.5 Model application

To build the model of *Demosponges* a generalized additive model was constructed that contained five explanatory variables (depth, slope, topographic position index, northness and oxygen). The dependent data was presence or absence of *Demosponges*. The full model was

$$y = \alpha + s(\text{depth}) + s(\text{slope}) + s(\text{TPI}) + s(\text{northness}) + s(\text{O}_2) + \sigma$$

A binomial error distribution ( $\sigma$ ) was used for the model fitting. A full model was fit initially containing all the variables with a basis degrees of freedom of 4 for each smooth. This model was reduced sequentially by removing the least significant term and comparing the AIC for the resulting reduced model following the methods of Rooper et al. (2016). This was repeated until there was a decline in model skill when removing a variable.

**6.4.5.1 Model settings** The default GAM settings in R were used (see `CobbSDM_Demosponge.Rmd`). The only setting that was modified was the specification of the binomial error distribution and the specified number of knots for the smooth of  $k = 4$ .

**6.4.5.2 Model complexity is assessed** The results of the sequential variable reduction resulted in the retention of 2 terms; depth, O<sub>2</sub>. The deviance explained by the model ( $D^2$ ) was 0.096.

The model complexity was assessed against simpler models with less terms during the sequential variable reduction step and the most complex model (containing these terms) was found to be the most appropriate (Table 3).

Table 3. Summary of GAM model predicting presence or absence of *Demosponges*.

Term	edf	F	p-value
depth	1.00	2.496	0.1141
O <sub>2</sub>	1.00	3.701	0.0544

Term	edf	F	p-value
residual	74.00		
GCV	-0.14		
Deviance explained (%)	9.60		

#### 6.4.6 Model response curves are generated (where appropriate) and compared to expectations

Model response curves are shown in Figure 51. Probability of presence of *Demosponges* was highest at depths < 500 m in low oxygen areas. None of the results were abnormal or unexpected.

##### 6.4.6.1 Modelling method-specific term estimates or coefficients are reported (where relevant)

The model specific term estimates are provided in Table 4.

Table 4. Model coefficients, significance and standard error estimates for GAM predicting *Demosponges* probability of presence.

	x
(Intercept)	-2.105
s(depth).1	0.000
s(depth).2	0.000
s(depth).3	-1.262
s(O2).1	0.000
s(O2).2	0.000
s(O2).3	-2.084

**6.4.6.2 Independent variable importance is reported** The relative importance of variables in the model was measured by sequentially removing the individual variables, fitting a new model and calculating the deviance explained. The deviance explained was then scaled to the full model to determine the relative drop in model goodness-of-fit with removal of each variable. The results showed that oxygen concentration and depth were of relatively equal importance in determining the probability of *Demosponges* presence (Figure 52).

## 6.5 Model uncertainty

### 6.5.1 Model specific goodness of fit statistics have been checked and reported

The *Demosponges* model AUC was 0.713, a good model according to the standards of Hosmer et al., (2013).

Using a threshold of 0.14 resulted in prediction of 11 of the 12 observed presences correctly, while predicting about 49% of the absences correctly (sensitivity = 0.917 and specificity = 0.492).

Table 5. Confusion matrix of predicted and observed presence and absence of *Demosponges* using a probability threshold 0.14.

	Observed	
Predicted	Presence	Absence
Presence	11	33
Absence	1	32

**6.5.1.1 Multiple measures of goodness of fit have been examined** Commonly used goodness-of-fit measures for binomial models are provided in Table 5 for the GLM predicting *Demosponges* probability of presence. These include the True Skill Statistic (Allouche et al., 2006), the root-mean-squared-error and the

Spearman's rank correlation. Other threshold dependent metrics can be calculated from the confusion matrix (Table 4).

Model diagnostics indicated some minor issues with the prediction of presence or absence (Figure 53). There were often absences in the higher probability areas, which could indicate the model did not fit well.

### 6.5.2 Spatial autocorrelation in the residuals has been assessed and reported

There was not significant spatial autocorrelation in the model residuals measured by Moran's I ( $I = 0.06$ ). However, this value was close to significant. This was not unexpected given the random-stratified sample design of observations in the study area.

### 6.5.3 Residuals have been tested against assumed distribution (where appropriate)

Not applicable for the binomial distribution. Figure 50 shows model residuals (on the logit scale are shown for each data point used to model *Demosponges* and diagnostics.

**6.5.3.1 Spatial patterns in residuals** Model residuals are shown in Figure 54. This confirms the results of the Moran's I, with little evidence of spatial patterns in the residuals.

## 6.6 Model validation

### 6.6.1 Training and testing data splitting method

Both internal model validation method and independent data was used as a validation data set. K-fold cross-validation was used here. Five (k) folds were chosen at random.

**6.6.1.1 Potential spatial biases were accounted for in splitting the data** The spatial blocking method (Valvani et al., 2019) was *not* used to split the data for the internal cross-validation.

**6.6.1.2 A standard method used for cross-validation** k-fold cross-validation is a standard method. The data was divided into 5 equal portions and a model then fit to 80% of the data and tested against the remaining 20% of the data. This was repeated for each subdivision of the data. The same maps and diagnostics were produced for each model fit on the k-folds.

The data folds appeared to show the same patterns as the full model.

The model performance was similar for all the training data sets (the full model and the individual folds). However the performance of the model on the testing folds was less impressive. For example, the True Skill Statistic and AUC for model folds 2, 3 and 5 was very poor, indicating some potential issues with model performance. There were relatively few presence observations in the data set, which may have resulted in these random splits of the data with few presence observations to fit the model.

### 6.6.2 Truly independent data used for model validation

The presence and absence observations from 58 transects completed in 2024 was also used to test the models developed on the 2022 survey data.

The *Demosponges* model AUC was 0.838, an excellent performing model according to the standards of Hosmer et al., (2013).

Using a threshold of 0.14, 0.14 resulted in prediction of 10 of the 13 observed presences correctly, while predicting about 76% of the absences correctly (sensitivity = 0.769 and specificity = 0.756)

Table 6. Confusion matrix of predicted and observed presence and absence of *Demosponges* using a probability threshold 0.14, 0.14 for the independently collected data set in 2024.

Observed		
Predicted	Presence	Absence
Presence	10	11
Absence	3	34

Table 6. Model goodness of fit measures for the full model and the individual model validation folds

Fold	AIC	threshold	AUC_training	AUC_testing	TSS_training	TSS_testing
Full model	66.257	0.140	0.713	NA	0.409	NA
Fold_1	60.187	0.130	0.602	0.714	0.242	0.571
Fold_2	42.411	0.080	0.576	0.650	0.252	0.200
Fold_3	52.273	0.125	0.642	0.583	0.342	-0.083
Fold_4	55.308	0.125	0.691	0.867	0.400	-0.667
Fold_5	59.505	0.130	0.626	0.571	0.262	0.500

Fold	Cor_training	Cor_testing	RMSE_training	RMSE_testing
Full model	0.267	NA	0.352	NA
Fold_1	0.136	0.186	0.378	0.253
Fold_2	0.078	0.252	0.296	0.545
Fold_3	0.173	0.116	0.345	0.401
Fold_4	0.254	-0.308	0.368	0.316
Fold_5	0.166	0.062	0.376	0.264

## 6.7 Model outputs

### 6.7.1 Maps of model predictions, model residuals and prediction error

Maps of model predictions are provided in Figure 56. Maps of residuals in Figure 54. Maps of prediction error in Figure 57. The model predicted that the highest probability of presence for *Demosponges* was near the summits of each of the seamounts.

### 6.7.2 Areas of model extrapolation are clearly defined

The model was not extrapolated outside the five seamounts, although within this region, there were some areas with little or no sampling. The model was extrapolated at depths from 850 - 1250 m where no sampling occurred.

### 6.7.3 The prediction unit is clearly defined (and explained if necessary)

The prediction unit is the probability of presence or absence of *Demosponges*.

### 6.7.4 Thresholding methods (for dichotomising probability into presence or absence) are clearly described and appropriate

No thresholding was done (beyond the thresholding for calculating goodness-of-fit measures). Probability of presence is presented as the result.

#### 6.7.4.1 The sensitivity of model outcomes to threshold value chosen has been explored

Sensitivity to threshold values was not explored, but in a formal analysis of the model could be completed using the provided model outputs.

## 6.8 Conclusions

The *Demosponges* model fit the observations from 2022 well. The internal model validation showed somewhat robust results. The independently collected data were predicted with excellent accuracy.

Model response curves showed the importance of depth. At depths above 500 m, there was a high probability of *Demosponges* presence on a randomly chosen transect.

PRELIMINARY

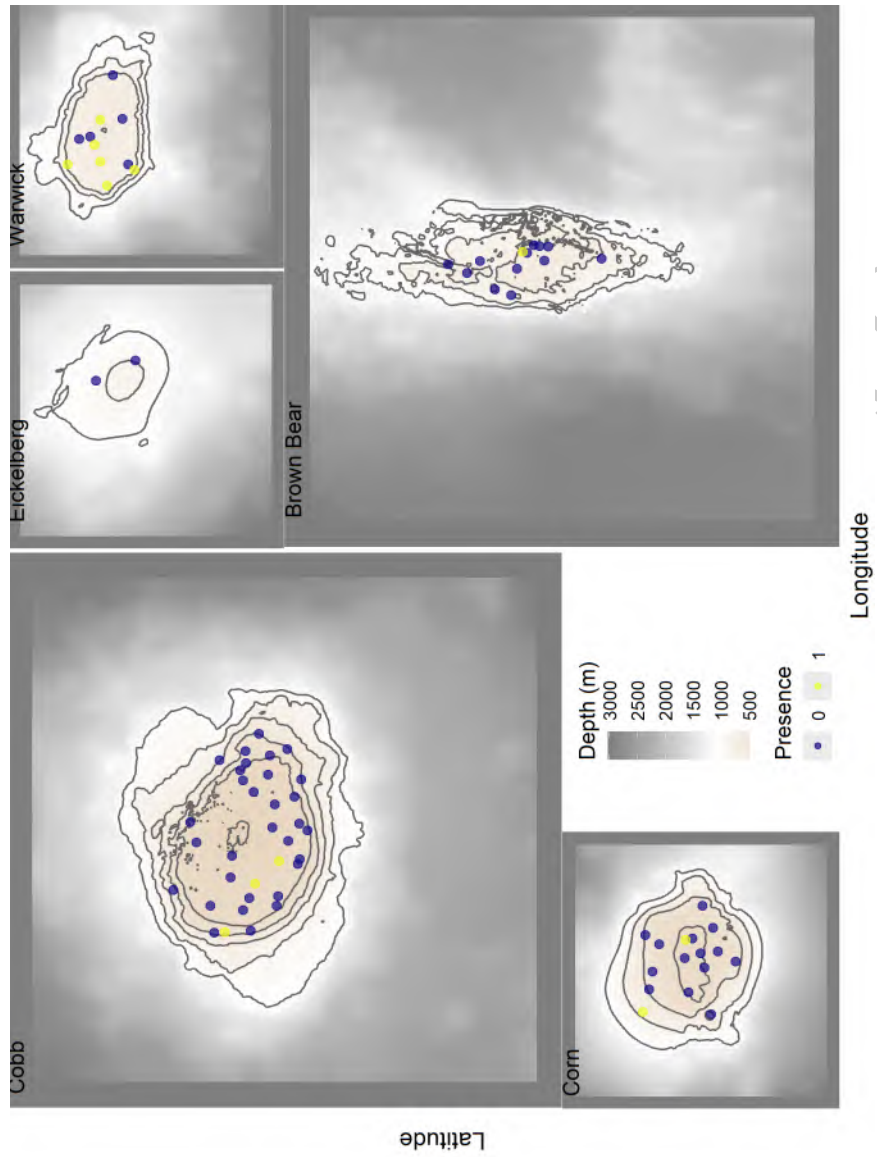


Figure 47: Locations of presence and absence transects for Demosponges from 2022 and 2024 stereo-camera survey

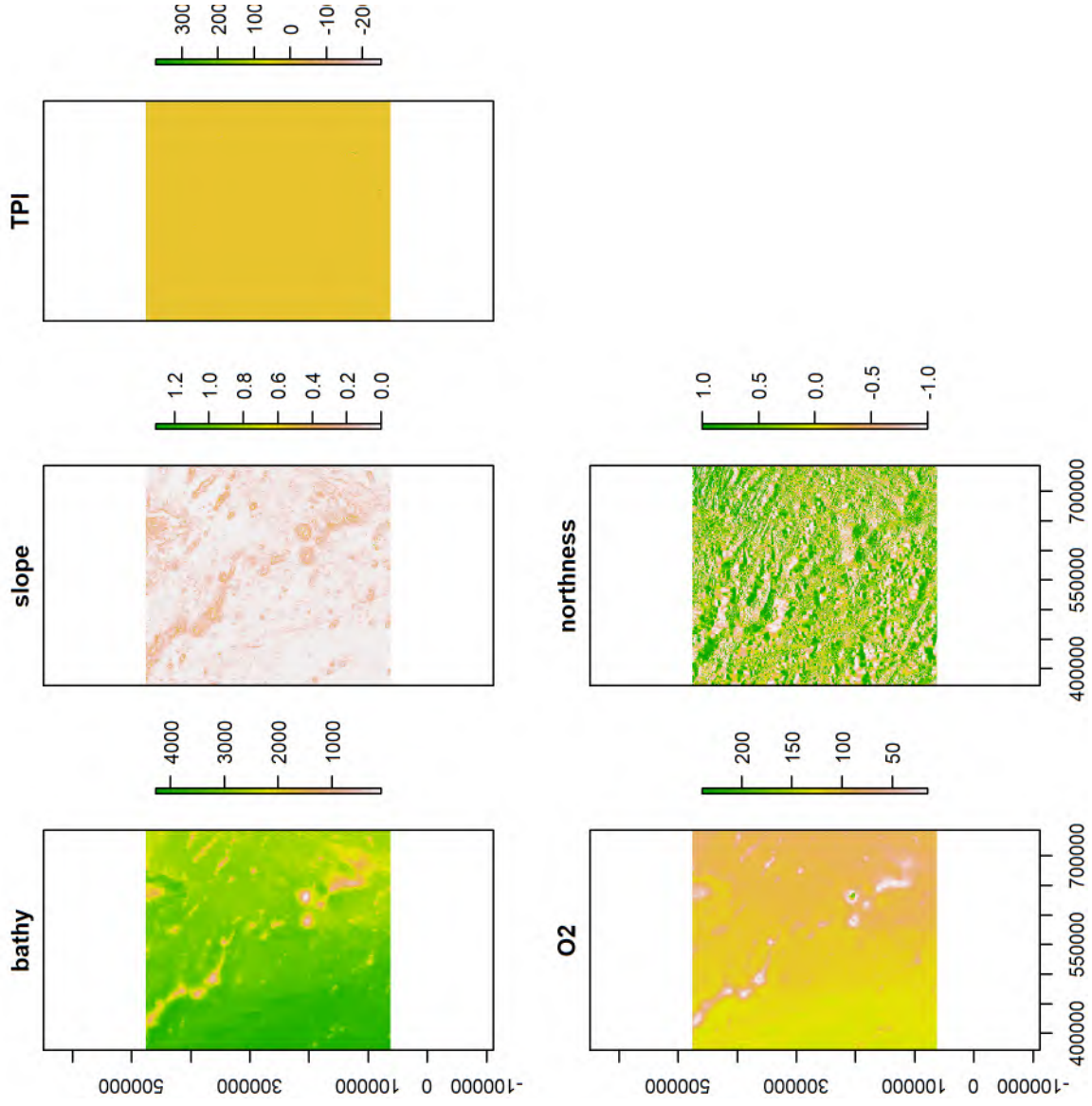


Figure 48: Map of bathymetry, slope, TPI, Oxygen and northness used as explanatory variables in this analysis of VME data

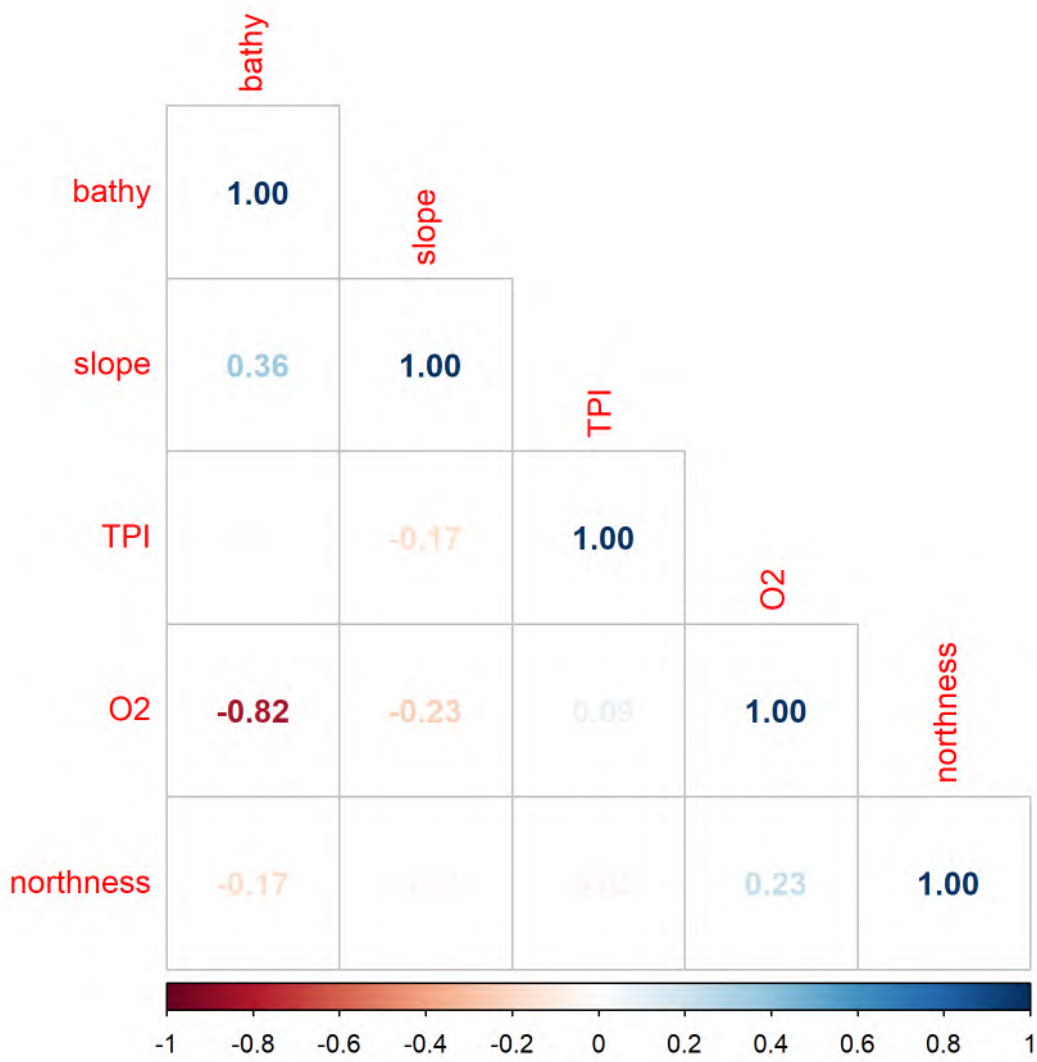


Figure 49: Correlation among independent variables used in modeling.

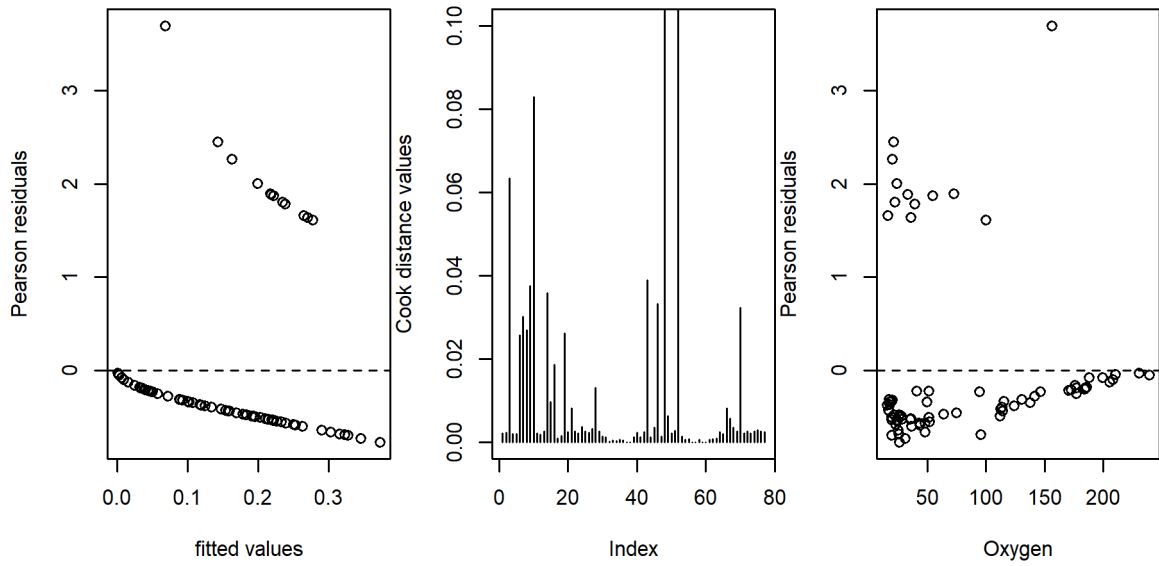


Figure 50: Diagnostic plots for GAM model assumptions.

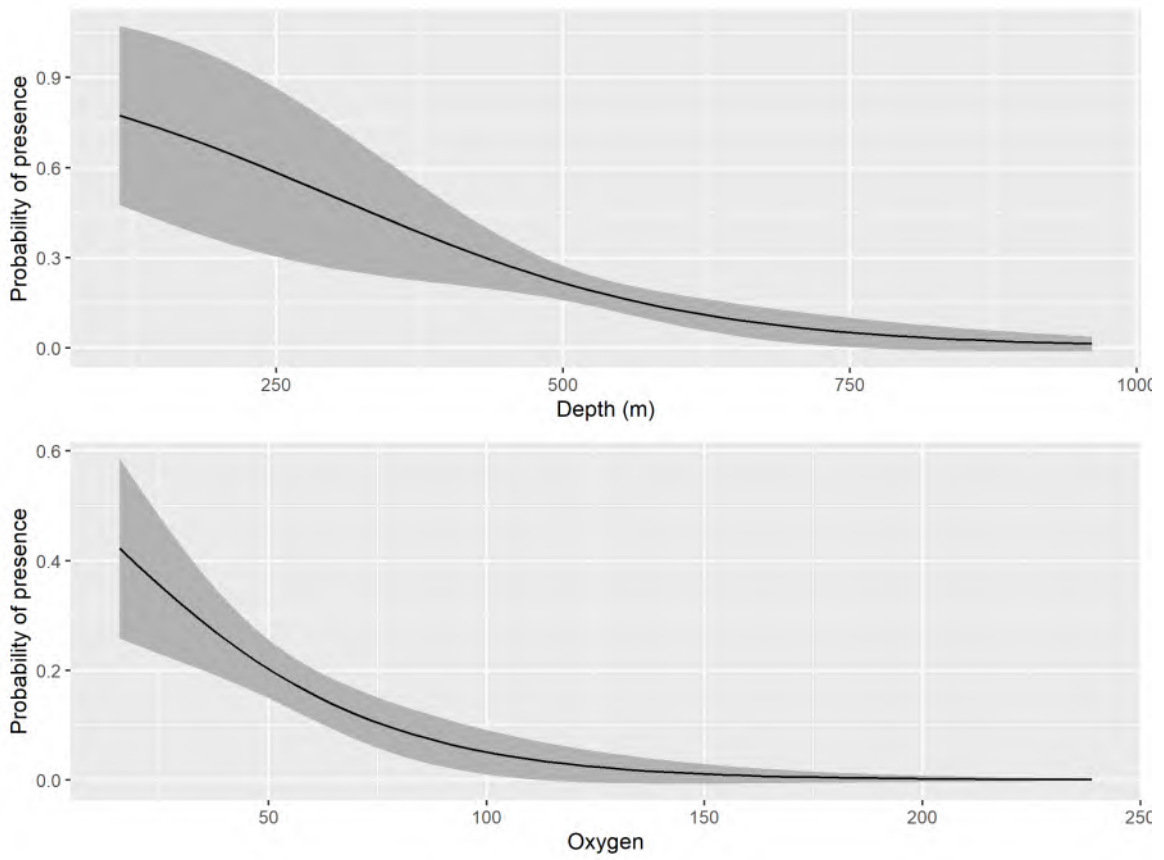


Figure 51: Response curves for independent variables used best-fitting GAM for presence or absence.

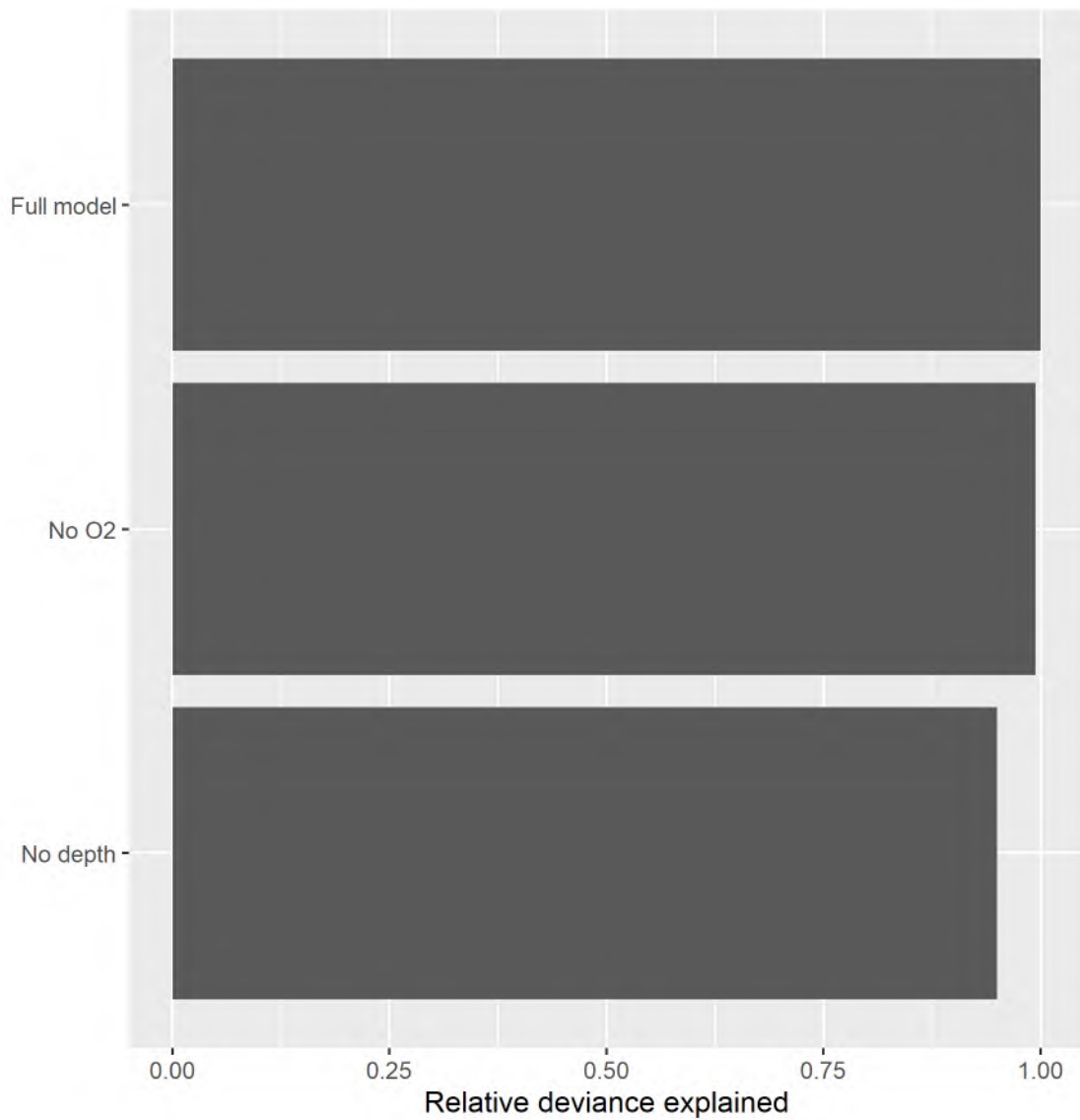


Figure 52: Relative importance of variables included in the Demosponge presence or absence GAM measured by their contribution to deviance explained when sequentially removed from the model.

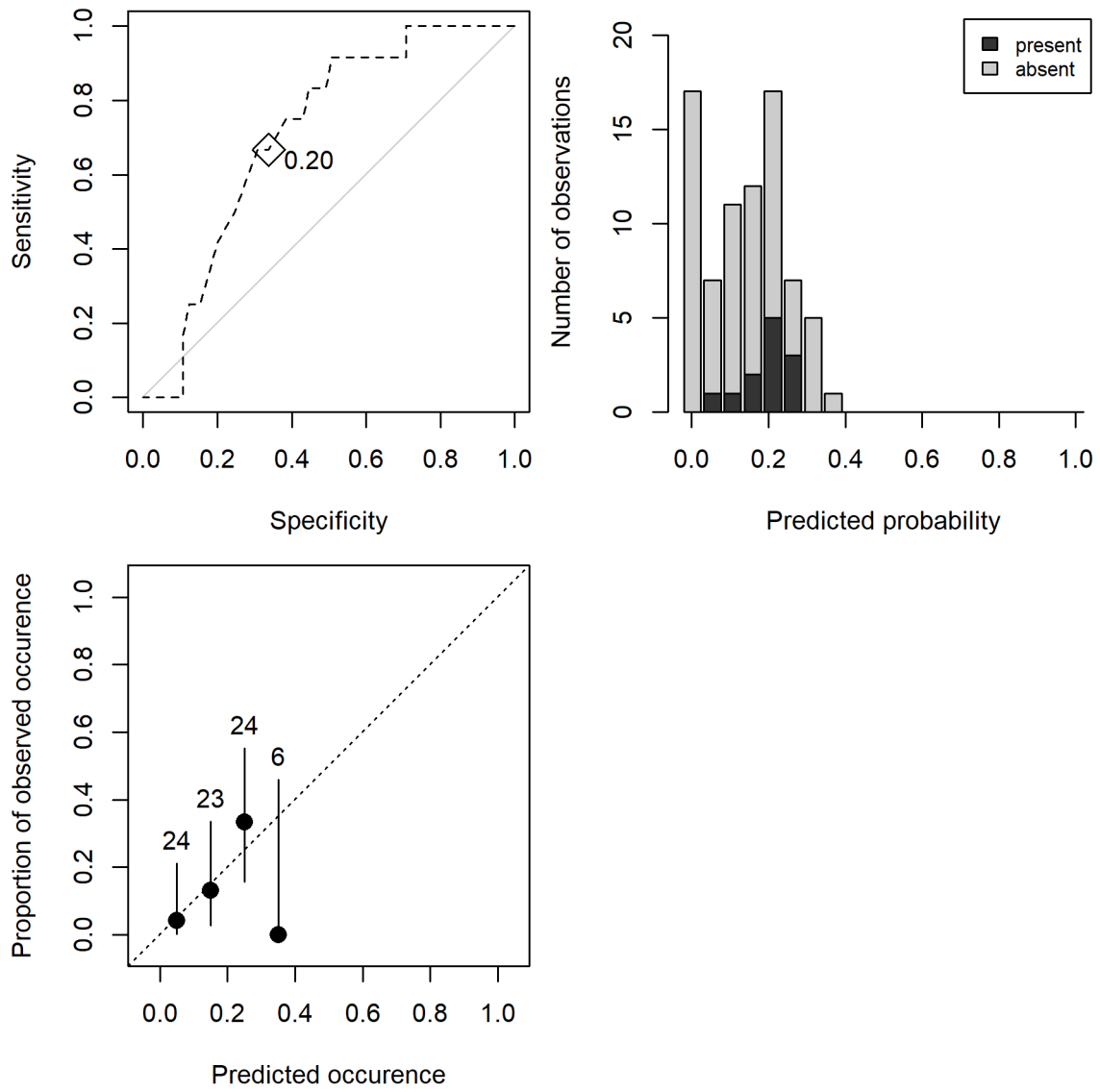


Figure 53: Model diagnostic plots for Demosponge presence or absence GAM.

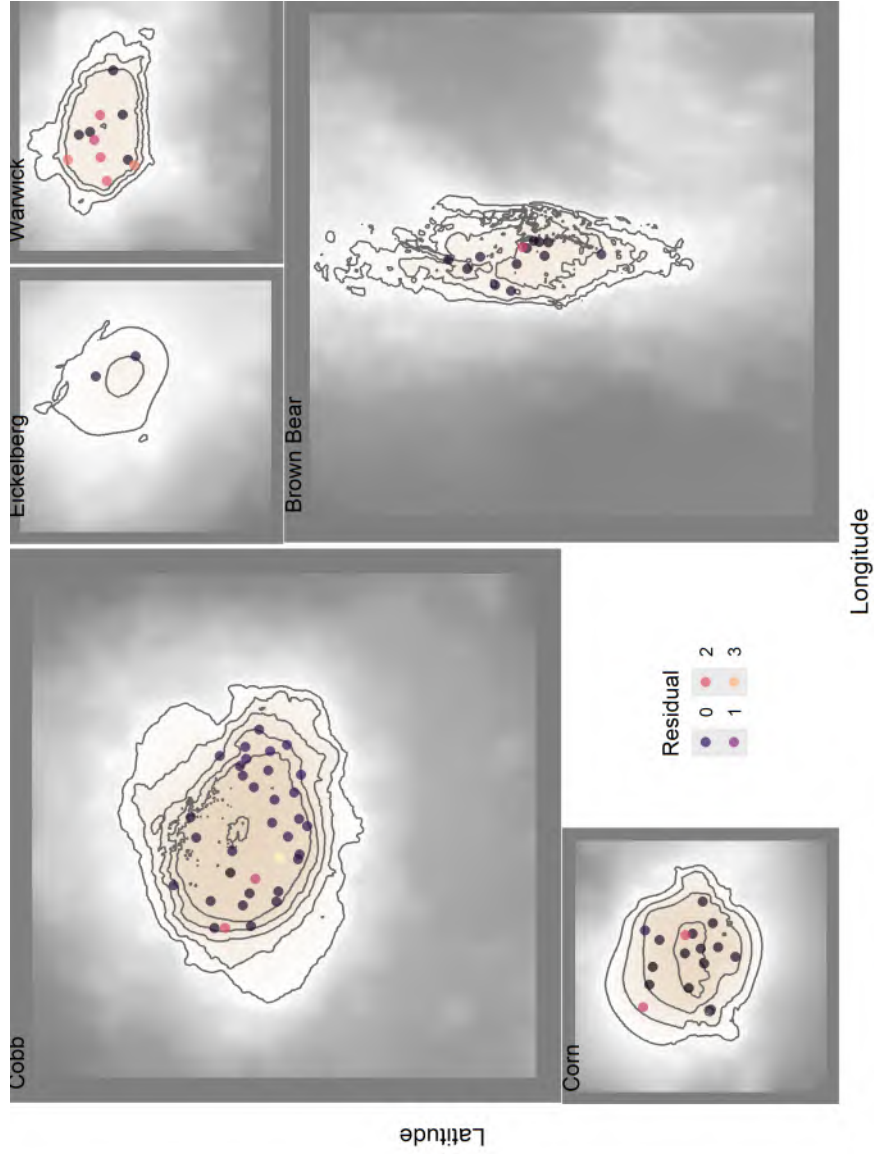


Figure 54: Spatial patterns in model Pearson residuals for GAM predicting probability of presence for Demosponges.

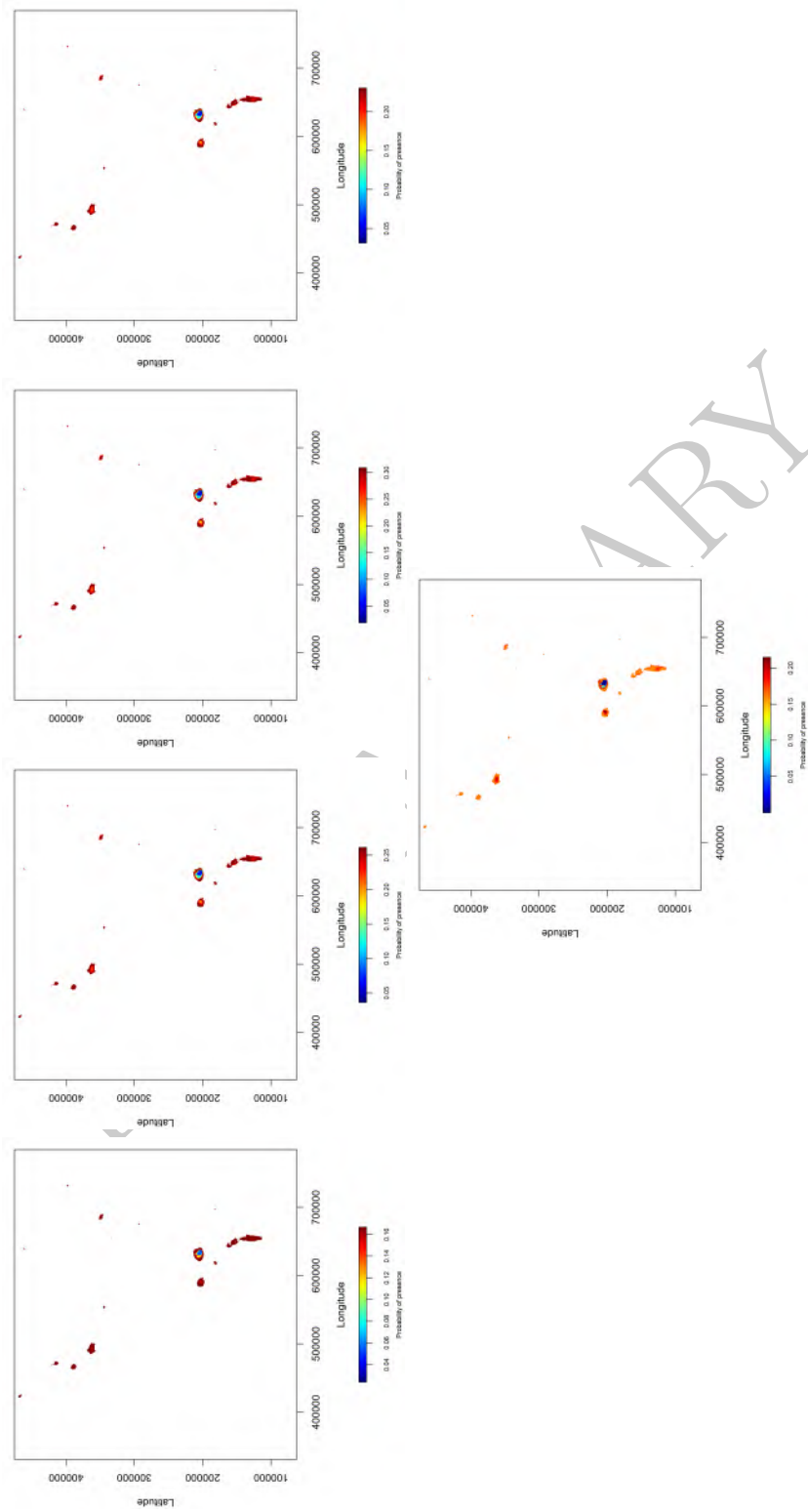


Figure 55: Maps of model predictions for 5 randomly selected folds of the data.

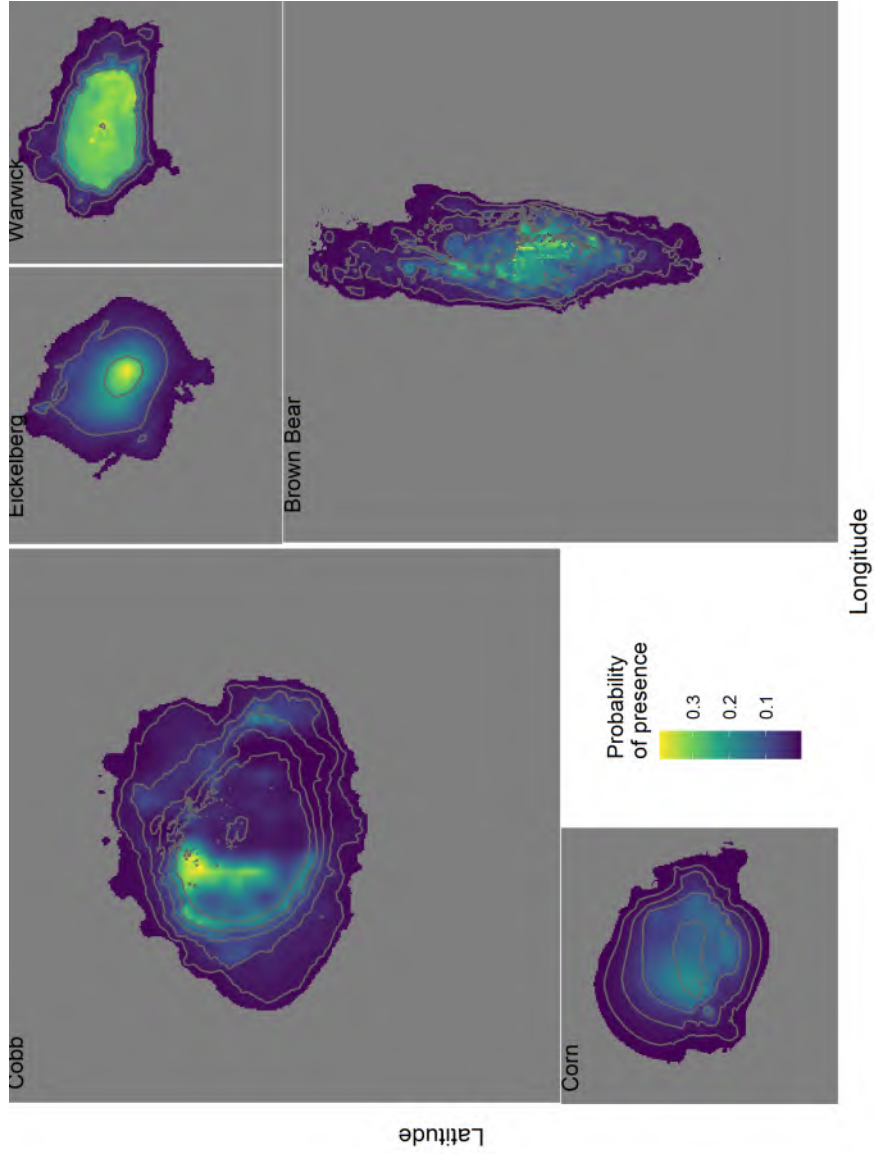


Figure 56: Predicted probability of presence for Demosponges at seamounts in the Cobb-Eickelberg seamount chain.

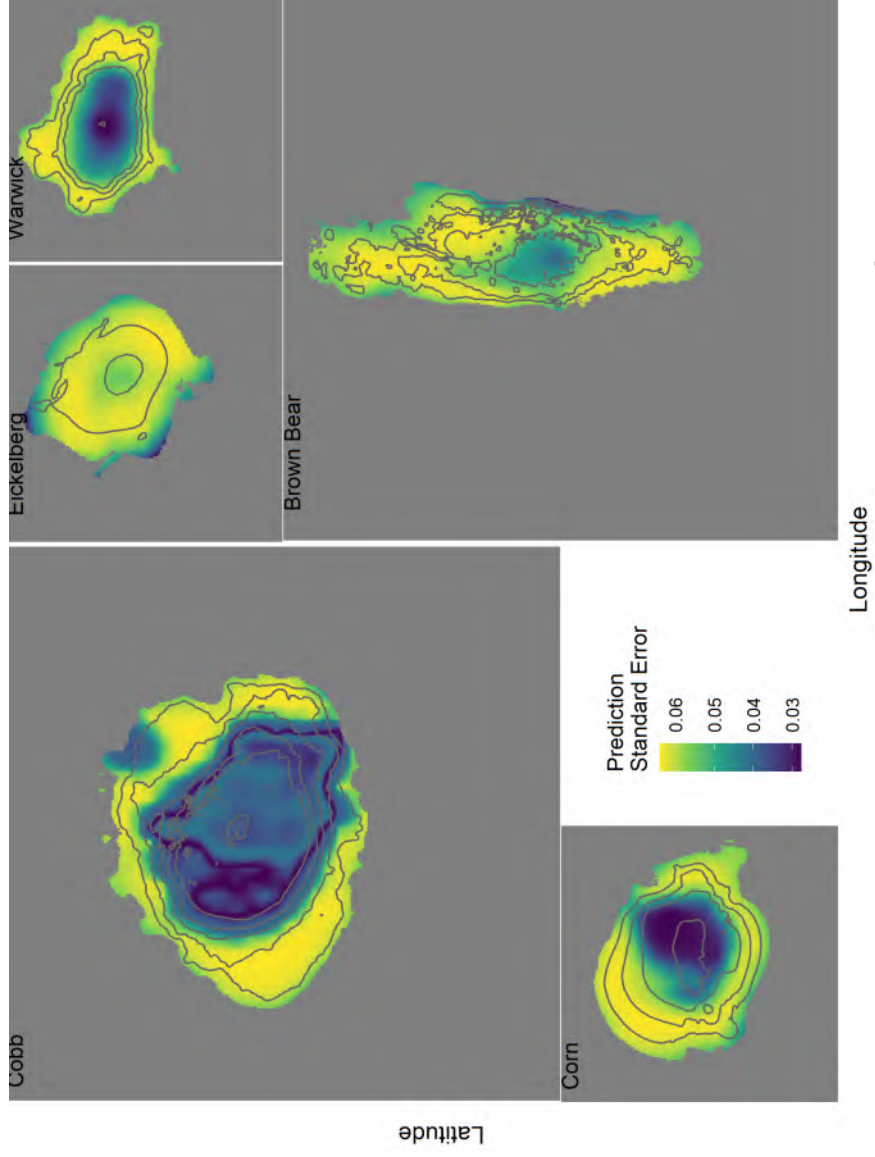


Figure 57: Spatial patterns in model prediction error for GAM predicting probability of Demosponges at seamounts in the Cobb-Eickelberg seamount chain.

## 7 Vulnerable Marine Indicator Taxa Group: *Pennatulaceans*

### 7.1 Study resolution

#### 7.1.1 Location of the study area (or management region)

This modelling was carried out for five seamounts in the Northeastern Pacific Ocean where fisheries are managed by the North Pacific Fisheries Commission. The five seamounts are shown in Figure 1 and are part of the Cobb-Eickelberg seamount chain.

**7.1.1.1 Spatial extent of the modelled area** The specific seamounts modeled were five North Pacific Seamounts (Cobb, Brown Bear, Eickelberg, Warwick and Corn). Modeling was conducted from depths of 0 - 1250 m. Data was collected from 0 to ~850 m.

**7.1.1.2 Spatial resolution of the model and independent variables** The spatial resolution of the modeling was 100 m by 100 m grid cells. The all data was projected into an Albers equal area projection (proj4 description = “+proj=aea +lat\_0=45 +lon\_0=-126 +lat\_1=50 +lat\_2=58.5 +x\_0=1000000 +y\_0=0 +ellps=GRS80 +towgs84=0,0,0,0,0,0 +units=m +no\_defs”).

**7.1.1.3 Spatial precision (of observations and independent variables)** The spatial precision of the observations was taken from the gps mounted on the research vessel. Based on tracking information, the camera system was towed slightly behind the vessel (~200 m typically), but along the same path as the vessel. The anticipated precision of the variation of the camera path was expected to be less than 20 m across the trackline.

**7.1.1.4 Depth resolution/range/extent (of the observations and independent variables)** The depth range of the observations of *Pennatulaceans* (from the depth sensor mounted on the camera) was from 61 to 808 m (mean = 442 m, SE = 206.28). The depth range of the modeled area was from 34 (the summit depth of Cobb Seamount) to 1250 m.

#### 7.1.2 Temporal extent of the data

**7.1.2.1 Dates of data extent** The dates observations used in model development were collected were September 6, 2022 to September 20, 2022. The dates for observations used for model testing were from September 3, 2024 to September 11, 2024.

**7.1.2.2 Precision of date/time** The precision of the date and the time of the data was assumed to be the closest second.

**7.1.2.3 Data/time resolution** The resolution of the date and time was fraction of a second.

**7.1.2.4 Impacts over time to consider in the data set (e.g. historical fishing effort)** Fishing occurred over the entire time frame from which these data points were collected. Fishing also has occurred historically since the 1970's. We did not attempt to account for historical fishing effort over this time. There may have been climate impacts occurring over the time frame of the data observations as well, however, these were not accounted for in the analyses.

### 7.2 Dependent data

The dependent data are shown in Figure 58.

Table 1. Number of records for each taxonomic grouping in the order *Pennatulaceans* from the survey database.

	Species or Taxa group	Count
2	Balticina	63
4	Pennatulacea	62
1	Anthoptilum sp	7
3	Lithoptilum lithophilum	4
5	Umbellula lindahli	1

### 7.2.1 Data type (presence, absence, abundance)

The data used for modeling *Pennatulaceans* distribution were observed presences ( $n = 41$ ) and absences ( $n = 36$ ) that occurred at the five seamounts.

### 7.2.2 Data source (e.g. type of survey(s) combined)

The data were entirely from random stratified surveys of the Cobb-Eickelberg seamount chain conducted in 2022.

### 7.2.3 Measure of sampling effort

Sampling effort was estimated by the distance the camera traveled along each transect multiplied by the field of view observed along the transect (Rooper et al. 2016). This provided an area observed for each transect which was used as the effort measure. Area observed ranged from 254 to 2469 m<sup>2</sup> with a median area observed of 1197 m<sup>2</sup>.

### 7.2.4 Detectability

Detectability of the width of the viewing area of the camera along the transect (area observed) was assumed to be 100% for VME indicator taxa. However, there were likely some individuals that were too small to be detected.

### 7.2.5 Taxonomic level

The taxonomic level modeled here was the taxonomic group *Pennatulaceans* (see Table 1 for individual families included in this grouping and refer to CMM for NPFC definitions).

### 7.2.6 Functional attributes (its ecology)

*Pennatulaceans* are a diverse, long-lived and fragile species. They occur in deep-water and are habitat forming structures important to many fishes, invertebrates other taxonomic groups.

### 7.2.7 Taxonomic confidence of species/assemblages

The taxonomic confidence of the assemblage was assumed to be good. Experts experienced in identification of corals and sponges from visual imagery in the North Pacific Ocean did all the identification and image analyses.

### 7.2.8 Rationale for taxonomic/assemblage level modeled

*Pennatulaceans* as defined here are a group that shares common habitat requirements and depth distribution. They are closely related and the order is globally distributed at deep depths. This Order has been previously modelled using Maximum entropy methods on a global extent and regional extent (Yesson et al., 2017, Chu et al. 2018, Doherty et al. 2019).

### 7.2.9 Source of absence data

Absences were observations of no individuals at transects. In total there were 36 absences in the dataset.

### 7.2.10 Other potential errors or biases in the data

There are some potential sources of error in the data, including errors in positioning of the records, errors in species identification (including both false positives and false negatives).

### 7.2.11 Data filtering steps

No data filtering was conducted.

### 7.2.12 Taxonomic aggregation steps

The records for the Order *Pennatulaceans* were aggregated by transect into presence or absence observations.

### 7.2.13 Method for combining dependent data sources (if done outside the modelling)

No other dependent data sources were used in this modelling.

## 7.3 Independent data

### 7.3.1 Independent data (environmental variables used)

Five independent variables were used in building a model of *Pennatulaceans* distribution; bathymetry, topographic position index, seafloor slope, Oxygen concentration and northness (Figure 59).

### 7.3.2 Independent data source (source of raw or derived data)

The bathymetry used here was downloaded from the NOAA website (<https://www.ncei.noaa.gov/maps/bathymetry/>). It consists of gridded bathymetry from a multibeam sources on a 3 arc-second grid for the region of interest. The details of the data sources can be found on the NOAA website. There were some gaps in the NOAA bathymetry layers. These were filled using single beam echosounder data collected during the 2022 and 2024 cruises and GEBCO bathymetry ([www.gebco.net/data\\_and\\_products/gridded\\_bathymetry\\_data](http://www.gebco.net/data_and_products/gridded_bathymetry_data)). The single beam echosounder data and GEBCO bathymetry was sampled into the missing grids in the NOAA bathymetry, with preference to the single beam echosounder data.

From the bathymetry two derived variables (slope and topographic position index) were calculated using the raster package (Hijmans 2019). Slope was calculated from the nearest 8 neighbors and TPI was calculated with a focal distance of ~300 m.

Northness was calculated as the cosine of the aspect (direction relative to 0 degrees that the slope was facing) for each grid cell based on bathymetry.

Oxygen data were based on the World Ocean Atlas data (2018 update). These data were clipped to the area of interest and resampled into the bathymetry grid using bilinear interpolation. The five explanatory variables are shown in Figure 59.

### 7.3.3 Native spatial and temporal resolution of the independent data

The native spatial resolution of the NOAA bathymetry was 3 arc-second grid. The native spatial resolution for the Oxygen data was 0.5 degrees longitude and latitude. It should be noted that the Oxygen data sources are conglomerations of data collected over varying spatial and temporal scales (e.g. the temporal scale is since ~1900's in the case of some measurements). For complete documentation of the spatial and temporal scale of the raw data the NODC respective website should be consulted ([www.gebco.net/data\\_and\\_products/gridded\\_bathymetry\\_data](http://www.gebco.net/data_and_products/gridded_bathymetry_data) and <https://www.nodc.noaa.gov/OC5/woa18/>).

All independent data layers were trimmed to include only observations and explanatory variables from this region and to depths of 1250 m.

### 7.3.4 Data processing and scaling (method for downscaling or aggregation)

Both the bathymetry (for gap filling) and oxygen layers were downscaled to a 100 m by 100 m grid in order to match the scale of the bathymetry. This downscaling was completed using bilinear interpolation.

**7.3.4.1 Goodness of fit for downscaled aggregated data** The downscaled data at the dependent data sites for both Oxygen and bathymetry represented the lower resolution very well ( $r > 0.9$ ).

**7.3.4.2 Measurement errors and bias** Measurement errors in the data or bias in the data were not accounted for beyond the processing conducted on the raw measurements by GEBCO or NODC.

### 7.3.5 Derivation methods and calculations for derived variables

From the bathymetry three derived variables (aspect, slope and topographic position index) were calculated using the raster package (Hijmans 2019). These variables were calculated on bathymetry aggregated (see below) to a 100 m by 100 m grid. The aspect variable was then converted to northness using a cosine function.

### 7.3.6 Rationale for inclusion of independent variables clearly stated and ecologically relevant

These five variables (depth, slope, topographic position index, northness and oxygen) have been found in previous studies to influence the distribution of *Pennatulaceans* (Huff et al., 2013, Yesson et al., 2017, Etnoyer et al., 2018).

## 7.4 Modelling approach

In this study generalized additive models (GAM) were developed to predict species distribution (Wood 2006).

### 7.4.1 Model steps

**7.4.1.1 Code for model provided** The code and data used for this model are not currently publicly available, but can be available on request from Chris Rooper (chris.rooper@dfo-mpo.gc.ca).

**7.4.1.2 Packages used are referenced** The packages used to develop this model are referenced in the above .Rmd file. The key packages used were “sf”, “rnatualearth”, “ggplot2”, “rgdal”, “rgeos”, “gstat”, “raster”, “mgcv” and are all available for download from CRAN. The R version used here was R version 3.6.0 (2019-04-26) – “Planting of a Tree” (R Core Development Team 2019).

**7.4.1.3 Data is made available as supplementary material** The independent variables are available from Chris Rooper (chris.rooper@dfo-mpo.gc.ca).

### 7.4.2 Biases (spatial, temporal and other) acknowledged and described

There were no inherent biases in the modeling method (although there may be biases in the dependent and independent data described above).

### 7.4.3 Methods and approaches to collinearity in independent variables

**7.4.3.1 Collinearity in independent variables** The five explanatory variables were examined for collinearity using a pearson correlations (Figure 60). Variance inflation factors (Zuur et al. 2002) were also examined. In both cases the values were low, suggesting that the variables were fairly independent of each other.

Table 2. Variance inflation factors for independent variables using in modeling.

Variable	VIF
Depth	3.592
Slope	1.231
TPI	1.091
Oxygen	3.372
Northness	1.065

**7.4.3.2 Criteria for variable/dimension reduction provided** None of the variance inflation factors exceeded 5, indicating that dimension reduction was not warranted.

#### 7.4.4 Choice of modelling method is explained and justified

The modelling method chosen was a generalized additive model (GAM). This model was primarily chosen for its simplicity of assumptions (stated below), its usefulness in fitting binomial (presence-absence) data, and the many previous applications of this method to predicting species distributions.

**7.4.4.1 Modelling assumptions are clearly stated** The basic GAM assumptions are; 1) Independence among data points, 2) The distribution of the residuals is binomially distributed, 3) homogenous variance across the fitted values, and 4) a non-linear relationship between response and predictor.

**7.4.4.2 Potential violations of model assumptions are explored** Diagnostic plots of Pearson residuals are shown in Figure 61. The residuals did not indicate any serious violations of GAM assumptions.

#### 7.4.5 Model application

To build the model of *Pennatulaceans* a generalized additive model was constructed that contained five explanatory variables (depth, slope, topographic position index, northness and oxygen). The dependent data was presence or absence of *Pennatulaceans*. The full model was

$$y = \alpha + s(\text{depth}) + s(\text{slope}) + s(\text{TPI}) + s(\text{northness}) + s(\text{O}_2) + \sigma$$

A binomial error distribution ( $\sigma$ ) was used for the model fitting. A full model was fit initially containing all the variables with a basis degrees of freedom of 4 for each smooth. This model was reduced sequentially by removing the least significant term and comparing the AIC for the resulting reduced model following the methods of Rooper et al. (2016). This was repeated until there was a decline in model skill when removing a variable.

**7.4.5.1 Model settings** The default GAM settings in R were used (see `CobbSDM_Pennatulacean.Rmd`). The only setting that was modified was the specification of the binomial error distribution and the specified number of knots for the smooth of  $k = 4$ .

**7.4.5.2 Model complexity is assessed** The results of the sequential variable reduction resulted in the retention of 3 terms; slope, O<sub>2</sub>, northness. The deviance explained by the model ( $D^2$ ) was 0.385.

The model complexity was assessed against simpler models with less terms during the sequential variable reduction step and the most complex model (containing these terms) was found to be the most appropriate (Table 3).

Table 3. Summary of GAM model predicting presence or absence of *Pennatulaceans*.

Term	edf	F	p-value
slope	1.000	6.112	0.0134
O <sub>2</sub>	2.935	9.941	0.0187

Term	edf	F	p-value
northness	2.912	10.037	0.0166
residual	69.153		
GCV	0.054		
Deviance explained (%)	38.500		

#### 7.4.6 Model response curves are generated (where appropriate) and compared to expectations

Model response curves are shown in Figure 62. Probability of presence of *Pennatulaceans* decreased with increasing slopes and was highest when those slopes were more west facing at low oxygen areas. None of the results were abnormal or unexpected.

##### 7.4.6.1 Modelling method-specific term estimates or coefficients are reported (where relevant)

The model specific term estimates are provided in Table 4.

Table 4. Model coefficients, significance and standard error estimates for GAM predicting *Pennatulaceans* probability of presence.

	x
(Intercept)	0.617
s(slope).1	0.000
s(slope).2	0.000
s(slope).3	-0.877
s(O2).1	9.620
s(O2).2	-19.263
s(O2).3	12.413
s(northness).1	5.779
s(northness).2	-4.210
s(northness).3	-5.498

**7.4.6.2 Independent variable importance is reported** The relative importance of variables in the model was measured by sequentially removing the individual variables, fitting a new model and calculating the deviance explained. The deviance explained was then scaled to the full model to determine the relative drop in model goodness-of-fit with removal of each variable. The results showed that slope was the least important variable determining the probability of *Pennatulaceans* presence, and Oxygen and northness were the most important (Figure 63).

## 7.5 Model uncertainty

### 7.5.1 Model specific goodness of fit statistics have been checked and reported

The *Pennatulaceans* model AUC was 0.883, an excellent model according to the standards of Hosmer et al., (2013).

Using a threshold of 0.6 resulted in prediction of 32 of the 41 observed presences correctly, while predicting about 86% of the absences correctly (sensitivity = 0.78 and specificity = 0.861).

Table 5. Confusion matrix of predicted and observed presence and absence of *Pennatulaceans* using a probability threshold 0.6.

	Observed	
Predicted	Presence	Absence

	Observed	
Presence	32	5
Absence	9	31

**7.5.1.1 Multiple measures of goodness of fit have been examined** Commonly used goodness-of-fit measures for binomial models are provided in Table 5 for the GAM predicting *Pennatulaceans* probability of presence. These include the True Skill Statistic (Allouche et al., 2006), the root-mean-squared-error and the Spearman’s rank correlation. Other threshold dependent metrics can be calculated from the confusion matrix (Table 4).

Model diagnostics indicated no issues with the prediction of presence or absence (Figure 64).

### 7.5.2 Spatial autocorrelation in the residuals has been assessed and reported

There was not significant spatial autocorrelation in the model residuals measured by Moran’s I ( $I = 0.27$ ). This was not unexpected given the random-stratified sample design of observations in the study area.

### 7.5.3 Residuals have been tested against assumed distribution (where appropriate)

Not applicable for the binomial distribution. Figure 61 shows model residuals (on the logit scale are shown for each data point used to model *Pennatulaceans* and diagnostics.

**7.5.3.1 Spatial patterns in residuals** Model residuals are shown in Figure 65. This confirms the results of the Moran’s I, with little evidence of spatial patterns in the residuals.

## 7.6 Model validation

### 7.6.1 Training and testing data splitting method

Both internal model validation method and independent data was used as a validation data set. K-fold cross-validation was used here. Five (k) folds were chosen at random.

**7.6.1.1 Potential spatial biases were accounted for in splitting the data** The spatial blocking method (Valvani et al., 2019) was *not* used to split the data for the internal cross-validation.

**7.6.1.2 A standard method used for cross-validation** k-fold cross-validation is a standard method. The data was divided into 5 equal portions and a model then fit to 80% of the data and tested against the remaining 20% of the data. This was repeated for each subdivision of the data. The same maps and diagnostics were produced for each model fit on the k-folds.

The data folds appeared to show the same patterns as the full model.

The model performance was similar for all the training data sets (the full model and the individual folds). The performance of the model on the testing folds was except for the True Skill Statistic and AUC for model fold 5 was very poor, indicating some potential issues with model performance.

### 7.6.2 Truly independent data used for model validation

The presence and absence observations from 58 transects completed in 2024 was also used to test the models developed on the 2022 survey data.

The *Pennatulaceans* model AUC was 0.524, an poor performing model according to the standards of Hosmer et al., (2013).

Using a threshold of 0.6, 0.6 resulted in prediction of 5 of the 19 observed presences correctly, while predicting about 72% of the absences correctly (sensitivity = 0.263 and specificity = 0.718).

Table 6. Confusion matrix of predicted and observed presence and absence of *Pennatulaceans* using a probability threshold 0.6, 0.6 for the independently collected data set in 2024.

	Observed	
Predicted	Presence	Absence
Presence	5	11
Absence	14	28

Table 6. Model goodness of fit measures for the full model and the individual model validation folds

Fold	AIC	threshold	AUC_training	AUC_testing	TSS_training	TSS_testing
Full model	81.127	0.600	0.883	NA	0.642	NA
Fold_1	62.974	0.570	0.904	0.727	0.642	0.477
Fold_2	66.404	0.370	0.881	0.810	0.699	0.317
Fold_3	69.045	0.525	0.876	0.870	0.635	0.611
Fold_4	72.446	0.650	0.854	0.952	0.632	0.460
Fold_5	61.262	0.360	0.915	0.571	0.698	-0.107

Fold	Cor_training	Cor_testing	RMSE_training	RMSE_testing
Full model	0.663	NA	0.374	NA
Fold_1	0.700	0.349	0.354	0.476
Fold_2	0.660	0.533	0.367	0.421
Fold_3	0.646	0.630	0.375	0.375
Fold_4	0.609	0.779	0.398	0.318
Fold_5	0.718	0.124	0.340	0.540

## 7.7 Model outputs

### 7.7.1 Maps of model predictions, model residuals and prediction error

Maps of model predictions are provided in Figure 67. Maps of residuals in Figure 65. Maps of prediction error in Figure 68. The model predicted that the highest probability of presence for *Pennatulaceans* was on the west facing slopes of seamounts and at specific patches near seamount summits.

### 7.7.2 Areas of model extrapolation are clearly defined

The model was not extrapolated outside the five seamounts, although within this region, there were some areas with little or no sampling. The model was extrapolated at depths from 850 - 1250 m where no sampling occurred.

### 7.7.3 The prediction unit is clearly defined (and explained if necessary)

The prediction unit is the probability of presence or absence of *Pennatulaceans*.

### 7.7.4 Thresholding methods (for dichotomising probability into presence or absence) are clearly described and appropriate

No thresholding was done (beyond the thresholding for calculating goodness-of-fit measures). Probability of presence is presented as the result.

**7.7.4.1 The sensitivity of model outcomes to threshold value chosen has been explored**  
Sensitivity to threshold values was not explored, but in a formal analysis of the model could be completed using the provided model outputs.

## 7.8 Conclusions

The *Pennatulaceans* model fit the observations from 2022 well. The internal model validation showed generally robust results. However, the independently collected data were predicted with poor accuracy.

Model response curves showed the importance of oxygen and northness as predictors. On west facing (and lower) slopes with low oxygen there was a high probability of *Pennatulaceans* presence at all seamounts on a randomly chosen transect.

PRELIMINARY

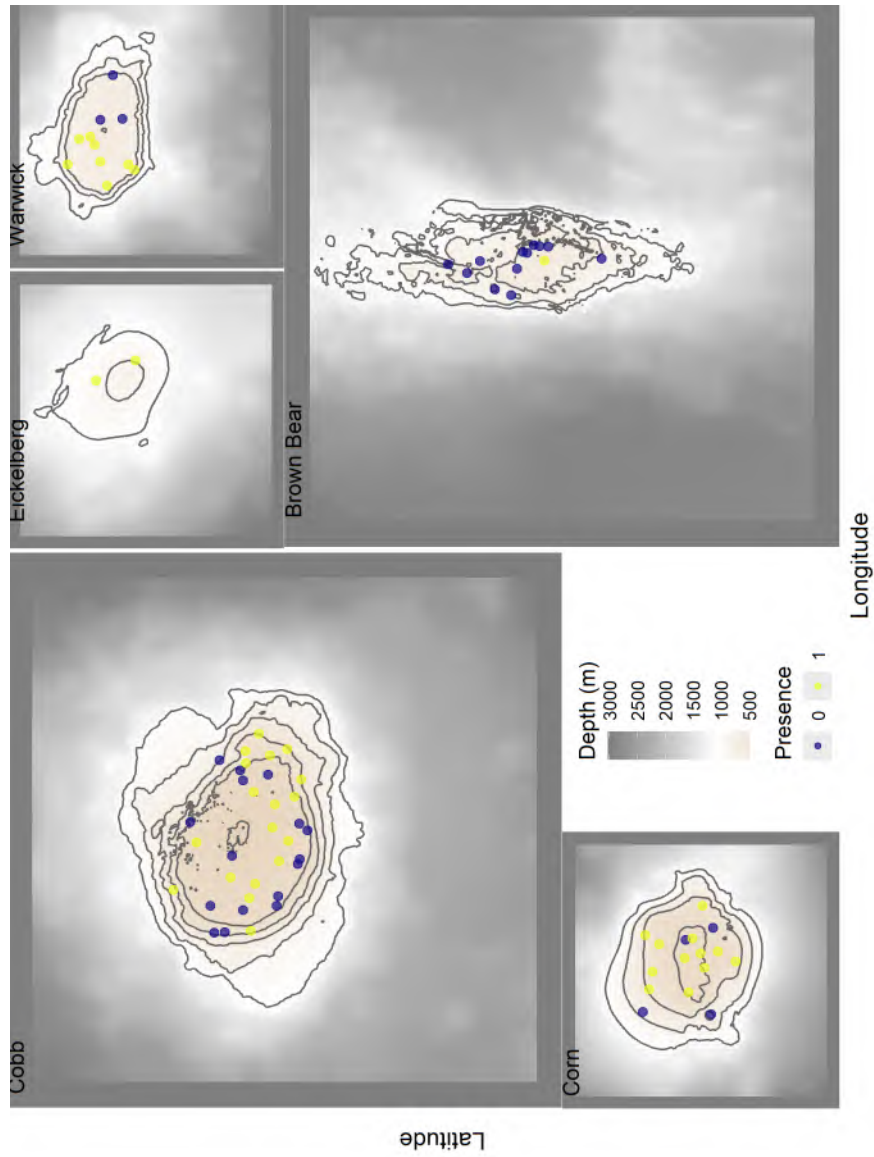


Figure 58: Locations of presence and absence transects for Pennatulaceans from 2022 and 2024 stereo-camera survey

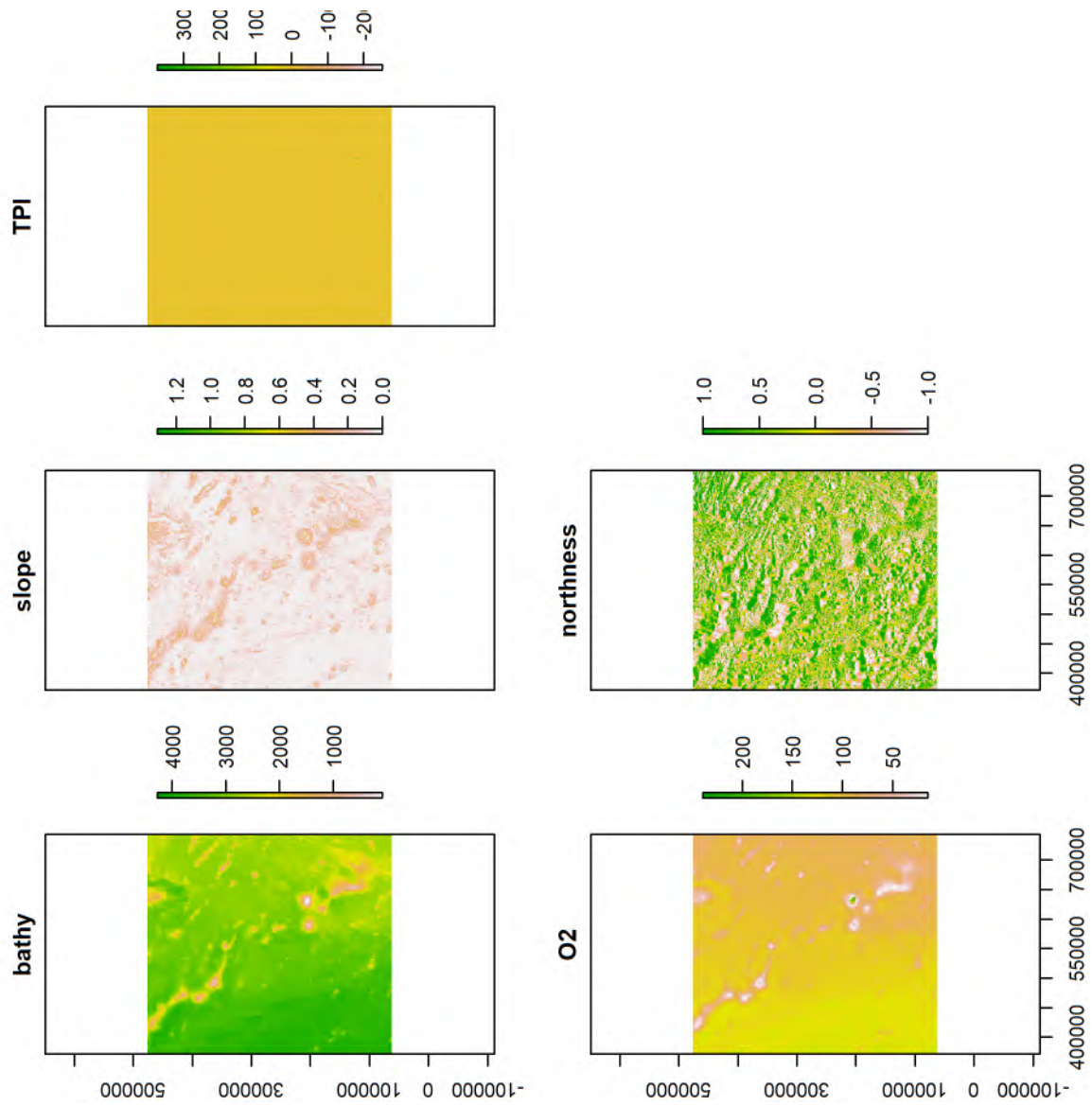


Figure 59: Map of bathymetry, slope, TPI, Oxygen and northness used as explanatory variables in this analysis of VME data

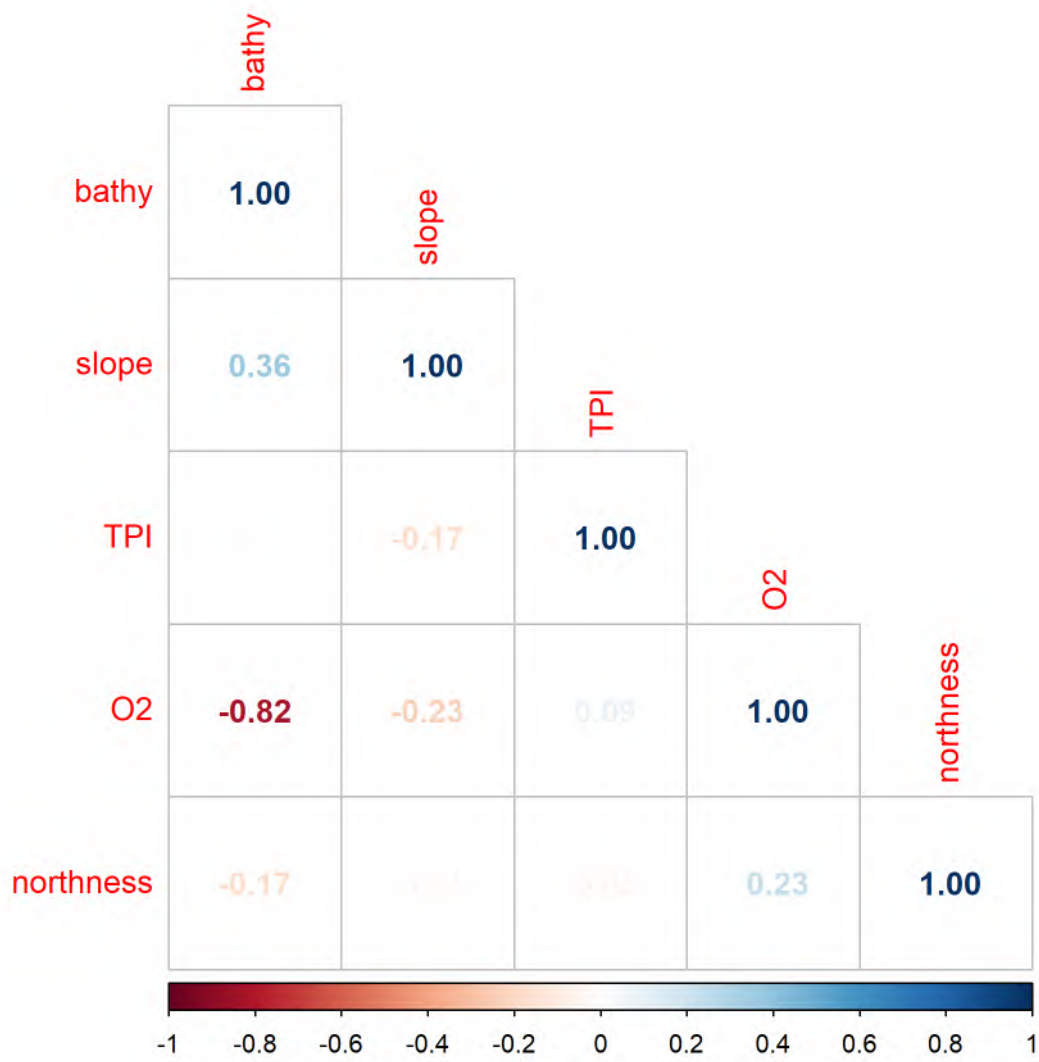


Figure 60: Correlation among independent variables used in modeling.

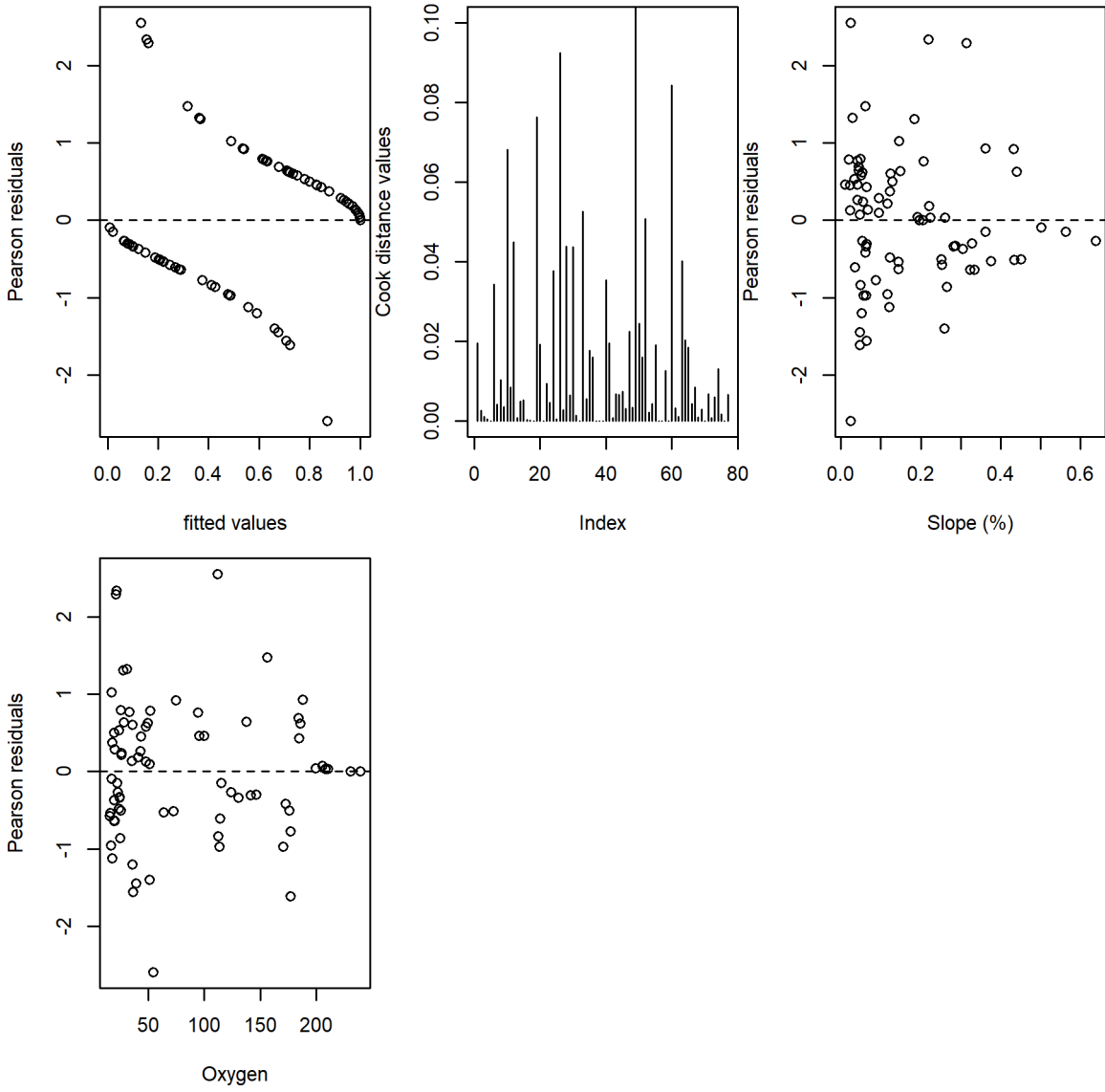


Figure 61: Diagnostic plots for GAM model assumptions.

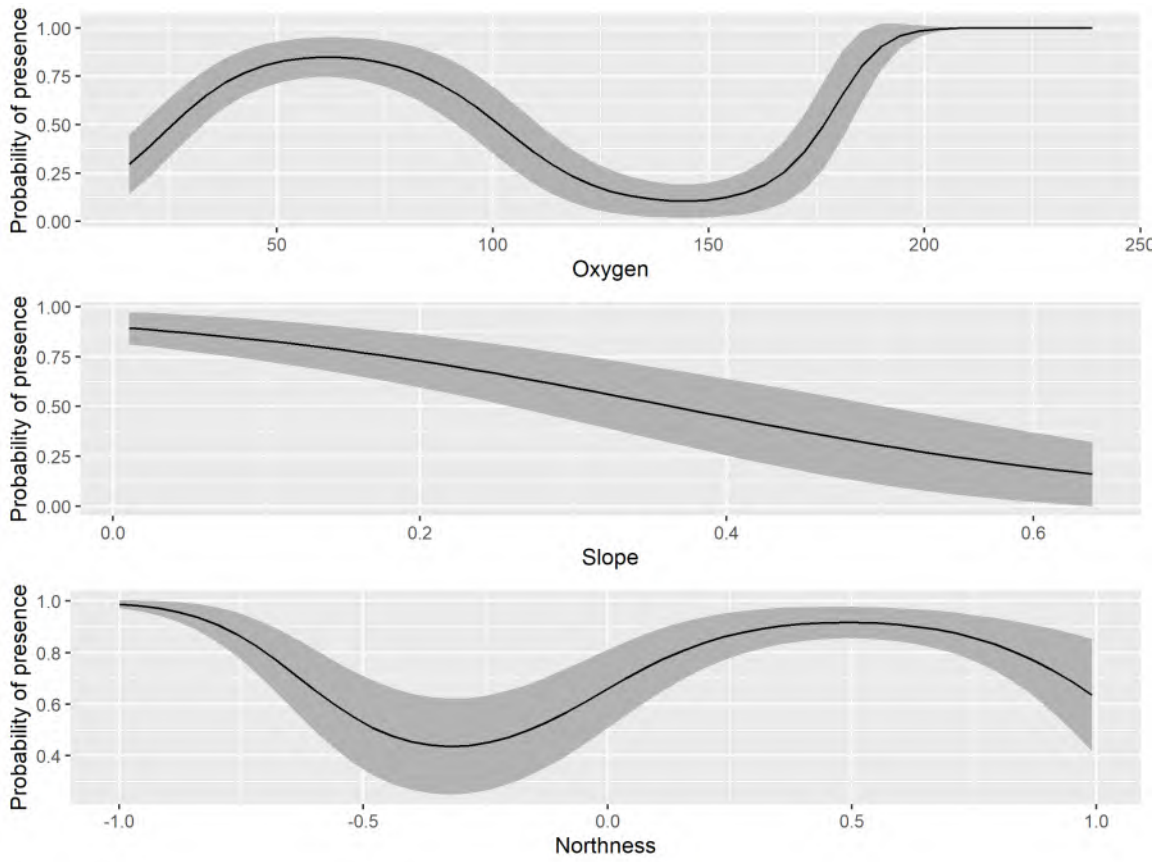


Figure 62: Response curves for independent variables used best-fitting GAM for presence or absence.

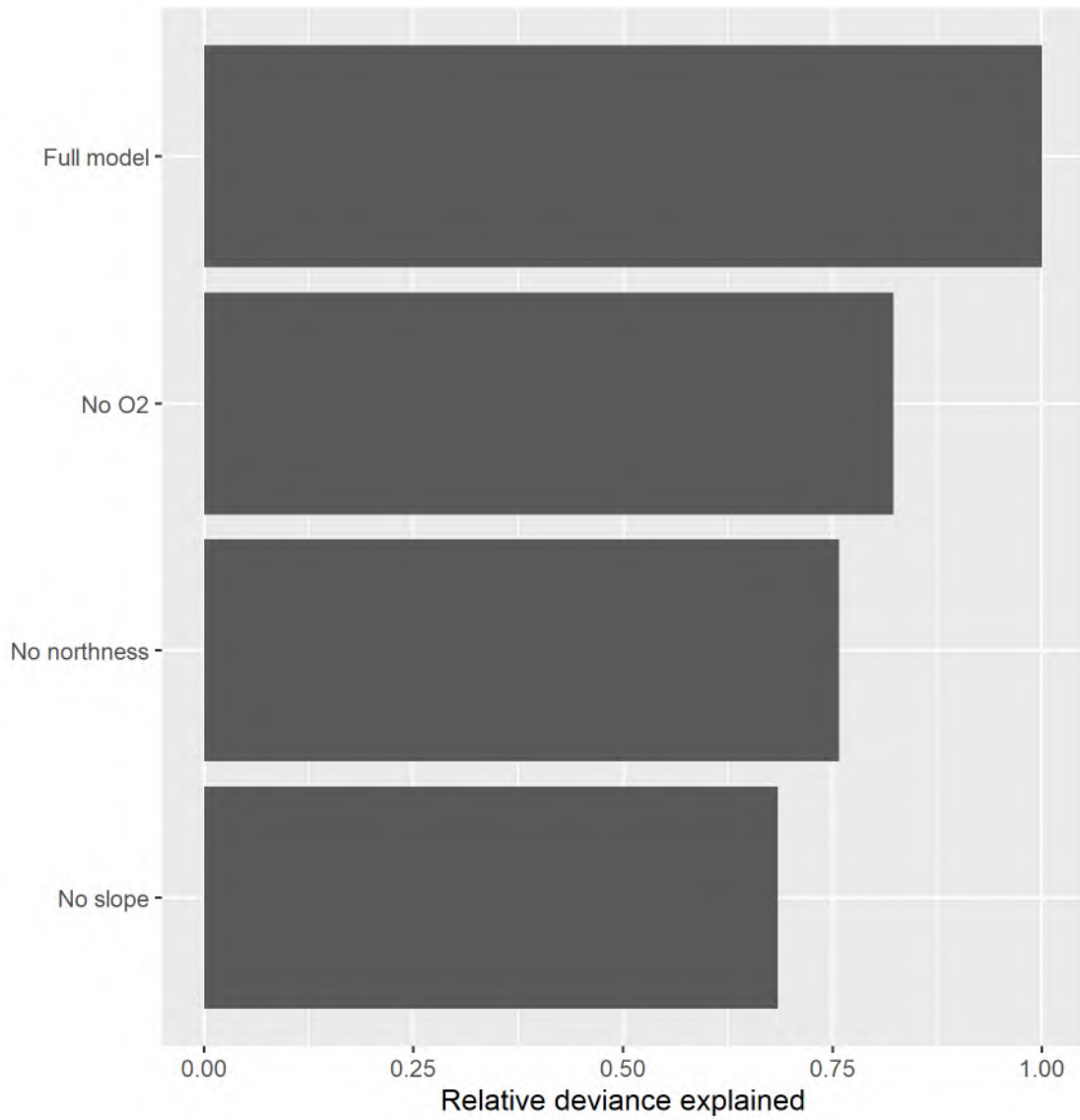


Figure 63: Relative importance of variables included in the Pennatulacean presence or absence GAM measured by their contribution to deviance explained when sequentially removed from the model.

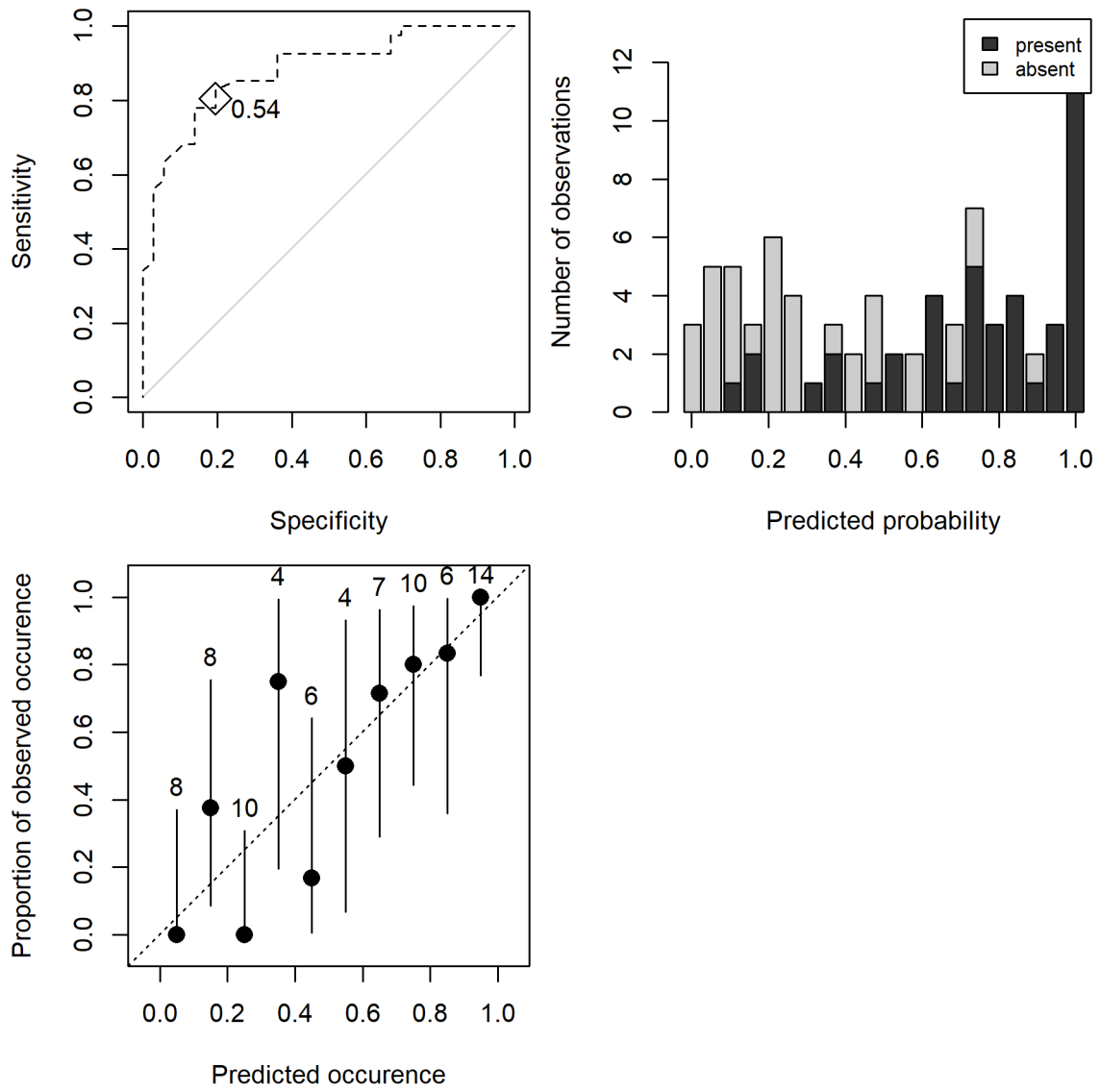


Figure 64: Model diagnostic plots for Pennatulacean presence or absence GAM.

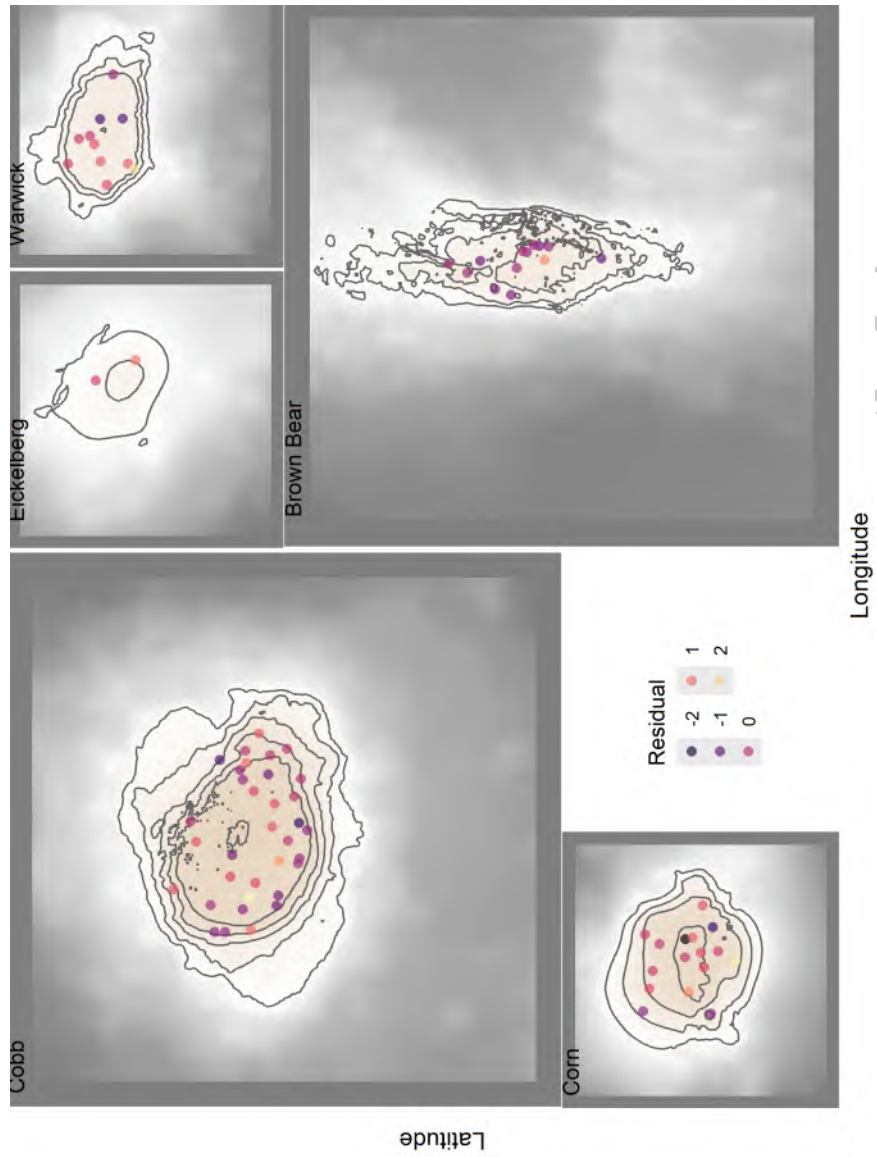


Figure 65: Spatial patterns in model Pearson residuals for GAM predicting probability of presence for Pennatulaceans.

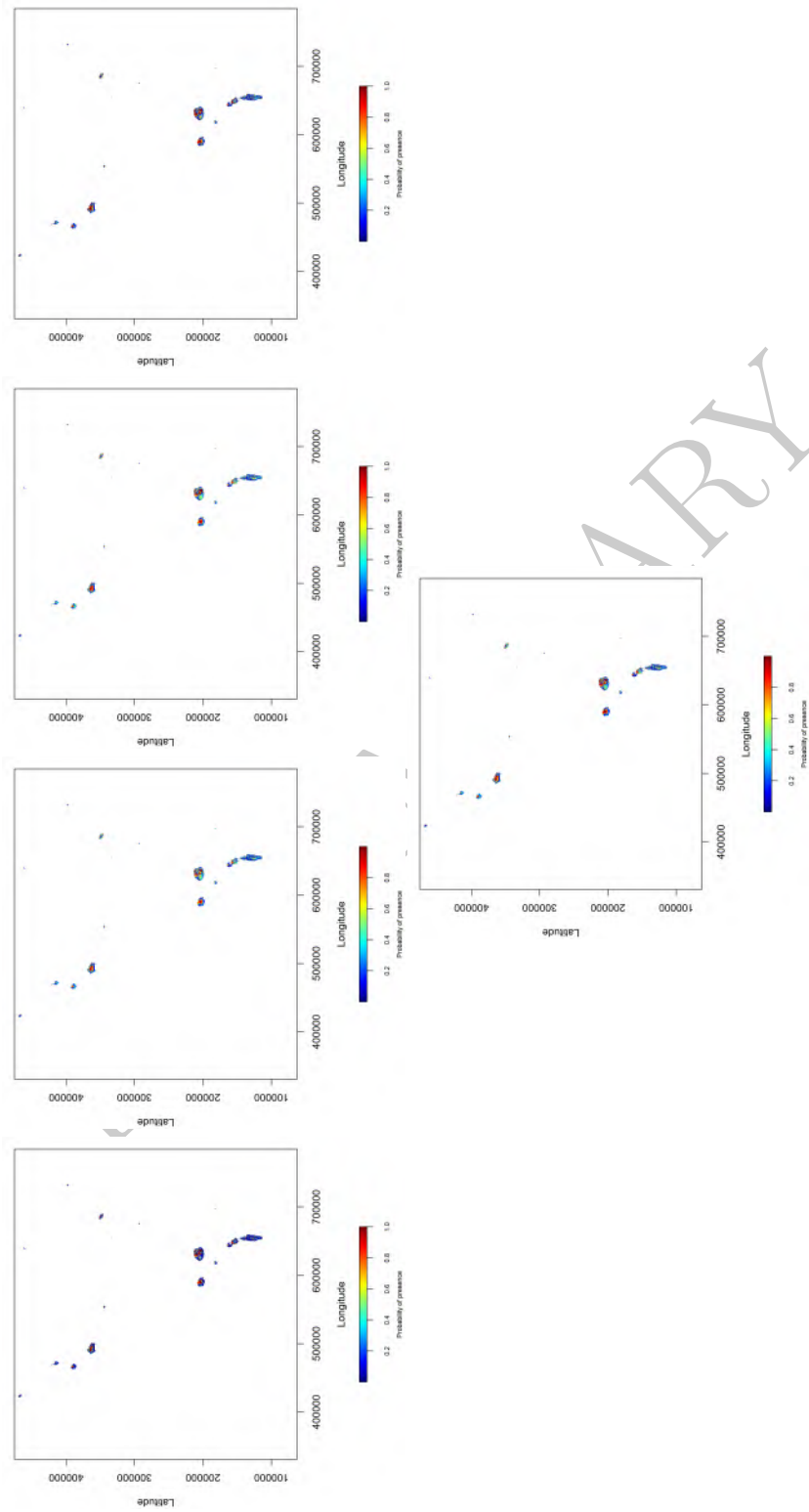


Figure 66: Maps of model predictions for 5 randomly selected folds of the data.

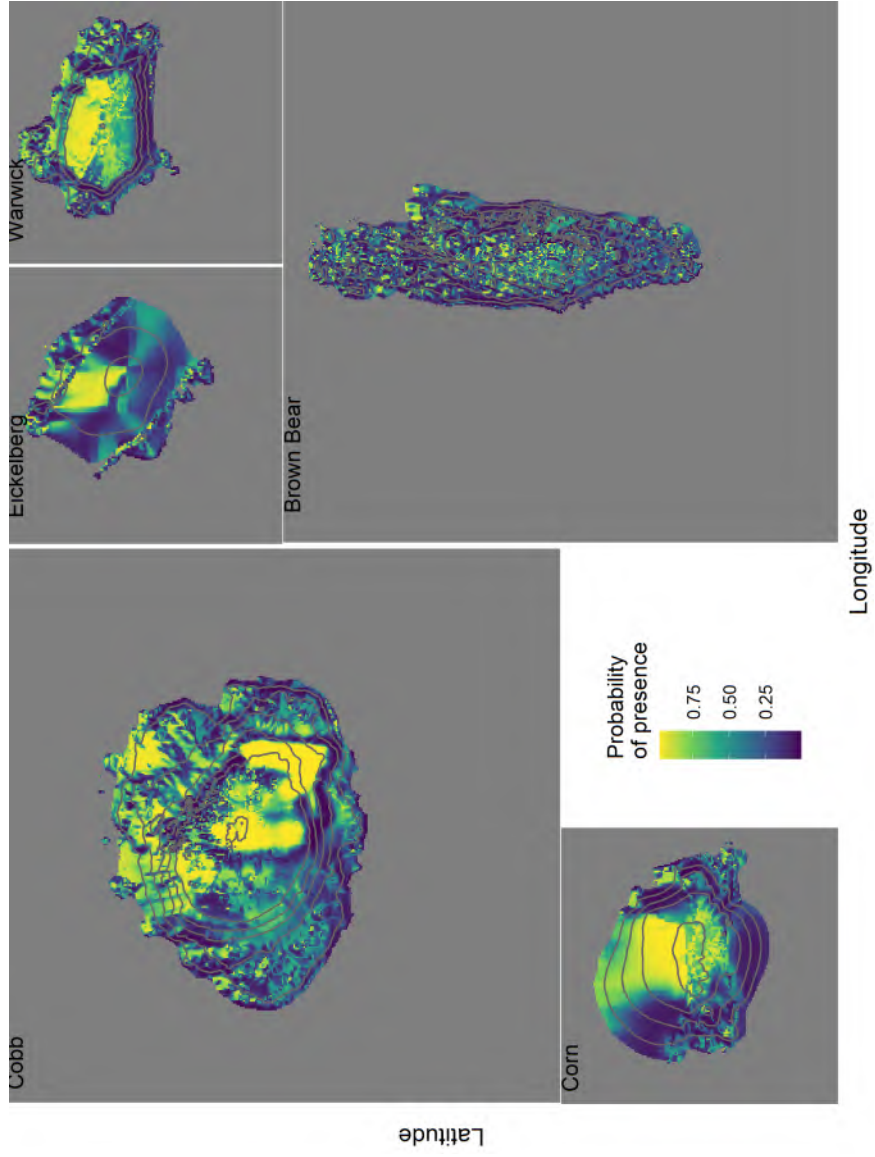


Figure 67: Predicted probability of presence for Pennatulaceans at seamounts in the Cobb-Eickelberg seamount chain.

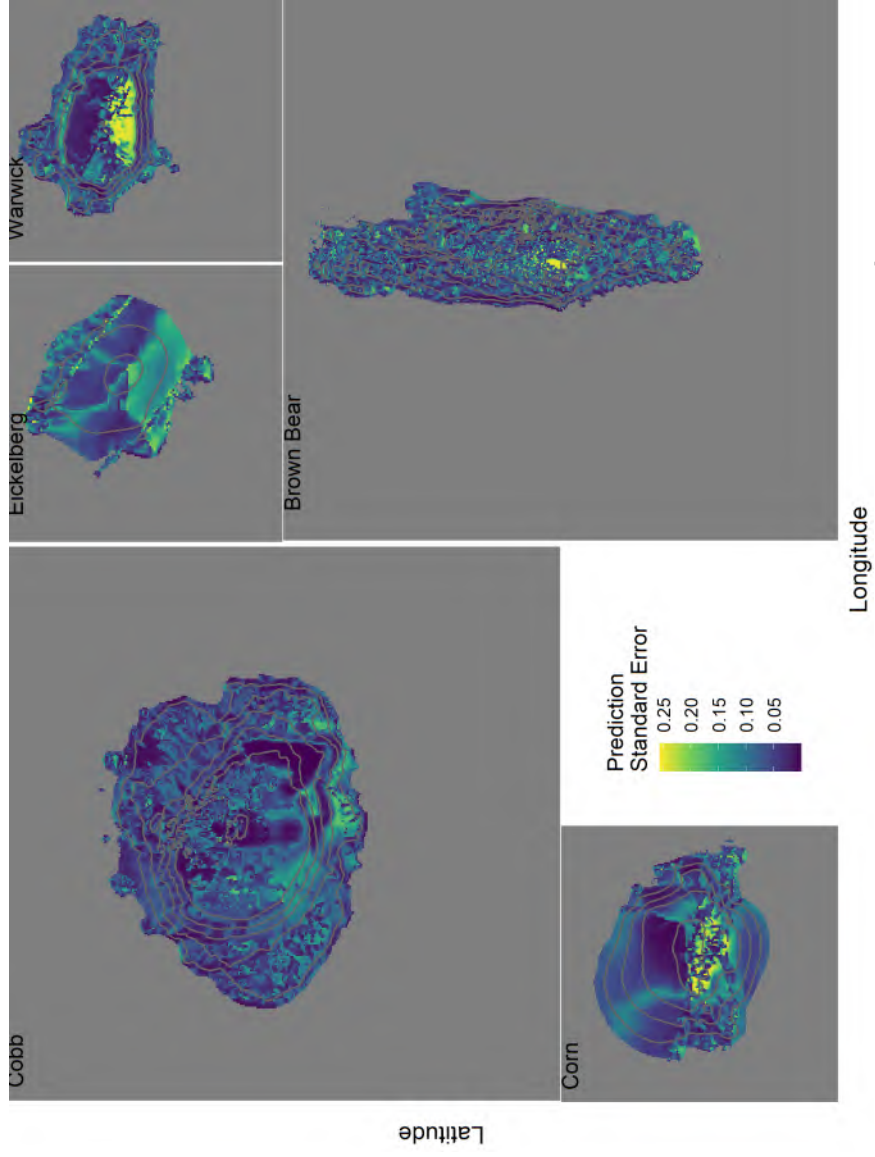


Figure 68: Spatial patterns in model prediction error for GAM predicting probability of Pennatulaceans at seamounts in the Cobb-Eickelberg seamount chain.

## 8 Vulnerable Marine Indicator Taxa Group: *Hydrocorals*

### 8.1 Study resolution

#### 8.1.1 Location of the study area (or management region)

This modelling was carried out for five seamounts in the Northeastern Pacific Ocean where fisheries are managed by the North Pacific Fisheries Commission. The five seamounts are shown in Figure 1 and are part of the Cobb-Eickelberg seamount chain.

**8.1.1.1 Spatial extent of the modelled area** The specific seamounts modeled were five North Pacific Seamounts (Cobb, Brown Bear, Eickelberg, Warwick and Corn). Modeling was conducted from depths of 0 - 1250 m. Data was collected from 0 to ~850 m.

**8.1.1.2 Spatial resolution of the model and independent variables** The spatial resolution of the modeling was 100 m by 100 m grid cells. The all data was projected into an Albers equal area projection (proj4 description = "+proj=aea +lat\_0=45 +lon\_0=-126 +lat\_1=50 +lat\_2=58.5 +x\_0=1000000 +y\_0=0 +ellps=GRS80 +towgs84=0,0,0,0,0,0 +units=m +no\_defs").

**8.1.1.3 Spatial precision (of observations and independent variables)** The spatial precision of the observations was taken from the gps mounted on the research vessel. Based on tracking information, the camera system was towed slightly behind the vessel (~200 m typically), but along the same path as the vessel. The anticipated precision of the variation of the camera path was expected to be less than 20 m across the trackline.

**8.1.1.4 Depth resolution/range/extent (of the observations and independent variables)** The depth range of the observations of *Hydrocorals* (from the depth sensor mounted on the camera) was from 61 to 808 m (mean = 442 m, SE = 206.28). The depth range of the modeled area was from 34 (the summit depth of Cobb Seamount) to 1250 m.

#### 8.1.2 Temporal extent of the data

**8.1.2.1 Dates of data extent** The dates observations used in model development were collected were September 6, 2022 to September 20, 2022. The dates for observations used for model testing were from September 3, 2024 to September 11, 2024.

**8.1.2.2 Precision of date/time** The precision of the date and the time of the data was assumed to be the closest second.

**8.1.2.3 Data/time resolution** The resolution of the date and time was fraction of a second.

**8.1.2.4 Impacts over time to consider in the data set (e.g. historical fishing effort)** Fishing occurred over the entire time frame from which these data points were collected. Fishing also has occurred historically since the 1970's. We did not attempt to account for historical fishing effort over this time. There may have been climate impacts occurring over the time frame of the data observations as well, however, these were not accounted for in the analyses.

### 8.2 Dependent data

The dependent data are shown in Figure 69.

Table 1. Number of records for each taxonomic grouping in the order *Hydrocorals* from the survey database.

Species or Taxa group	Count
Stylasteridae	1340

### 8.2.1 Data type (presence, absence, abundance)

The data used for modeling *Hydrocorals* distribution were observed presences (n = 36) and absences (n = 41) that occurred at the five seamounts.

### 8.2.2 Data source (e.g. type of survey(s) combined)

The data were entirely from random stratified surveys of the Cobb-Eickelberg seamount chain conducted in 2022.

### 8.2.3 Measure of sampling effort

Sampling effort was estimated by the distance the camera traveled along each transect multiplied by the field of view observed along the transect (Rooper et al. 2016). This provided an area observed for each transect which was used as the effort measure. Area observed ranged from 254 to 2469 m<sup>2</sup> with a median area observed of 1197 m<sup>2</sup>.

### 8.2.4 Detectability

Detectability of the width of the viewing area of the camera along the transect (area observed) was assumed to be 100% for VME indicator taxa. However, there were likely some individuals that were too small to be detected.

### 8.2.5 Taxonomic level

The taxonomic level modeled here was the taxonomic group *Hydrocorals* (see Table 1 for individual families included in this grouping and refer to CMM for NPFC definitions).

### 8.2.6 Functional attributes (its ecology)

*Hydrocorals* are a diverse, long-lived and fragile species. They occur in deep-water and are habitat forming structures important to many fishes, invertebrates other taxonomic groups.

### 8.2.7 Taxonomic confidence of species/assemblages

The taxonomic confidence of the assemblage was assumed to be good. Experts experienced in identification of corals and sponges from visual imagery in the North Pacific Ocean did all the identification and image analyses.

### 8.2.8 Rationale for taxonomic/assemblage level modeled

*Hydrocorals* as defined here are a group that shares common habitat requirements and depth distribution. They are closely related and the order is globally distributed at deep depths. This Order has been previously modelled using Maximum entropy methods on a global extent and regional extent (Yesson et al., 2017, Chu et al. 2018, Doherty et al. 2019).

### 8.2.9 Source of absence data

Absences were observations of no individuals at transects. In total there were 41 absences in the dataset.

### 8.2.10 Other potential errors or biases in the data

There are some potential sources of error in the data, including errors in positioning of the records, errors in species identification (including both false positives and false negatives).

### 8.2.11 Data filtering steps

No data filtering was conducted.

### 8.2.12 Taxonomic aggregation steps

The records for the Order *Hydrocorals* were aggregated by transect into presence or absence observations.

### 8.2.13 Method for combining dependent data sources (if done outside the modelling)

No other dependent data sources were used in this modelling.

## 8.3 Independent data

### 8.3.1 Independent data (environmental variables used)

Five independent variables were used in building a model of *Hydrocorals* distribution; bathymetry, topographic position index, seafloor slope, Oxygen concentration and northness (Figure 70).

### 8.3.2 Independent data source (source of raw or derived data)

The bathymetry used here was downloaded from the NOAA website (<https://www.ncei.noaa.gov/maps/bathymetry/>). It consists of gridded bathymetry from a multibeam sources on a 3 arc-second grid for the region of interest. The details of the data sources can be found on the NOAA website. There were some gaps in the NOAA bathymetry layers. These were filled using single beam echosounder data collected during the 2022 and 2024 cruises and GEBCO bathymetry ([www.gebco.net/data\\_and\\_products/gridded\\_bathymetry\\_data](http://www.gebco.net/data_and_products/gridded_bathymetry_data)). The single beam echosounder data and GEBCO bathymetry was sampled into the missing grids in the NOAA bathymetry, with preference to the single beam echosounder data.

From the bathymetry two derived variables (slope and topographic position index) were calculated using the raster package (Hijmans 2019). Slope was calculated from the nearest 8 neighbors and TPI was calculated with a focal distance of ~300 m.

Northness was calculated as the cosine of the aspect (direction relative to 0 degrees that the slope was facing) for each grid cell based on bathymetry.

Oxygen data were based on the World Ocean Atlas data (2018 update). These data were clipped to the area of interest and resampled into the bathymetry grid using bilinear interpolation. The five explanatory variables are shown in Figure 70.

### 8.3.3 Native spatial and temporal resolution of the independent data

The native spatial resolution of the NOAA bathymetry was 3 arc-second grid. The native spatial resolution for the Oxygen data was 0.5 degrees longitude and latitude. It should be noted that the Oxygen data sources are conglomerations of data collected over varying spatial and temporal scales (e.g. the temporal scale is since ~1900's in the case of some measurements). For complete documentation of the spatial and temporal scale of the raw data the NODC respective website should be consulted ([www.gebco.net/data\\_and\\_products/gridded\\_bathymetry\\_data](http://www.gebco.net/data_and_products/gridded_bathymetry_data) and <https://www.nodc.noaa.gov/OC5/woa18/>).

All independent data layers were trimmed to include only observations and explanatory variables from this region and to depths of 1250 m.

### 8.3.4 Data processing and scaling (method for downscaling or aggregation)

Both the bathymetry (for gap filling) and oxygen layers were downscaled to a 100 m by 100 m grid in order to match the scale of the bathymetry. This downscaling was completed using bilinear interpolation.

**8.3.4.1 Goodness of fit for downscaled aggregated data** The downscaled data at the dependent data sites for both Oxygen and bathymetry represented the lower resolution very well ( $r > 0.9$ ).

**8.3.4.2 Measurement errors and bias** Measurement errors in the data or bias in the data were not accounted for beyond the processing conducted on the raw measurements by GEBCO or NODC.

### 8.3.5 Derivation methods and calculations for derived variables

From the bathymetry three derived variables (aspect, slope and topographic position index) were calculated using the raster package (Hijmans 2019). These variables were calculated on bathymetry aggregated (see below) to a 100 m by 100 m grid. The aspect variable was then converted to northness using a cosine function.

### 8.3.6 Rationale for inclusion of independent variables clearly stated and ecologically relevant

These five variables (depth, slope, topographic position index, northness and oxygen) have been found in previous studies to influence the distribution of *Hydrocorals* (Huff et al., 2013, Yesson et al., 2017, Etnoyer et al., 2018).

## 8.4 Modelling approach

In this study generalized additive models (GAM) were developed to predict species distribution (Wood 2006).

### 8.4.1 Model steps

**8.4.1.1 Code for model provided** The code and data used for this model are not currently publicly available, but can be available on request from Chris Rooper (chris.rooper@dfo-mpo.gc.ca).

**8.4.1.2 Packages used are referenced** The packages used to develop this model are referenced in the above .Rmd file. The key packages used were “sf”, “rnaturalearth”, “ggplot2”, “rgdal”, “rgeos”, “gstat”, “raster”, “mgcv” and are all available for download from CRAN. The R version used here was R version 3.6.0 (2019-04-26) – “Planting of a Tree” (R Core Development Team 2019).

**8.4.1.3 Data is made available as supplementary material** The independent variables are available from Chris Rooper (chris.rooper@dfo-mpo.gc.ca).

### 8.4.2 Biases (spatial, temporal and other) acknowledged and described

There were no inherent biases in the modeling method (although there may be biases in the dependent and independent data described above).

### 8.4.3 Methods and approaches to collinearity in independent variables

**8.4.3.1 Collinearity in independent variables** The five explanatory variables were examined for collinearity using a pearson correlations (Figure 71). Variance inflation factors (Zuur et al. 2002) were also examined. In both cases the values were low, suggesting that the variables were fairly independent of each other.

Table 2. Variance inflation factors for independent variables using in modeling.

Variable	VIF
Depth	3.592
Slope	1.231
TPI	1.091
Oxygen	3.372
Northness	1.065

**8.4.3.2 Criteria for variable/dimension reduction provided** None of the variance inflation factors exceeded 5, indicating that dimension reduction was not warranted.

#### 8.4.4 Choice of modelling method is explained and justified

The modelling method chosen was a generalized additive model (GAM). This model was primarily chosen for its simplicity of assumptions (stated below), its usefulness in fitting binomial (presence-absence) data, and the many previous applications of this method to predicting species distributions.

**8.4.4.1 Modelling assumptions are clearly stated** The basic GAM assumptions are; 1) Independence among data points, 2) The distribution of the residuals is binomially distributed, 3) homogenous variance across the fitted values, and 4) a non-linear relationship between response and predictor.

**8.4.4.2 Potential violations of model assumptions are explored** Diagnostic plots of Pearson residuals are shown in Figure 72. The residuals did not indicate any serious violations of GAM assumptions.

#### 8.4.5 Model application

To build the model of *Hydrocorals* a generalized additive model was constructed that contained five explanatory variables (depth, slope, topographic position index, northness and oxygen). The dependent data was presence or absence of *Hydrocorals*. The full model was

$$y = \alpha + s(\text{depth}) + s(\text{slope}) + s(\text{TPI}) + s(\text{northness}) + s(O_2) + \sigma$$

A binomial error distribution ( $\sigma$ ) was used for the model fitting. A full model was fit initially containing all the variables with a basis degrees of freedom of 4 for each smooth. This model was reduced sequentially by removing the least significant term and comparing the AIC for the resulting reduced model following the methods of Rooper et al. (2016). This was repeated until there was a decline in model skill when removing a variable.

**8.4.5.1 Model settings** The default GAM settings in R were used (see CobbSDM\_Hydrocoral.Rmd). The only setting that was modified was the specification of the binomial error distribution and the specified number of knots for the smooth of  $k = 4$ .

**8.4.5.2 Model complexity is assessed** The results of the sequential variable reduction resulted in the retention of 4 terms; depth, TPI, slope, O<sub>2</sub>. The deviance explained by the model ( $D^2$ ) was 0.317.

The model complexity was assessed against simpler models with less terms during the sequential variable reduction step and the most complex model (containing these terms) was found to be the most appropriate (Table 3).

Table 3. Summary of GAM model predicting presence or absence of *Hydrocorals*.

Term	edf	F	p-value
depth	2.949	14.674	0.0018
TPI	1.988	5.003	0.0914

Term	edf	F	p-value
slope	1.965	2.954	0.2816
O2	1.000	2.286	0.1305
residual	68.098		
GCV	0.175		
Deviance explained (%)	31.700		

#### 8.4.6 Model response curves are generated (where appropriate) and compared to expectations

Model response curves are shown in Figure 73. The probability of presence of *Hydrocorals* was highest above 500 m depth at low oxygen regions. The probability of presence was also higher in when TPI values were around zero and in moderate slopes. None of the results were abnormal or unexpected.

##### 8.4.6.1 Modelling method-specific term estimates or coefficients are reported (where relevant)

The model specific term estimates are provided in Table 4.

Table 4. Model coefficients, significance and standard error estimates for GAM predicting *Hydrocorals* probability of presence.

	x
(Intercept)	-0.507
s(depth).1	-5.347
s(depth).2	4.592
s(depth).3	2.257
s(TPI).1	3.241
s(TPI).2	5.868
s(TPI).3	-1.929
s(slope).1	0.295
s(slope).2	2.302
s(slope).3	0.483
s(O2).1	0.000
s(O2).2	0.000
s(O2).3	-0.805

**8.4.6.2 Independent variable importance is reported** The relative importance of variables in the model was measured by sequentially removing the individual variables, fitting a new model and calculating the deviance explained. The deviance explained was then scaled to the full model to determine the relative drop in model goodness-of-fit with removal of each variable. The results showed that slope was the least important variable determining the probability of *Hydrocorals* presence, and TPI and depth were the most important (Figure 74).

## 8.5 Model uncertainty

### 8.5.1 Model specific goodness of fit statistics have been checked and reported

The *Hydrocorals* model AUC was 0.849, an excellent model according to the standards of Hosmer et al., (2013).

Using a threshold of 0.46 resulted in prediction of 29 of the 36 observed presences correctly, while predicting about 76% of the absences correctly (sensitivity = 0.806 and specificity = 0.756).

Table 5. Confusion matrix of predicted and observed presence and absence of *Hydrocorals* using a probability threshold 0.46.

	Observed	
Predicted	Presence	Absence
Presence	29	10
Absence	7	31

**8.5.1.1 Multiple measures of goodness of fit have been examined** Commonly used goodness-of-fit measures for binomial models are provided in Table 5 for the GLM predicting *Hydrocorals* probability of presence. These include the True Skill Statistic (Allouche et al., 2006), the root-mean-squared-error and the Spearman’s rank correlation. Other threshold dependent metrics can be calculated from the confusion matrix (Table 4).

Model diagnostics indicated no issues with the prediction of presence or absence (Figure 75).

### 8.5.2 Spatial autocorrelation in the residuals has been assessed and reported

There was marginally significant spatial autocorrelation in the model residuals measured by Moran’s I ( $I = 0.047$ ). This was unexpected given the random-stratified sample design of observations in the study area.

### 8.5.3 Residuals have been tested against assumed distribution (where appropriate)

Not applicable for the binomial distribution. Figure 72 shows model residuals (on the logit scale are shown for each data point used to model *Hydrocorals* and diagnostics.

**8.5.3.1 Spatial patterns in residuals** Model residuals are shown in Figure 76. This confirms the results of the Moran’s I, with some evidence of clumped spatial patterns in the residuals, especially on Brown Bear seamount.

## 8.6 Model validation

### 8.6.1 Training and testing data splitting method

Both internal model validation method and independent data was used as a validation data set. K-fold cross-validation was used here. Five (k) folds were chosen at random.

**8.6.1.1 Potential spatial biases were accounted for in splitting the data** The spatial blocking method (Valvani et al., 2019) was *not* used to split the data for the internal cross-validation.

**8.6.1.2 A standard method used for cross-validation** k-fold cross-validation is a standard method. The data was divided into 5 equal portions and a model then fit to 80% of the data and tested against the remaining 20% of the data. This was repeated for each subdivision of the data. The same maps and diagnostics were produced for each model fit on the k-folds.

The data folds appeared to show the same patterns as the full model.

The model performance was similar for all the training data sets (the full model and the individual folds). However the performance of the model on the testing folds was less impressive. For example, the True Skill Statistic and AUC for model folds 5 was very poor, indicating some potential issues with model performance.

### 8.6.2 Truly independent data used for model validation

The presence and absence observations from 58 transects completed in 2024 was also used to test the models developed on the 2022 survey data.

The *Hydrocorals* model AUC was 0.749, a good performing model according to the standards of Hosmer et al., (2013).

Using a threshold of 0.46, 0.46 resulted in prediction of 17 of the 22 observed presences correctly, while predicting about 67% of the absences correctly (sensitivity = 0.773 and specificity = 0.667).

Table 6. Confusion matrix of predicted and observed presence and absence of *Hydrocorals* using a probability threshold 0.46, 0.46 for the independently collected data set in 2024.

		Observed	
Predicted		Presence	Absence
Presence		17	12
Absence		5	24

Table 6. Model goodness of fit measures for the full model and the individual model validation folds

Fold	AIC	threshold	AUC_training	AUC_testing	TSS_training	TSS_testing
Full model	90.491	0.460	0.849	NA	0.562	NA
Fold_1	76.070	0.325	0.857	0.648	0.563	0.056
Fold_2	71.291	0.575	0.874	0.719	0.629	0.250
Fold_3	71.546	0.490	0.866	0.760	0.652	0.100
Fold_4	74.360	0.605	0.856	0.778	0.565	0.492
Fold_5	72.610	0.420	0.872	0.500	0.590	-0.115

Fold	Cor_training	Cor_testing	RMSE_training	RMSE_testing
Full model	0.603	NA	0.400	NA
Fold_1	0.613	0.252	0.397	0.498
Fold_2	0.646	0.380	0.381	0.484
Fold_3	0.626	0.426	0.380	0.507
Fold_4	0.615	0.478	0.392	0.451
Fold_5	0.641	0.000	0.384	0.595

## 8.7 Model outputs

### 8.7.1 Maps of model predictions, model residuals and prediction error

Maps of model predictions are provided in Figure 78. Maps of residuals in Figure 76. Maps of prediction error in Figure 79. The model predicted that the highest probability of presence for *Hydrocorals* was in a band from 200-400 m and deeper and in some patchy areas near the summits of seamounts.

### 8.7.2 Areas of model extrapolation are clearly defined

The model was not extrapolated outside the five seamounts, although within this region, there were some areas with little or no sampling. The model was extrapolated at depths from 850 - 1250 m where no sampling occurred.

### 8.7.3 The prediction unit is clearly defined (and explained if necessary)

The prediction unit is the probability of presence or absence of *Hydrocorals*.

### 8.7.4 Thresholding methods (for dichotomising probability into presence or absence) are clearly described and appropriate

No thresholding was done (beyond the thresholding for calculating goodness-of-fit measures). Probability of presence is presented as the result.

**8.7.4.1 The sensitivity of model outcomes to threshold value chosen has been explored**  
Sensitivity to threshold values was not explored, but in a formal analysis of the model could be completed using the provided model outputs.

## 8.8 Conclusions

The *Hydrocorals* model fit the observations from 2022 well. The internal model validation showed robust results. The independently collected data were predicted with good accuracy.

Model response curves showed the importance of depth. At depths from 200-400 m, there was a high probability of *Hydrocorals* presence at all seamounts on a randomly chosen transect.

PRELIMINARY

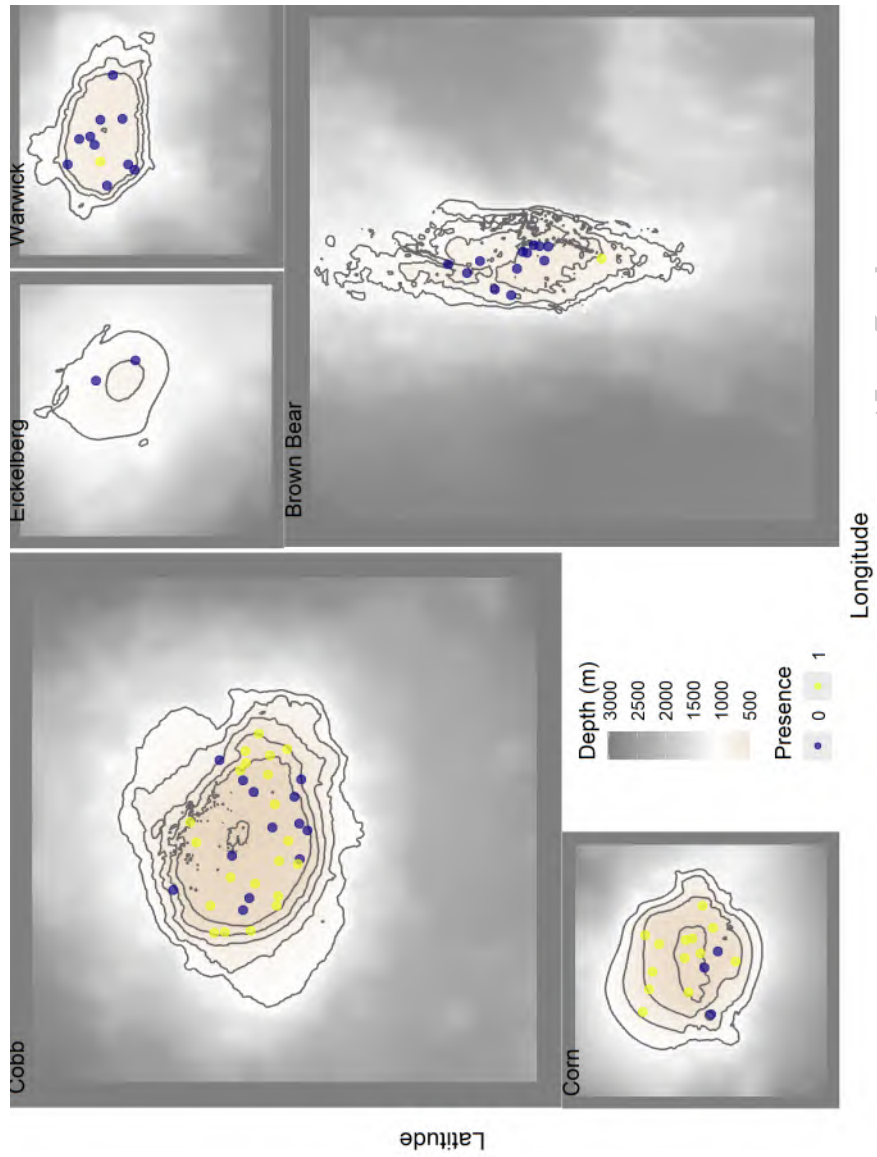


Figure 69: Locations of presence and absence transects for Hydrocorals from 2022 and 2024 stereo-camera survey

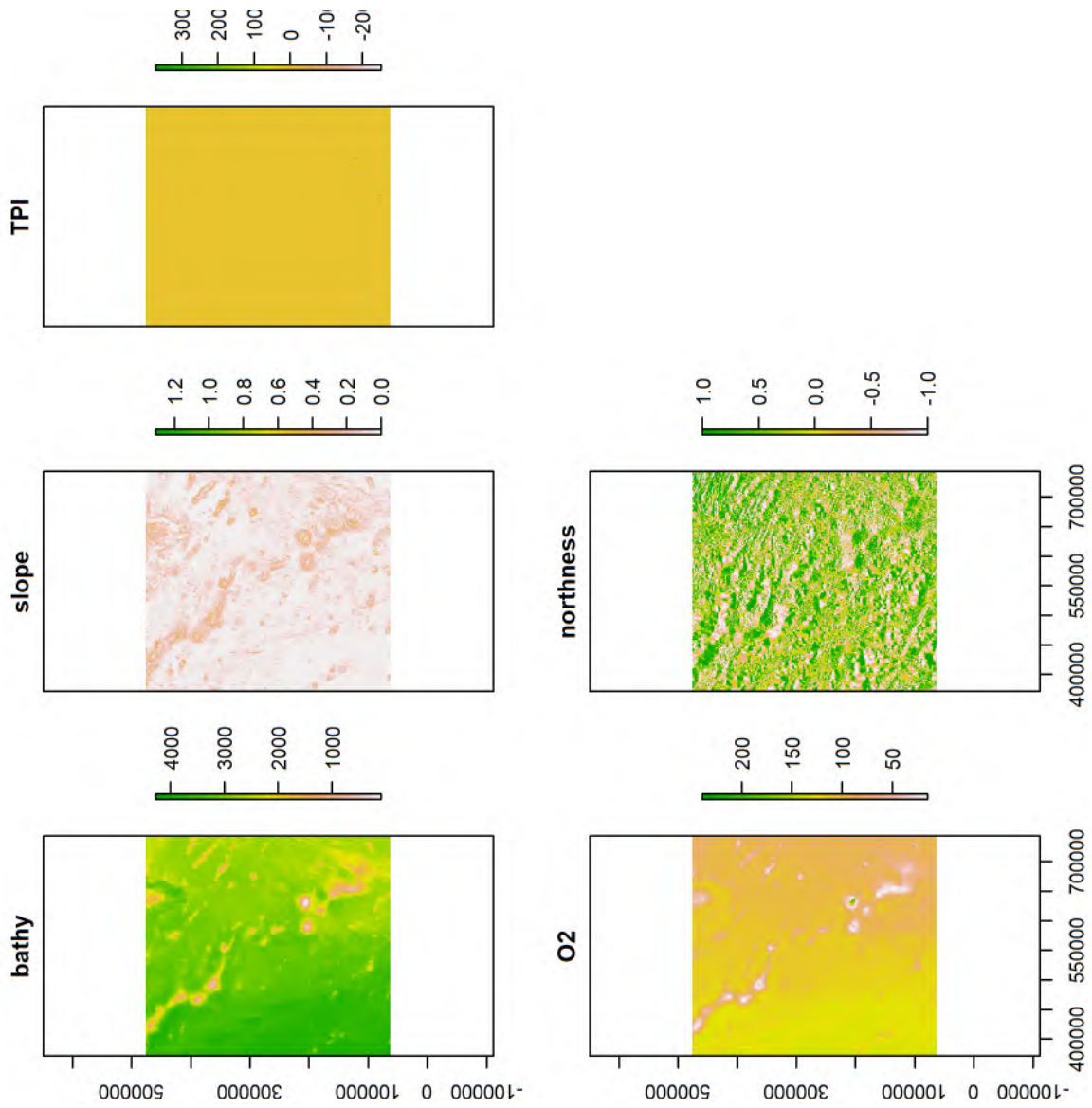


Figure 70: Map of bathymetry, slope, TPI, Oxygen and northness used as explanatory variables in this analysis of VME data

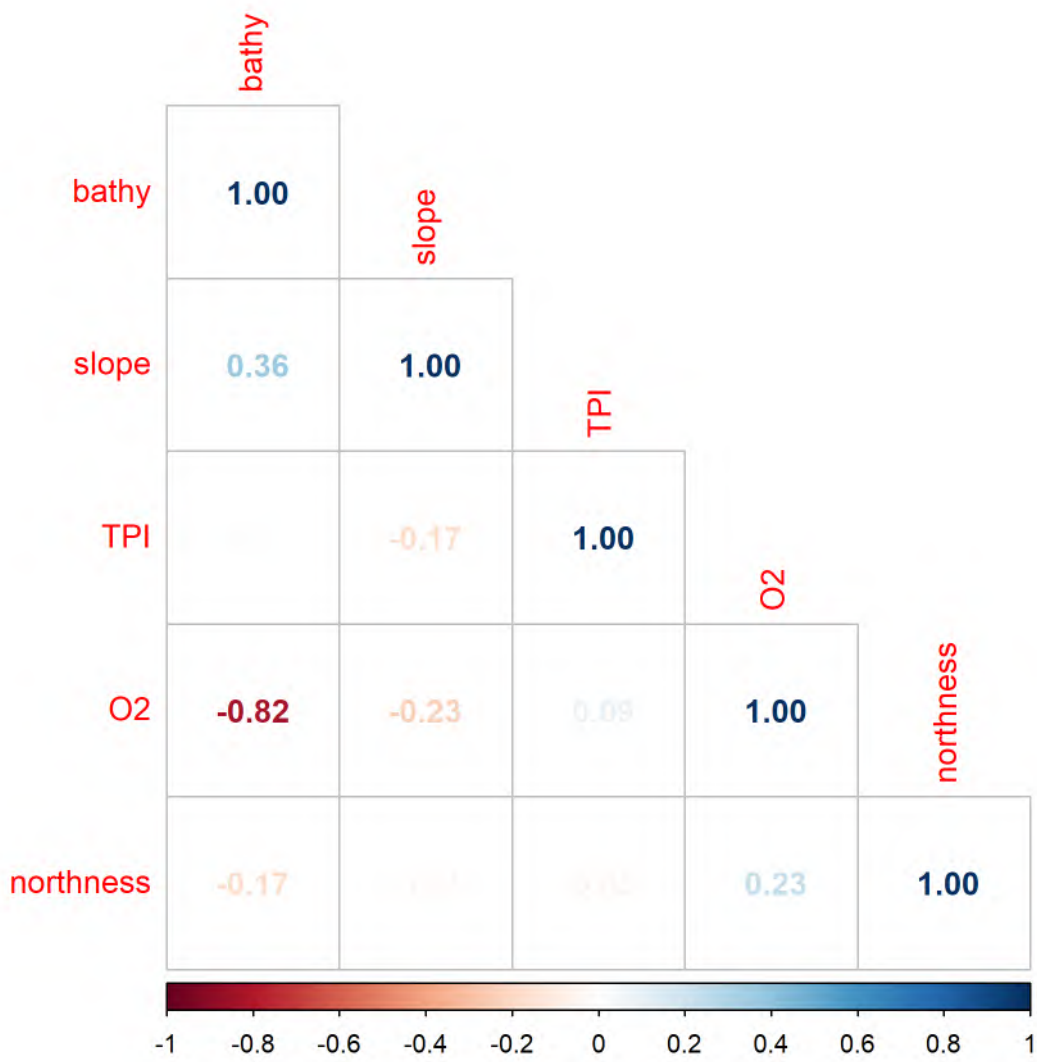


Figure 71: Correlation among independent variables used in modeling.

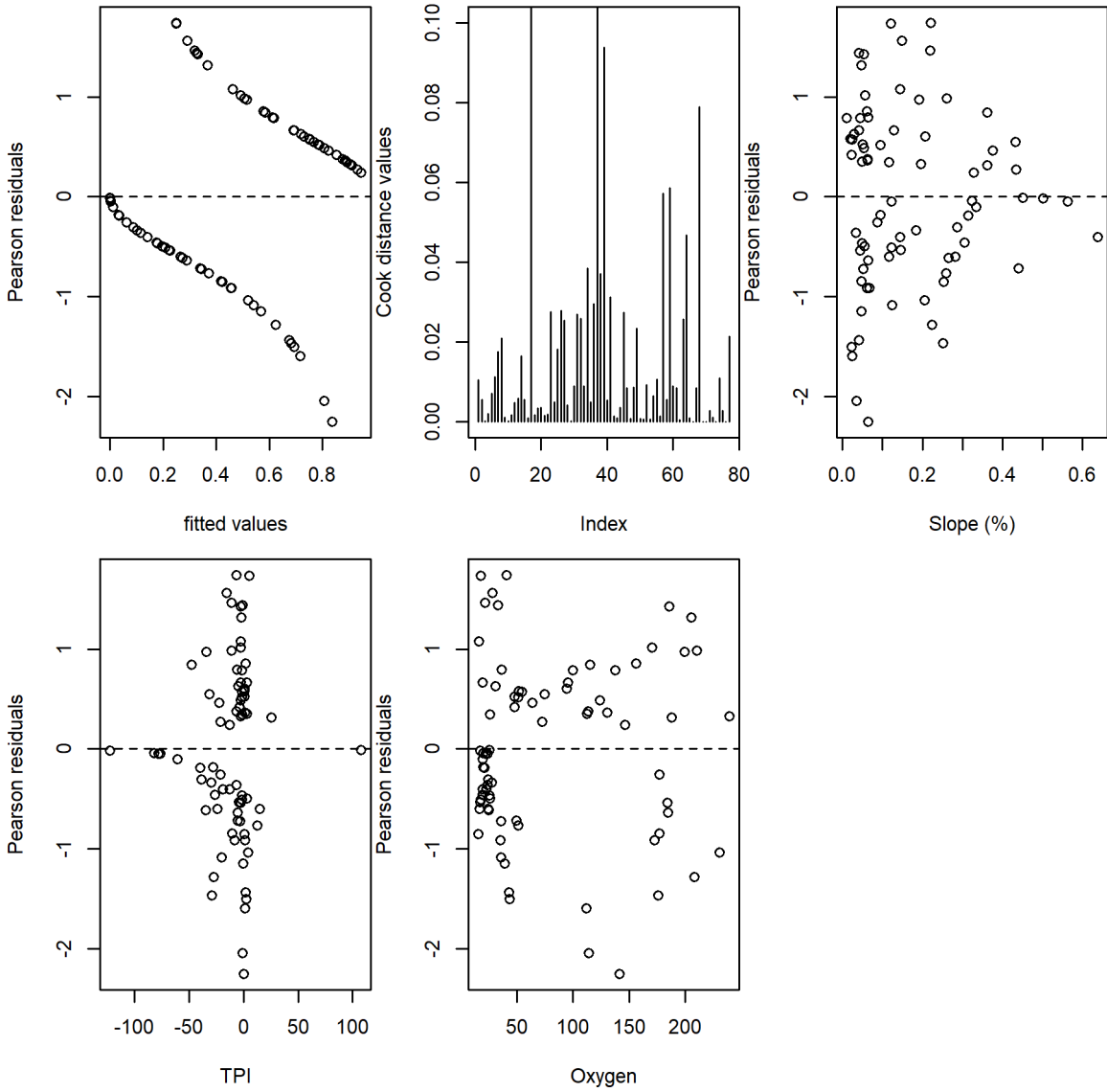


Figure 72: Diagnostic plots for GAM model assumptions.

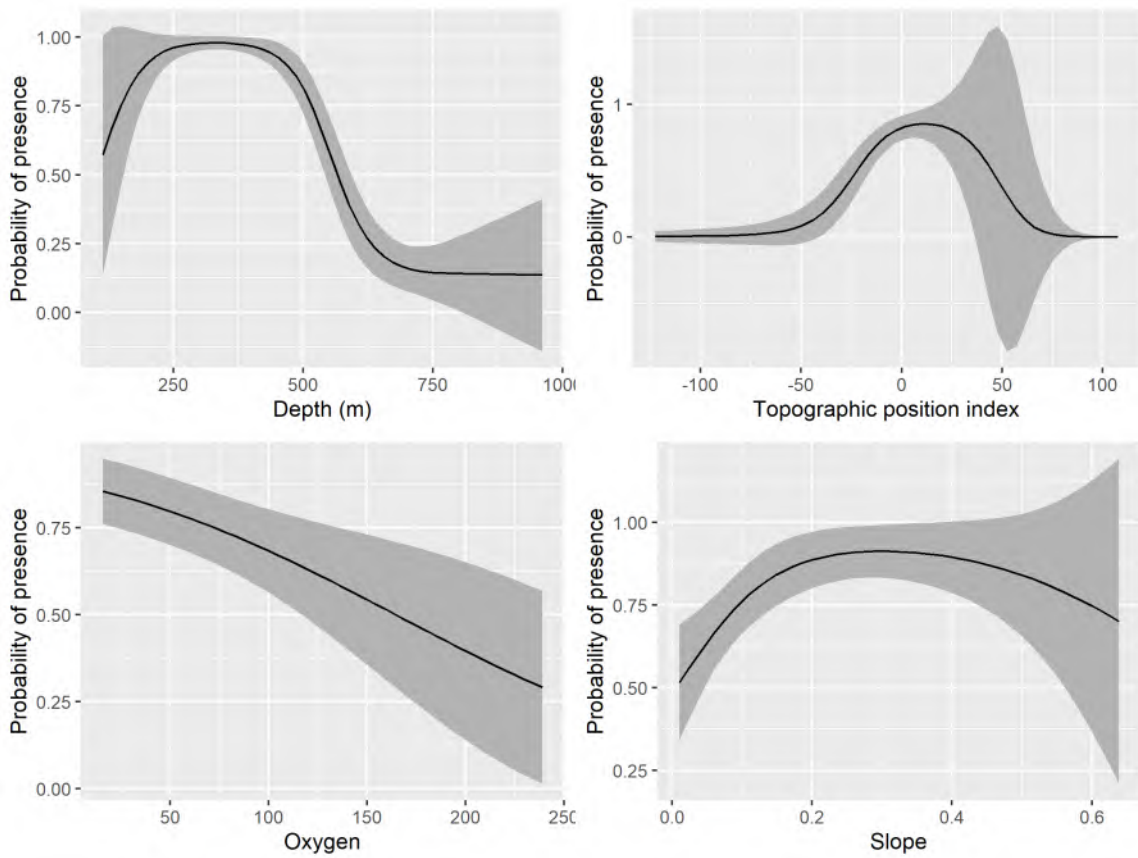


Figure 73: Response curves for independent variables used best-fitting GAM for presence or absence.

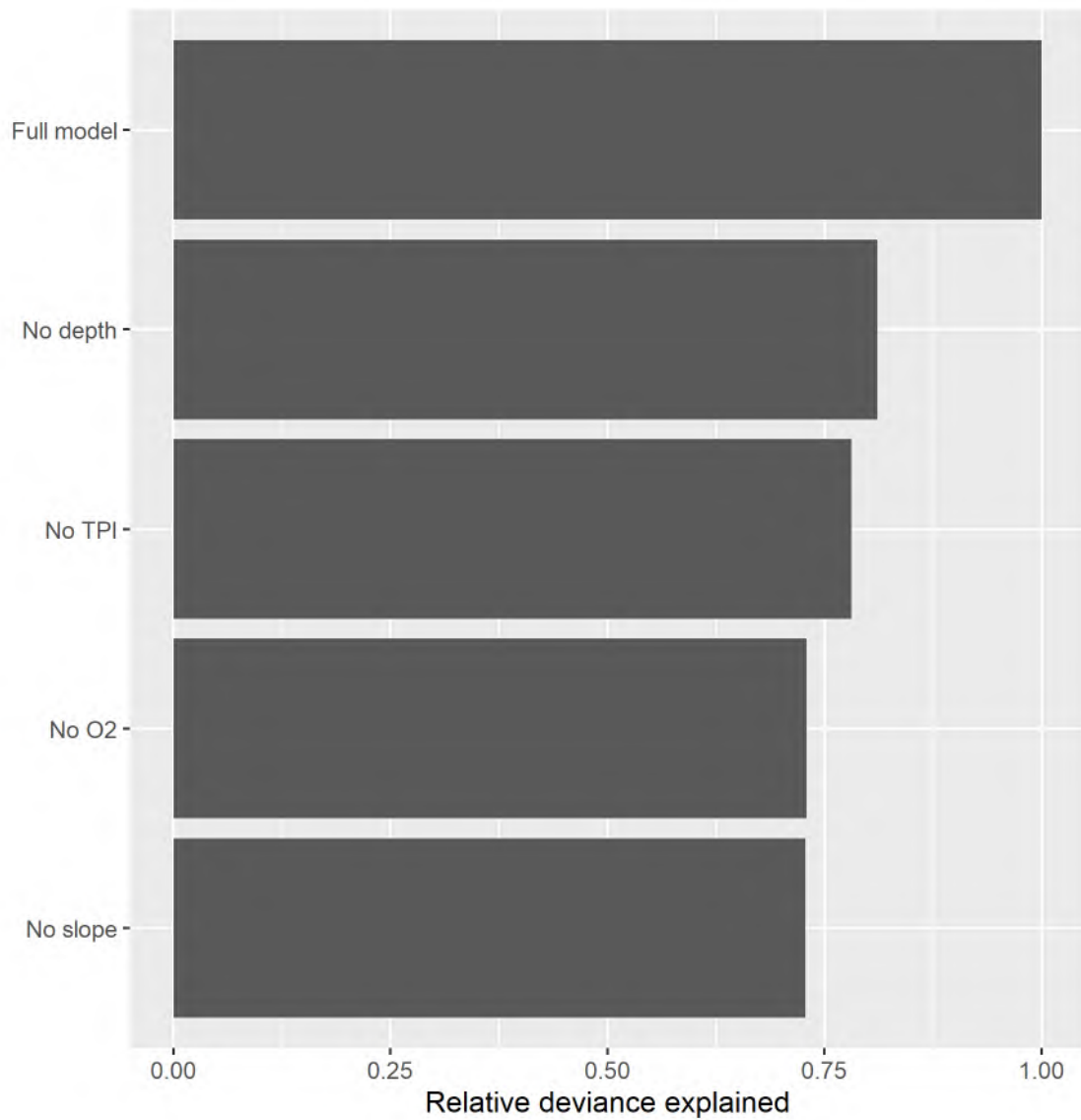


Figure 74: Relative importance of variables included in the Hydrocoral presence or absence GAM measured by their contribution to deviance explained when sequentially removed from the model.

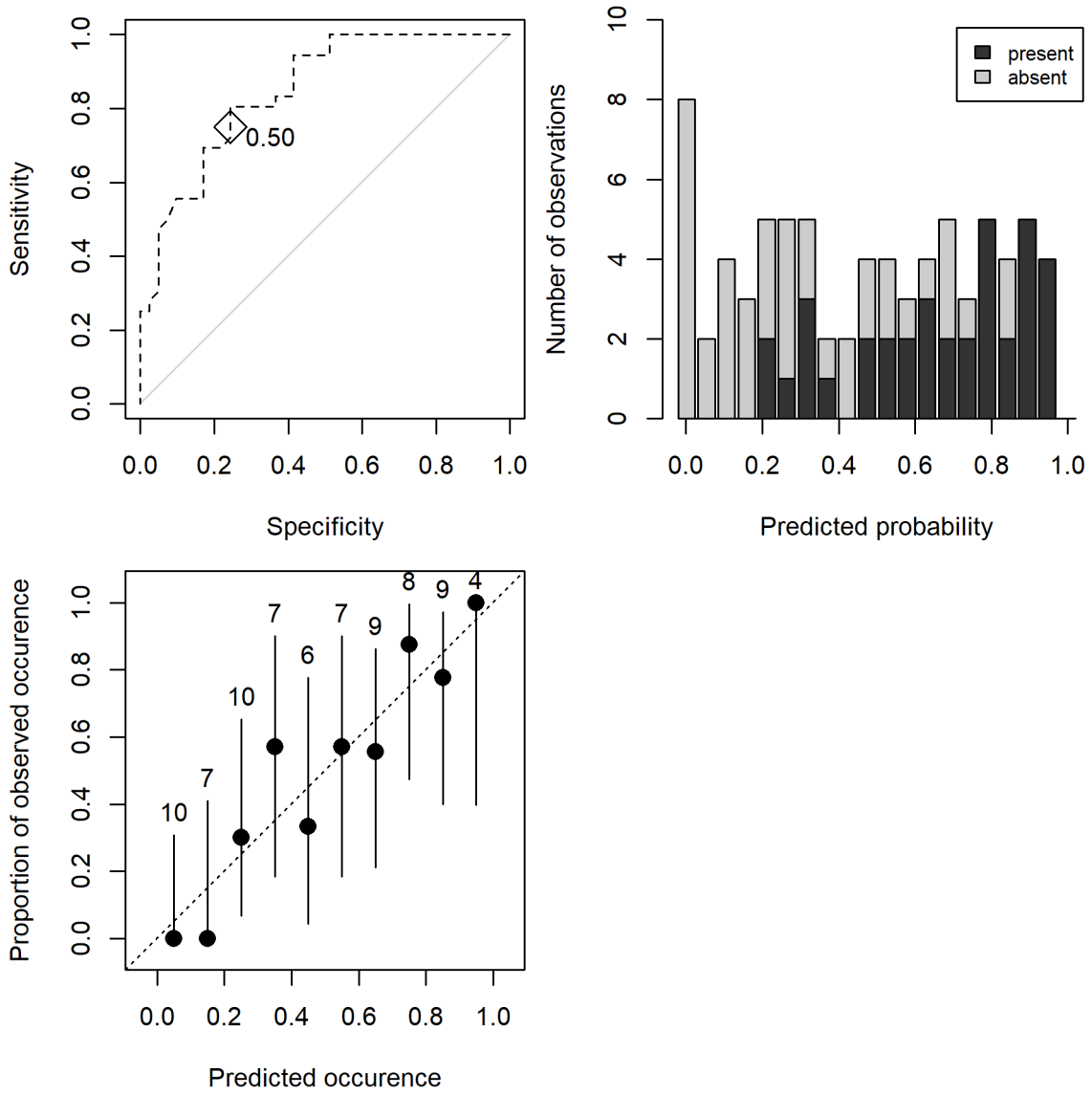


Figure 75: Model diagnostic plots for Hydrocoral presence or absence GAM.

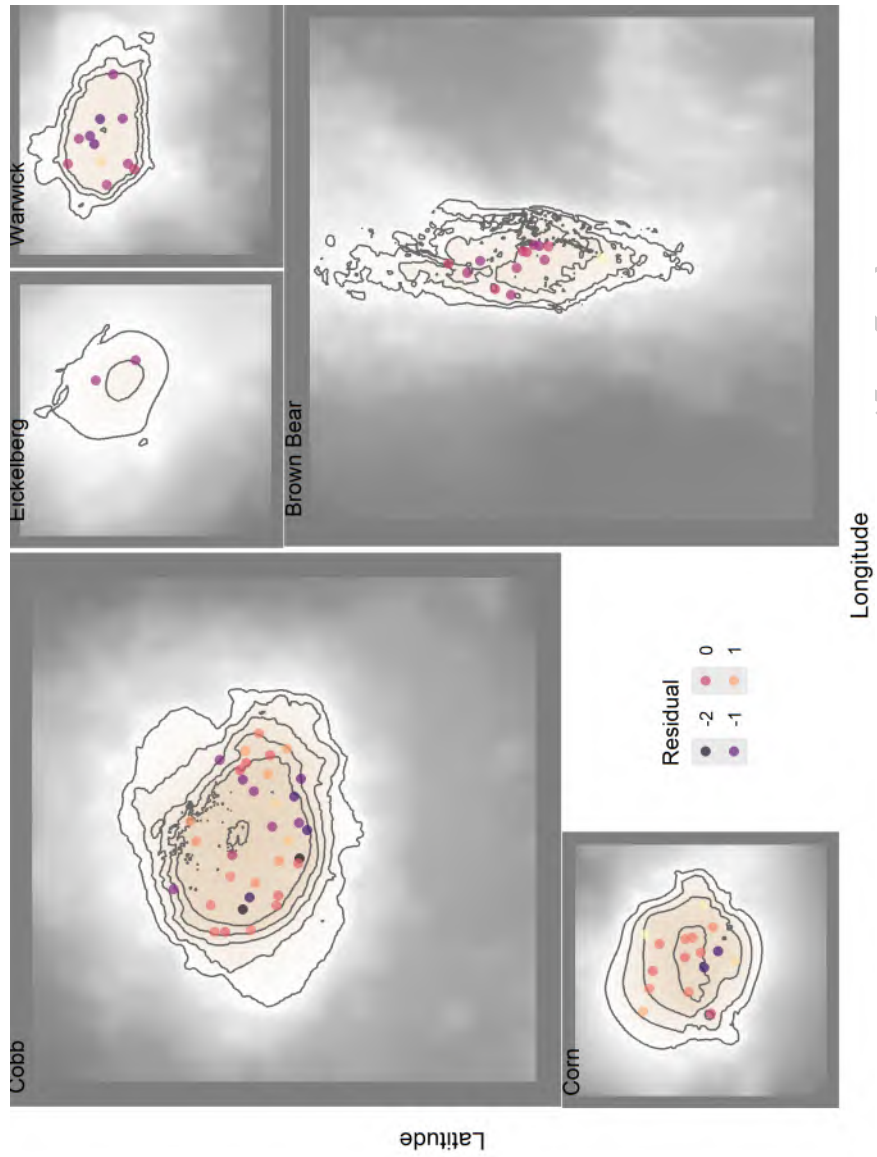


Figure 76: Spatial patterns in model Pearson residuals for GAM predicting probability of presence for Hydrocorals.

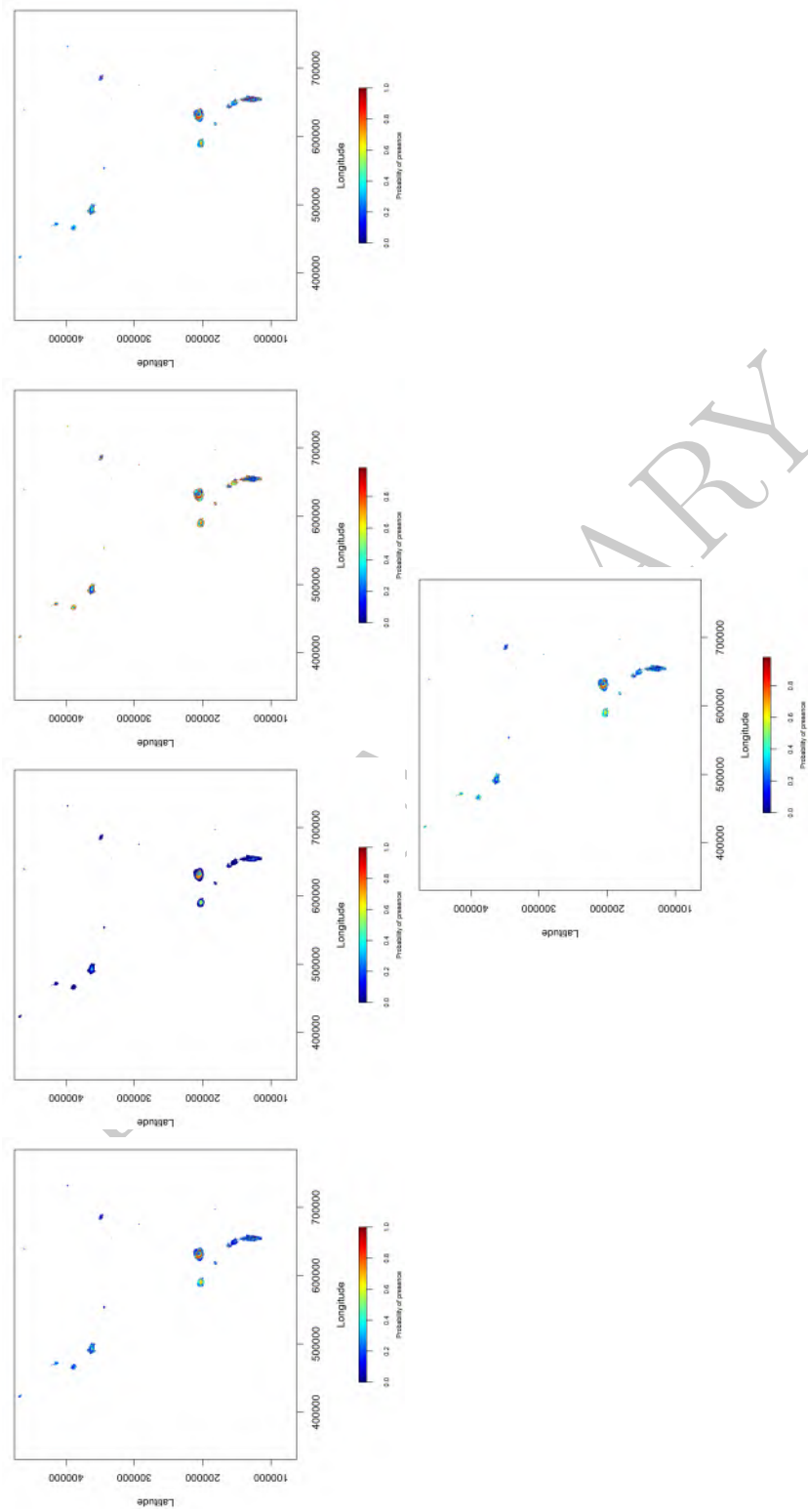


Figure 77: Maps of model predictions for 5 randomly selected folds of the data.

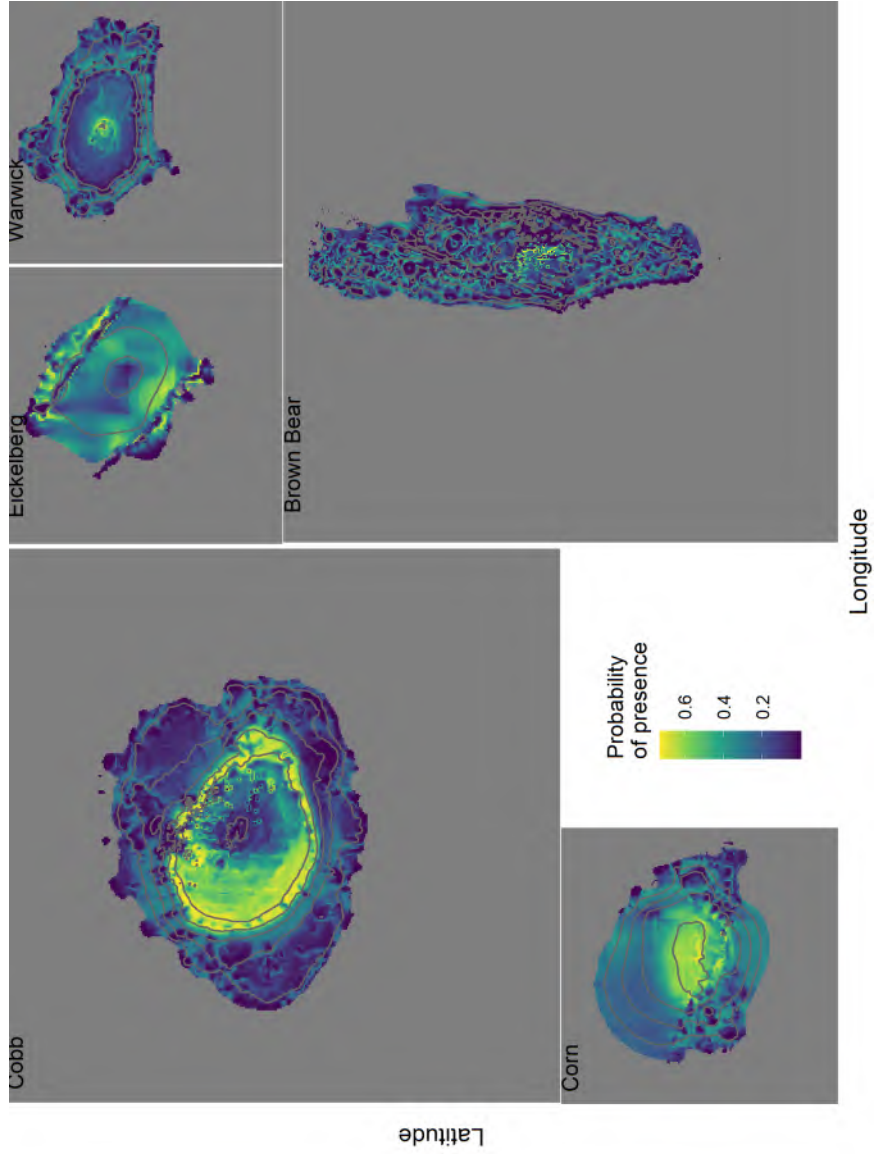


Figure 78: Predicted probability of presence for Hydrocorals at seamounts in the Cobb-Eickelberg seamount chain.

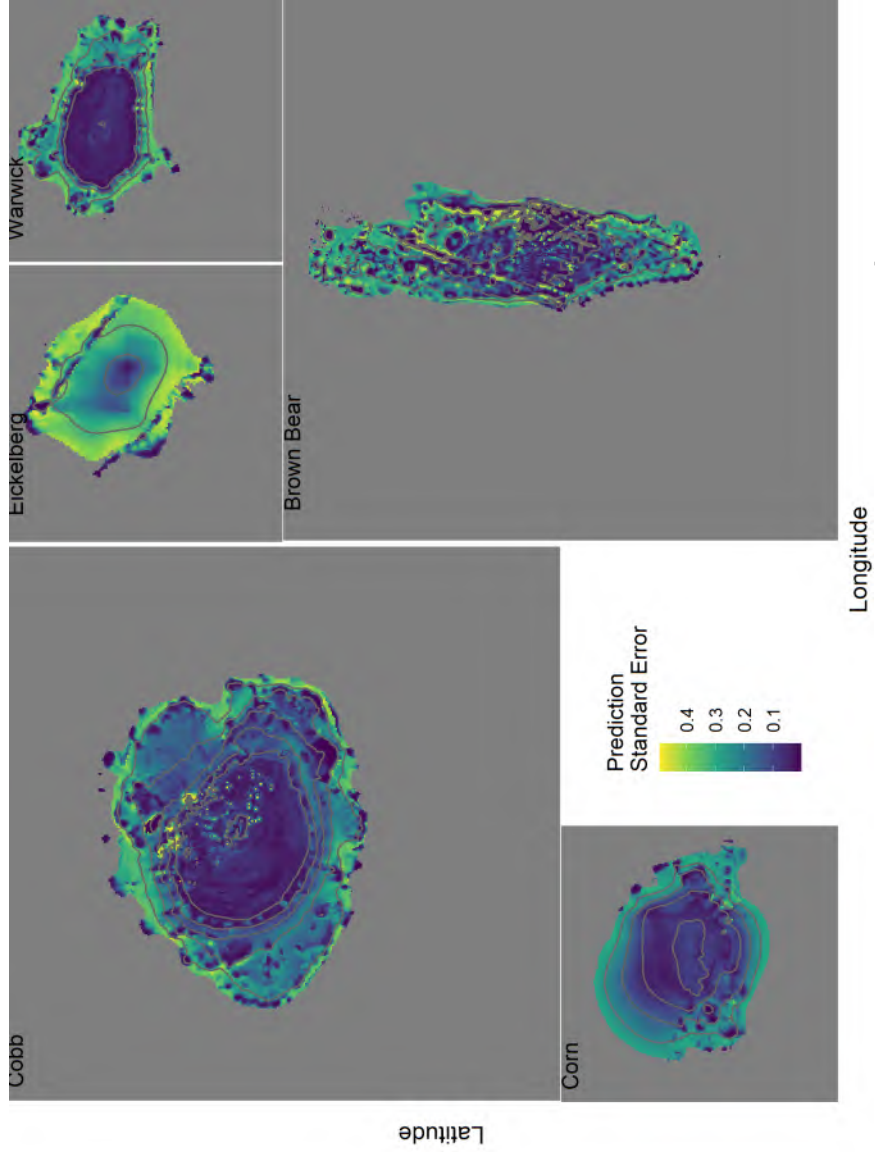


Figure 79: Spatial patterns in model prediction error for GAM predicting probability of Hydrocorals at seamounts in the Cobb-Eickelberg seamount chain.

## 9 Summary

Models were successfully constructed and tested using the survey data collected in 2022 and 2024 at Cobb-Eickelberg seamount chain. Most of these models showed good to excellent performance on training data, but were less accurate when tested either against random subsets of the data or against the independently collected data.

Gorgonian models generally performed well in both training and testing scenarios. These models predicted high probability of encountering Gorgonians at depths less than 600 m across all seamounts. Similarly, the Antipatharian models were good performers and predicted high probability of presence at depths below 350 m.

Scleractinian reefs were observed at only about 10% of transects in 2022. This made their presence or absence difficult to model. Although the training models performed well, when tested against independently acquired data the models were deficient. Most of the observations of Scleractinian reefs were at depths above 400 m. More work should be done on this important taxa group.

For sponges, both the demosponge and hexactinellid models performed well against training and testing data sets. Hexactinellids were predicted to have high probabilities of presence below 500 m depth, while demosponges were more prevalent near the summits of seamounts at depths less than 500 m.

Pennatulacean were predicted to occur on westward facing slopes in regions of low oxygen. The models performed well against both the training and internal testing data. However they did not perform well when tested against the survey data from 2024.

Hydrocoral models performed well for all training and testing scenarios. The model showed that hydrocorals are most prevalent in a band of depths from ~200 - 400 m.

Overall, the models generally fit well and produce useful predictions. At deeper depths there are generally uniformly high probabilities of finding at least one VME indicator taxa. This reflects the overall high occurrence rate of these taxa at the deeper transects.

More work could be done to incorporate additional variables that might explain some of the variability on a smaller scale. It has been noted that densities of VME indicator taxa were relatively low at most of the seamounts, so modeling of the density data should be a next step in order to identify areas of high density of VME indicator taxa.

## 10 References

- Allouche, O., Tsoar, A., & Kadmon, R. (2006). Assessing the accuracy of species distribution models: Prevalence, kappa and the true skill statistic (TSS). *Journal of Applied Ecology*, 43, 1223–1232. <https://doi.org/10.1111/j.1365-2664.2006.01214.x>
- Etnoyer, P. J., Wagner, D., Fowle, H. A., Poti, M., Kinlan, B., Georgian, S. E., & Cordes, E. E. (2018). Models of habitat suitability, size, and age-class structure for the deep-sea black coral *Leiopathes glaberrima* in the Gulf of Mexico. *Deep-Sea Research Part II: Topical Studies in Oceanography*, 150, 218–228. <https://doi.org/10.1016/j.dsr2.2017.10.008>
- Hijmans R. J. (2019). raster: Geographic Data Analysis and Modeling. R package version 3.0-7. <https://CRAN.R-project.org/package=raster>
- Hosmer, D. W. Jr., Lemeshow, S., and Sturdivant, R. X. (2013). *Assessing the Fit of the Model*. Applied Logistic Regression, 3rd Edn. John Wiley & Sons. doi: 10.1002/9781118548387.ch5
- Huff, D. D., Yoklavich, M. M., Love, M. S., Watters, D. L., Chai, F., & Lindley, S. T. (2013). Environmental factors that influence the distribution, size, and biotic relationships of the Christmas tree coral *Antipathes dendrochristos* in the Southern California Bight. *Marine Ecology Progress Series*, 494, 159–177. <https://doi.org/10.3354/meps10591>
- R Core Team (2019). R: A language and environment for statistical computing. R Foundation for Statistical Computing, Vienna, Austria. URL <https://www.R-project.org/>.

Valavi R, Elith J, Lahoz-Monfort JJ, Guillera-Arroita G. blockCV: An R package for generating spatially or environmentally separated folds for k-fold cross-validation of species distribution models. *Methods Ecol Evol.* 2019; 10:225–232. <https://doi.org/10.1111/2041-210X.13107>

Yesson, C., Bedford, F., Rogers, A. D., & Taylor, M. L. (2017). The global distribution of deep-water Antipatharia habitat. *Deep-Sea Research Part II: Topical Studies in Oceanography*, 145, 79–86. <https://doi.org/10.1016/j.dsr2.2015.12.004>

PRELIMINARY